Rivalta, E., Taisne, B., Bunger, A. P., Katz, R. F. (2015): A review of mechanical models of dike propagation: Schools of thought, results and future directions. - *Tectonophysics*, *638*, pp. 1—42.

DOI: http://doi.org/10.1016/j.tecto.2014.10.003

A review of mechanical models of dike propagation: schools of thought, results and future directions

E. Rivalta[a,b,c], B. Taisne[d], A. Bunger[e], R. Katz[f]

[a]*Deutsches GeoForschungsZentrum GFZ, Section 2.1, Potsdam, Germany*
[b]*Institute of Geophysics, University of Hamburg, Germany*
[c]*Earthquake Research Institute, University of Tokyo, Japan*
[d]*Earth Observatory of Singapore, Nanyang Technological University, Singapore*
[e]*Department of Civil and Environmental Engineering, Department of Chemical and Petroleum Engineering, University of Pittsburgh, Pittsburgh, PA, USA*
[f]*Department of Earth Science, University of Oxford, United Kingdom*

Abstract

Magma transport in brittle rock occurs by diking. Understanding the dynamics of diking and its observable consequences is essential to deciphering magma propagation in volcanic areas. Furthermore, diking plays a key role in tectonic phenomena such as continental rifting and plate divergence at mid-ocean ridges. Physics-based models of propagating dikes usually involve coupled transport of a viscous fluid with rock deformation and fracture. But the behaviour of dikes is also affected by the exchange of heat with the surroundings and by interaction with rock layering, pre-existing cracks, and the external stress field, among other factors. This complexity explains why existing models of propagating dikes are still relatively rudimentary: they are mainly 2D, and generally include only a subset of the factors described above. Here, we review numerical models on dike propagation focusing on the most recent studies (from the last 15–20 years). We track the influence of two main philosophies, one in which fluid dynamics are taken to control the behavior and the other which focuses on rock fracturing. It appear that uncertainties in the way that rock properties such as fracture toughness vary from laboratory to field scale remains one of the critical issues to be resolved. Finally, we present promising directions of research that include emerging approaches to numerical modeling and insights from hydraulic fracturing as an industrial analogue.

Keywords: Dike propagation, fluid-filled fractures, lubrication theory, Weertman cracks, Boundary element method, layered media, induced

seismicity, volcano deformation, rifting, hydraulic fracture.

Contents

1. Introduction

The motivation to improve and extend models of diking comes from several key scientific areas. Firstly, most basaltic eruptions occur in the form of dikes; the characteristics of these volcanic events are thus determined by the dynamics of the dikes. Secondly, plate divergence and crustal accretion at mid-ocean ridges and continental rift-zones occurs mostly in form of repeated episodes of diking. Thirdly, models of dikes can be applied to industrially important processes related to fluid transport and storage in the crust, such as hydraulic fracturing of hydrocarbon reservoirs and formation of diamond-bearing kimberlite deposits. The barriers to progress in modelling dikes stem from the mathematical complexity and/or computational impracticality of models that account for every possible mechanism affecting dike propagation. At their most basic, propagating dikes can be considered as a hot, compressible fluid flowing between cold elastic walls. However, non-linear rock behavior such as fracture and plasticity must be considered to model the motion of the fracture tip. Furthermore, magma rheology and buoyancy change during propagation due to gas exsolution and crystallization. Hence some of the most difficult problems in mathematical physics are closely linked to the dynamics of dikes. To make the problem tractable, most models of propagating dikes are simplified by some combination of reducing the problem to two-dimensions, linearizing the behavior of the rock when it deforms and breaks, neglecting thermal processes, linearizing and/or neglecting the changes in magma rheology, and simplifying the geometry or neglecting altogether the pre-existing structures within the host rock.

Nevertheless, in recent years our understanding of dikes has increased significantly, due both to a wealth of geophysical data now available and to progress in modelling. Some of the questions that have engaged researchers during the last two decades include: What is the three-dimensional shape of propagating dikes? What factors control their dynamics, and in particular their geometry? How can we explain the details of the seismicity or deformation field associated with dike emplacement? What is the effect of an external stress field? What are the effects of the free surface, layering or topography? What is the role played by the coupling with a magma reservoir?

In this review, we present an overview on how those questions have been addressed and indicate short and long-term perspectives on what questions might be answered in the future. In particular we present:

1. Geometrical and dynamical properties of dikes and the main observa-

tions available to constrain these (Sec. 2 and 3);
2. Different schools of thought in deriving models of dikes, with consideration of their strengths and limitations (Sec. 4);
3. The main results achieved in modelling the interplay of propagating dikes with a range of external factors in various tectonic settings (Sec. 5);
4. Applications to hydraulic fracturing and other industry-related problems (Sec. 6);
5. Perspectives on future research direction and open problems (Sec. 7).

2. Geometrical properties of dikes and relationship to magma and rock rheology

Magma-filled dikes have different manifestations often associated with different magma compositions and tectonic settings. In some active volcanic environments, such as Kilauea volcano in Hawai'i, magma may intrude in the host rock as a propagating dike and then flow through a stable, tabular conduit. This last manifestation of stable flow is sometimes referred to as a dike. None of the models presented in this review correspond to this stable configuration; see instead Montagna and Gonnermann (2013), for example. Here we consider the unstable configuration of a dike with a tip that propagates through more or less intact rock.

The thickness of dikes is much less than their breadth and length (Fig. 2). This aspect ratio is shared with sills, which are similar to dikes but emplaced horizontally along bedding planes rather than cutting through them. It distinguishes dikes and sills from other magma-filled bodies, such as diapirs, laccoliths or cylindrical conduits. Modern geophysical monitoring has enabled an accumulation of measurements of dike characteristics. These observations show that the thickness (also referred to as width or opening) typically ranges from tens of centimeters to several meters, while the length L (here defined as their dimension along the direction of propagation, which is sometimes referred to as height if propagation is vertical) ranges from several hundreds meters to a few kilometers, or even several tens of kilometers for horizontally propagating intrusions (Tryggvason, 1984, 1986; Toda and Stein, 2002; Wright et al., 2006). The third dimension of dikes (here called breadth b) is generally of the same order of magnitude as their length, but somewhat smaller, especially for horizontally propagating dikes (Fig. 2A,B). Anomalously large dikes, tens of meters thick and hundreds to thousands of kilometers long, can be identified in the field, sometimes in the

Figure 1: Left and right: The width of the dike, H, is much smaller that the other horizontal extension highlighted by the red line. The left picture was taken by N. Villeneuve at Piton des Neiges, the right picture by J.-C. Komorowski at Nyragongo. The origin of 2-D approximations in modeling dykes comes from field observations.

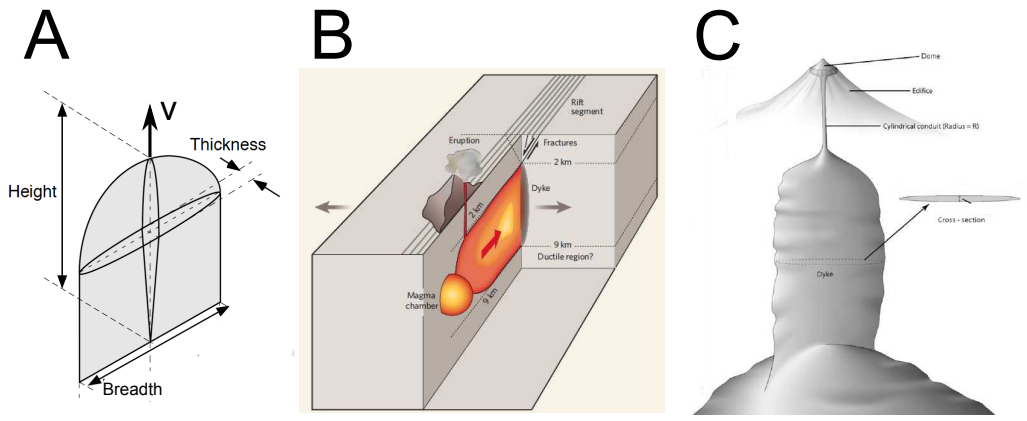

Figure 2: A) Simplified image of a vertically propagating dike (Modified from Fig. 3 in Watanabe et al. (2002), with permission). B) Dike propagating horizontally from a magma chamber (Fig. 2 in Sigmundsson (2006), with permission). C) Dike-like root developing from a magma reservoir into a cylindrical conduit in the volcanic edifice (Fig. 1 from Costa et al. (2007), with permission).

form of swarms (Pollard, 1987; Ernst et al., 1995; Jolly and Sanderson, 1995; Fialko and Rubin, 1999).

In general, dikes will open against the minimum compressive stress, σ_3, and propagate on a plane perpendicular to σ_3 (Anderson, 1951). In 2D, they propagate in the direction of maximum compressive stress, σ_1. When both horizontal stresses are similar ($\sigma_{hmin} \sim \sigma_{Hmax}$), intrusions will still have a thin aspect ratio but will orient randomly; this can occur, for instance, near a free surface. Examples of this behaviour are observed in laboratory experiments that entail fluid injection into solidified gelatin. For a simple gelatin block with hydrostatic stress conditions, $\sigma_{hmin} \sim \sigma_{Hmax}$; if the gelatin is brittle, fluid-filled cracks form vertically and in an essentially random horizontal direction, apparently according to small perturbations within the specimens. If the gelatin is viscoelastic (viscoelastic properties arise for specific types of gelatin), then the fluid-filled fractures assume a diapir-shaped aspect (Sumita and Ota, 2011). In nature, dikes may also form in $\sigma_{hmin} \sim \sigma_{Hmax}$ stress conditions: for example at volcanoes such as Etna, where in consequence of several dike injections in a specific direction, σ_{Hmax} may become very similar to σ_{hmin}, or the principle stresses may rotate. The dike pattern becomes radial in such stratovolcanoes, where it is also linked to the gravitational load of the edifice (Nakamura, 1977; Acocella and Neri, 2009).

Dikes take a tabular shape because they are fractures driven by internal

fluid pressure, opening in brittle materials. Other types of conduits, such as low-aspect-ratio cylindrical pipes, are energetically disfavored in the brittle crust, or need very long time scales and sustained, high temperatures to stabilize. They are observed for volcanoes such as Montserrat, where the viscosity of the magma is very high. Recent models (Costa et al., 2007, 2012) suggest that close to the surface, where the viscosity gradient of dacitic magmas is steep, flat-bottle shaped volcanic conduits might form, with a deep dike-like root transporting low-viscosity magma developing into a cylindrical conduit where the magma viscosity becomes high. This configuration may help to explain observed patterns of deformation (Fig. 2C).

What is the minimum rock/magma viscosity contrast such that rock responds in a brittle rather than ductile manner? Rubin (1993a) calculated self-similar solutions of fluid-filled, pressurized cracks in viscoelastic materials to study the rheological conditions promoting ascent by fracture versus viscous deformation of the host rock. He concluded that if the ratio of rock to magma viscosity η_r/η_m is larger than 10^{11}–10^{14}, the crust behaves elastically at the time scale of magmatic intrusion, such that basaltic magmas and low-viscosity rhyolitic magmas ($\eta_m \leq 10^4 - 10^6\,\mathrm{Pa\,s}$) will generate dikes in crustal rocks. If the viscosity contrast is smaller than 10^6–10^8, then magma transport occurs via equi-dimensional diapirs inducing ductile flow in the host rock. For intermediate viscosity contrasts (10^6–$10^8 \leq \eta_r/\eta_m \leq 10^{11}$–$10^{14}$) the form of transport is hybrid, with an emergent tabular aspect ratio; there is progressively more fracture and less ductile deformation of the host rock with increasing viscosity. Sumita and Ota (2011) describe their experimental study on the aspect ratio of buoyancy-driven fluid-filled fractures in a host material with a rheological transition from ductile to brittle. They find the fluid migrates as a hybrid of a diapir (the head) and a dike (the tail). The diapir is a bulging crack fracturing the agar at its propagating tip and closing at its tail to form a dyke. A small amount of fluid is left along its trail and the fluid decelerates with time. Sumita and Ota (2011) study how the shape and velocity of a constant-volume fluid batch change as the agar concentration, C, and the density difference between the fluid and the agar, $\Delta\rho$, vary (Fig. 3 and supplementary videos at http://www.sciencedirect.com/science/article/pii/S0012821X11000562). As C decreases, the medium becomes ductile and the 3D shape of the fluid batch changes from dike-like (with a blade-like section as seen from above) to a meandering or a bifurcating dike, and finally to a diapir–dike hybrid (the section as seen from above becomes a cusped ellipse). A similar transition is

also observed when $\Delta\rho$ increases under a fixed C. The experiments suggest that fluids may migrate as a diapirdike hybrids around the depth where a transition from brittle to ductile rheology occurs and that fluid migration of various styles can coexist at the same depth, if the fluids have different buoyancy.

It is generally agreed that in the crust, dikes have sufficient energy to propagate upward through intact rock; pre-existing fractures are not needed to transport magma. Analogously, a pre-existing fracture network is not required for a volcanic eruption to occur. However, if buoyant magma enters into pre-existing zones of weakness it may exploit those paths, provided that the weak zones are oriented in a favourable way relative to the stress field (Delaney et al., 1986; Ziv et al., 2000). This phenomenon is sometimes observed (Valentine and Krogh, 2006; Hooper et al., 2011), however it is not universal because faults are generally oriented in the stress field differently from fluid-filled fractures.

3. Observations

3.1. Field observations

Observations of propagating dikes represent a constraint on models and a means to identify open questions. In this section we review the main hurdles related to using data from different disciplines to constrain numerical models of dike propagation. For more comprehensive reviews of field and laboratory observations on dikes and sills refer to Menand (2011) and Tait and Taisne (2013).

3.1.1. Structural geology

While a wealth of observations on frozen dikes in the field is available (e.g. Gudmundsson, 1983), structural geology has rarely been used in combination with models, due to scarce communication between these disciplines. Exceptions to this trend that make this link within a single investigation include Pollard (1976); Pollard and Muller (1976); Pollard (1987); Valentine and Krogh (2006); Kavanagh and Sparks (2011); Geshi et al. (2012); Daniels et al. (2012). Even in the absence of complementary modeling efforts, valuable information can be obtained by studying outcrops in the field. For example, a partial 3D view of frozen dikes has been obtained by Kavanagh and Sparks (2011) by taking advantage of mining. However, fossil structures exposed by weathering or mining represent the final, static

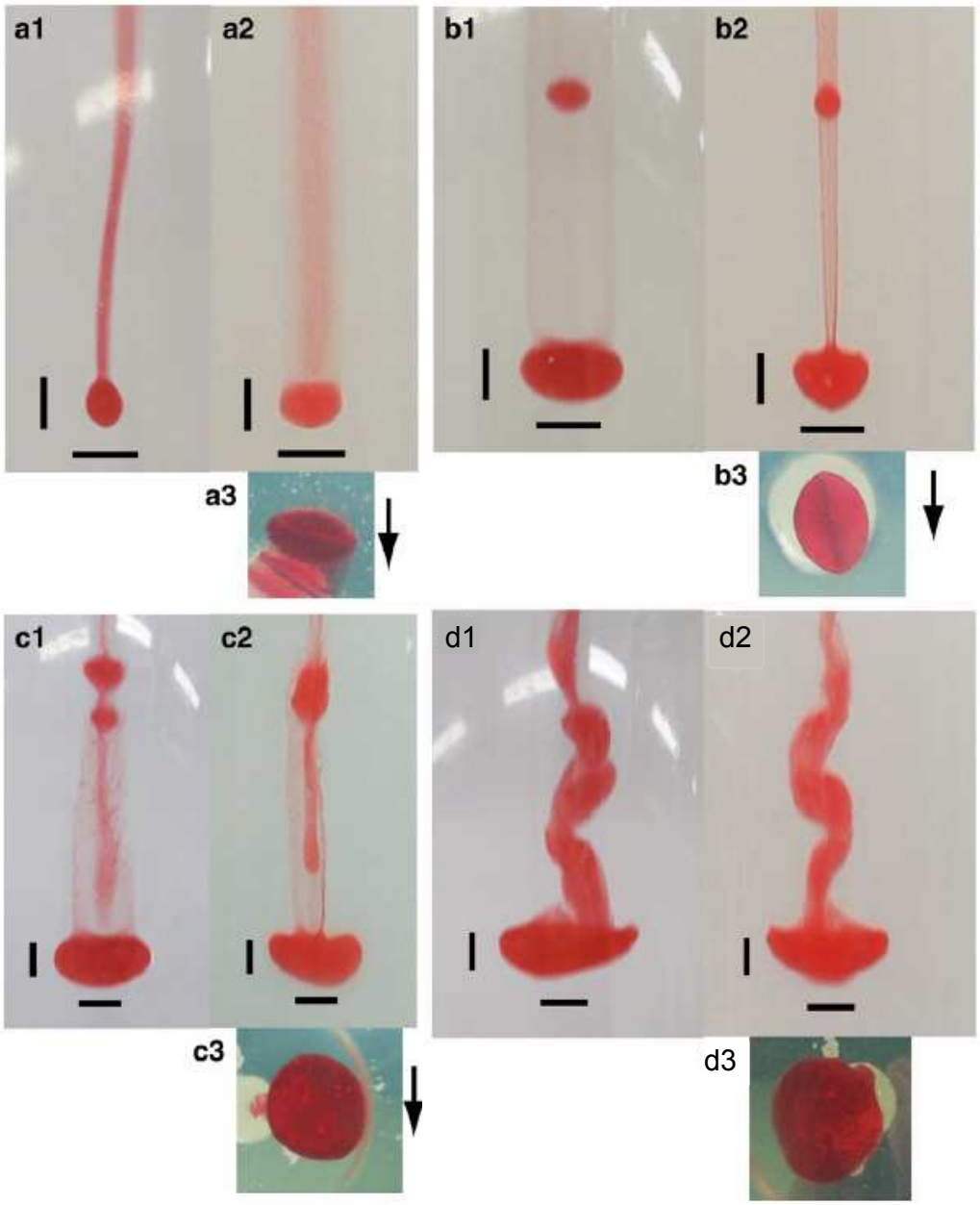

Figure 3: Examples of buoyancy-driven fluid-filled cracks propagating in Agar with different concentration C () and with a different density difference $\Delta\rho$ between gelatin and the aqueous solutions used for the injections. The cracks are viewed from 3 orthogonal angles (1, 2 and 3). A scale bar is 10 mm. (a) $C = 0.08\,\mathrm{wt.\%}$, $\Delta\rho$=31 $\mathrm{kg\,m^{-}3}$, (b) $C = 0.08\,\mathrm{wt.\%}$, $\Delta\rho$= 300 $\mathrm{kg\,m^{-}3}$ (see also video), (c) $C = 0.07\,\mathrm{wt.\%}$, $\Delta\rho$ = 604 $\mathrm{kg\,m^{-}3}$, and (d) $C = 0.06\,\mathrm{wt.\%}$, $\Delta\rho$=604 $\mathrm{kg\,m^{-}3}$. (Figs. 6 and 7 from Sumita and Ota (2011), with permission).

state of magma intrusion. It is difficult to use them to constrain numerical models of dike propagation because the link between the dynamic shape of dikes and their final frozen state is poorly understood. Therefore, caution is required when attempting to infer the elastic properties of the host rock on the basis of the final, static geometry of a dike.

Other geological and geophysical techniques useful to evaluate dynamic aspects include examining the magnetic (Kirton and Donato, 1985; Knight and Walker, 1988; Craddock et al., 2008; Chadima et al., 2008; Silva et al., 2010; Neres et al., 2014) or flow fabric of frozen dikes (e.g. Correa-Gomes et al., 2001), gravity (e.g. Carbone, 2003 and review by Battaglia et al., 2008); magnetic (e.g. Del Negro et al., 2003), and magnetotelluric data (Siniscalchi et al., 2012). Structural geology can also provide strong constraints, but it must be carried out with the recognition that the resulting observations are typically a sparse and dimensionally limited view of what are usually extensive, three-dimensional structure. For this reason, the value of these studies can be greatly increased when modelling is used to assist with interpretation of 3D morphologies and probable conditions that governed emplacement.

3.1.2. Crustal deformation

Inversion of GPS and/or InSAR deformation data can be used to estimate the shape and the volume of magma-filled dikes and sills and the of volume change of magma chambers. Recent developments in satellite interferometry allow highly resolved measurements of ground deformation. This enables the recognition of complex interactions between different feeding sources and intrusions (Wright et al., 2006; Grandin et al., 2009; Hamling, 2010; Grandin et al., 2010a,b; Montgomery-Brown et al., 2010; Bagnardi and Amelung, 2012). In some cases evidence of deflating sources is lacking, suggesting that magma was probably sourced very deep (Pallister et al., 2010).

The temporal period of InSAR data acquisition is much larger than the time scale of dike intrusions (several hours to a few days), so that it is very rare to measure an actively propagating dike. Thus, inversions of InSAR data generally give information on the ground deformation accumulated over the entire emplacement phase; they seldom provide information on the detailed dynamics. There are exceptions to this pattern, such as the work of Bagnardi and Amelung (2012) and Nobile et al. (2012), who obtained interferograms spanning the early and late intrusion phases of a sill and a dike, respectively.

The potentially high temporal resolution of GPS or strain data in prin-

ciple allows for inversion with respect to the evolving shape of dikes or sills. However, this has been performed only in a few cases (Aoki et al., 1999; Segall et al., 2001; Irwan et al., 2006; Aloisi et al., 2006; Montgomery-Brown et al., 2011). In some earlier work, forward models were used to explain temporal changes in the deformation field (Okada and Yamamoto, 1991; Linde et al., 1993). Peltier et al. (2005) modelled changes in direction of a propagating dike using data from tiltmeters; that work shows that flank eruptions at Piton de la Fournaise volcano are preceded by a relatively fast vertical dike migration, $\sim 2\ m/s$ followed by a slower horizontal propagation, $0.2\ m/s$ to $0.8\ m/s$.

In general, dike models for inversions of crustal deformation data are calculated by discretising the dikes into a mosaic of rectangular dislocation patches (Okada, 1985, 1992) or, for magma chambers, one or more dilatational point sources (Yamakawa, 1955; Mogi, 1958). In some instances, the inclusion of graben faulting is required to achieve a good match between the modeled and observed deformation field and consistency with seismic observations of larger events (Wright et al., 2006; Pallister et al., 2010; Nobile et al., 2012). In most studies, the dislocations and point sources involved are taken to be non-interacting, though Pascal et al. (2013) suggests that this might cause relatively large errors. Furthermore, smoothing/regularization and positivity constraints are applied in order to obtain (subjectively) realistic solutions (Wright et al., 2006; Montgomery-Brown et al., 2010; Nobile et al., 2012). In some cases, physical constraints are instead applied, such as requiring constant pressure drop or a linear pressure gradient on the dike/sill plane (Yun et al., 2006; Sigmundsson et al., 2010; Hooper et al., 2011). Both using physical constraints and smoothing the opening over the dike's plane results in approximately penny-shaped crack (Fig. 4). Horizontally elongated systems are obtained for dikes propagating laterally in rift systems (Montgomery-Brown et al., 2010; Nobile et al., 2012)(Fig. 4D and C respectively). Vertically elongated systems are found for dikes ascending to the surface from deep crustal levels (Pallister et al., 2010) (Fig. 4B). In the inversion by Nobile et al. (2012) (Fig. 4C), a thin channel connecting a Mogi-Yamakawa source and the dike is visible. However, the spatial resolution of the data is generally too low to constrain fine-scale details of dikes and sills shapes in the inversions.

As for longer time scales, while post-seismic deformation studies have contributed considerably to the understanding of the mechanics of faulting during the seismic cycle, studies of post- or inter-diking deformation phases

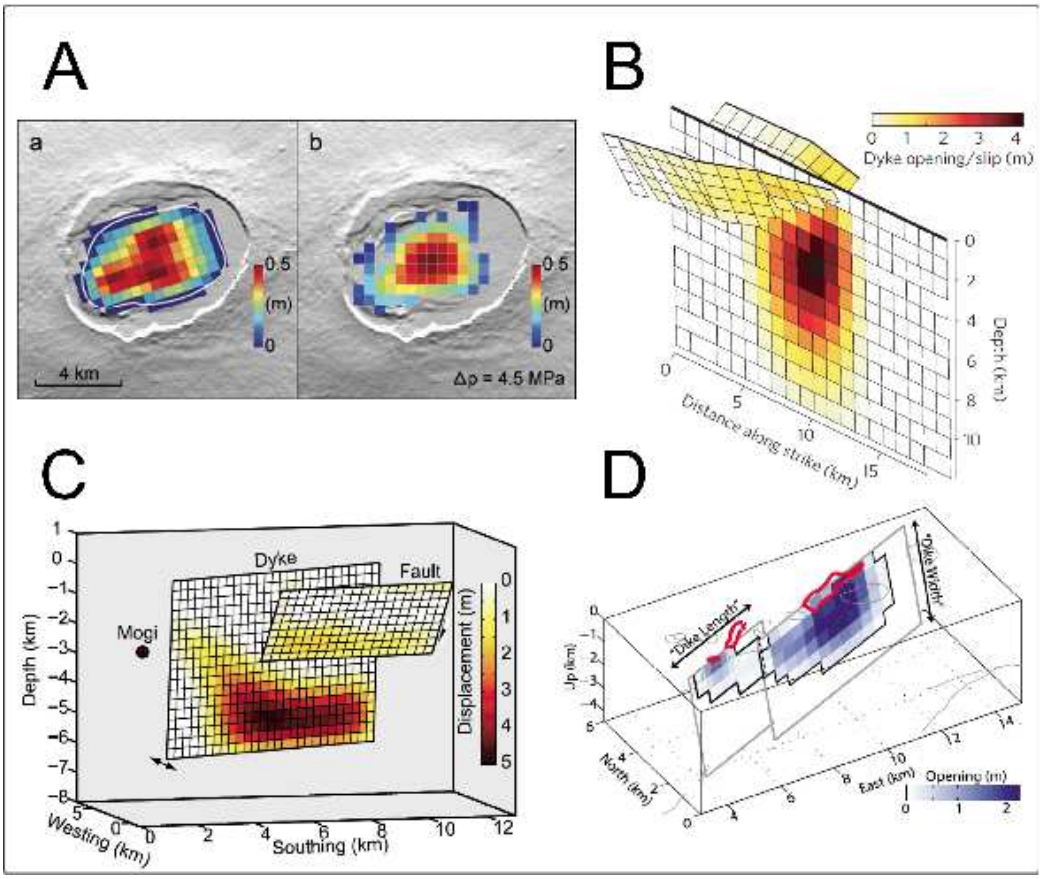

Figure 4: A) Inversion of a horizontal sill at Fernandina (Galapagos), the right panel solution was obtained with uniform pressure boundary conditions. Fig. 10 from (Yun et al., 2006), with permission. B) Inversion of a dike and related graben faulting at Harrat Lunayyir, Saudi Arabia. No feeding source was detected in this case. From Fig. 5 by (Pallister et al., 2010), with permission. C) Inversion of a dike including deflation at a Mogi-Yamakawa point source and graben faulting. From Fig. 2 by (Nobile et al., 2012), with permission. D) Inversion of an en-echelon dike during the 2007 father's day intrusion at Kilauea. From (Montgomery-Brown et al., 2010), Fig. 12, with permission.

are rare (Desmarais and Segall, 2007; Pedersen et al., 2009; Hughes, 2010; Ali et al., 2014). Grandin et al. (2010a) studied inter-diking deformation for the Manda-Hararo dike sequence. InSAR data for the inter-diking period highlights deflation or inflation at the magma chambers, reflecting maintained connectivity between the deeper reservoirs, but separation between the northern magma chambers and the after-dikes intruded further South. Grandin et al. (2010a) also detect inflation of a ∼25 kilometers deep reservoir, probably at the crust-mantle boundary.

For a review of progress in SAR imagery applied to the field of volcanology, see Pinel et al. (2014).

3.1.3. Dike-induced seismicity

The association of magmatic intrusions with earthquake swarms is an important motivation for the study of dikes. Dike-induced seismicity carries a wealth of information on the physics of diking. This information has typically been obtained by measuring the timing and location of events, but this can be enriched by assessing focal mechanisms (Passarelli et al., 2014a), seismic productivity (Rubin and Gillard, 1998; Pedersen et al., 2007) or by including earthquake nucleation models in the inversion of crustal deformation data (Segall et al., 2013).

Observations from 1975–1984 rifting episode at Krafla volcano in Iceland (Einarsson and Brandsdóttir, 1978; Brandsdóttir and Einarsson, 1979) made clear that propagating dikes induce migrating seismicity, and that this seismicity can be loosely associated with the propagating tip of the dike. Migrating seismicity associated with diking has also been commonly reported on and close to stratovolcanoes — for example, by Battaglia et al. (2005) before the 1998 eruption at Piton de la Fournaise; by Patanè et al. (2002) and Aloisi et al. (2006) for the 2001 and 2002 dike intrusion at Etna, respectively; by Klein et al. (1987); Gillard et al. (1996); Rubin and Gillard (1998) and Rubin et al. (1998) for the 1983 dike at Kilauea; by Toda and Stein (2002); Uhira et al. (2005) for the 2000 intrusion at Izu islands, Japan; Baer and Hamiel (2010) for the dike event in Arrat Lunayyir, Saudi Arabia; by Dziak et al. (1995) for mid-ocean ridges; and more recently for the Manda-Harraro rifting episode by Ayele et al. (2009); Keir et al. (2009); Belachew et al. (2011).

The exceptionally long seismic phase observed in March 1998 at Piton de la Fournaise presented a clear upward migration (Fig. 5B, from Battaglia et al. (2005)). The data highlight a sudden decrease in the upward velocity at a depth of 1.5 kilometers below the surface that could be explained by a lower

density of the upper-layer host rock (Taisne and Jaupart, 2009; Maccaferri et al., 2011). According to Taisne and Jaupart (2009) the velocity variation may correspond to a factor-of-two decrease in the density difference between rock and magma. Closer to the free surface, the upward migration of the seismicity accelerates, ending with the eruption. Rivalta and Dahm (2006) attributed this to the effect of the free surface; alternatively, late degassing may decrease the magma density and induce an acceleration of the dike (Taisne and Jaupart, 2011). The analysis of the seismic crises spanning 25 years of activity at Piton de la Fournaise volcano (Roult et al., 2012) also shows that the early stage of the seismic crisis is not necessarily related to magma migration. Instead, by looking at the ratio of the seismic amplitude, Taisne et al. (2011a) show that the migration of the radiated seismic energy that is associated with the migration of the magma was delayed with respect to the onset of the seismic crisis. This observation suggest that magma migration is preceded by a phase of rupture/damage of the magma storage region.

Following the above considerations, a caveat regarding the relationship between tip migration and seismicity is appropriate. While the data hint at an equivalence between tip migration and seismicity, there is evidence that the tip is not the only, and sometimes not even the primary source of seismicity. For example, Rubin et al. (1998) evaluate the seismicity induced by the 1983 dike intrusion at Kilauea, which included a re-location of seismic sources. Most of the hypocenters collapsed onto a few tightly spaced clusters, sometimes linked to areas with high background seismicity, suggesting that pre-existing weakness and high differential stress are needed to reach failure. This is consistent with rate-state earthquake nucleation theory (Dieterich, 1994): positive Coulomb stresses are predicted to increase pre-stressing seismicity rates. Therefore, areas with high pre-diking seismic rates but low dike-induced Coulomb stresses may appear more active than areas with very high dike-induced stresses, such as the tips, if pre-diking seismicity there was very low or below the detection threshold. This highlights that for a correct interpretation of dike-induced seismicity we need both to estimate Coulomb stress changes and assess pre-existing seismic rates.

Production of seismicity can also occur on a different time scale to the migration of the dike tip. Aoki et al. (1999) noticed that the migration of seismicity for the swarm accompanying the 1997 intrusion at Izu Islands, Japan, had a time scale of 12 hours in contrast to the time scale of several days for the vertical migration of deformation. They concluded that the

migration of the seismicity does not necessarily reflect the migration of the dike; rather, the seismicity is linked to the evolution of the stress field associated to the opening of the dike and to the stress previously stored in the crust. Later, Hayashi and Morita (2003) and Morita et al. (2006) offered a contrasting view based on precisely relocated earthquakes from a 1998 swarm in the same region. They argue that the swarm seismicity actually marks the edge of the propagating dike. As of 1997, the seismic network was not good enough for an accurate assessment of the relationship between the dike trajectory and seismicity. This highlights the importance of well-designed and dense seismic networks for correctly inferring dike trajectories.

Patterns of dike-induced seismicity can have other peculiar aspects that have not yet been fully explained. For example, an advancing front of migrating epicenters (blue lines in Fig. 5A to D), often with a convex-upward trend if migration is lateral, is very often trailed by a retreating front, which delimits a spatio-temporal frame where the seismicity is active (green lines in Fig. 5A to D). While the advancing front generally has a simple shape, the retreating front sometimes shows a complex functional trend, with the distance between the two changing in time (this is true in particular for lateral injections). Sometimes, bi-directional migration of the seismicity is observed; this is probably associated with an initial bi-lateral propagation of dike (Fig. 5D), generally followed by uni-lateral propagation.

Tarasewicz et al. (2012) discuss another peculiar pattern of seismicity, associated with the 2011 eruptive phase of Eyjafjallajökull volcano, which was characterized by downward migration. They interpreted their observations in terms of a downward-migrating decompression wave that started at the top of the volcano with the removal of 200m of ice cap and progressed with the subsequent removal of magma from a series of stacked sills into the eruptive conduit and then into the atmosphere.

Additional information on the orientation and shape of the dikes and on their pressurization level can be obtained by studying the focal mechanisms of the induced earthquakes. Fault plane solutions of large induced earthquakes are often used in crustal deformation models to constrain the orientation of co-diking faulting processes (Wright et al., 2006; Pallister et al., 2010; Nobile et al., 2012). Roman et al. (2004) and Roman and Cashman (2006) observed rotations of the maximum compressive stress axis during isolated periods of time in volcanic areas and interpreted this in terms of pressurization of dike-like conduits, possibly precursor to volcanic eruptions.

Volcanic seismicity often involves large non-double-couple (non-DC) com-

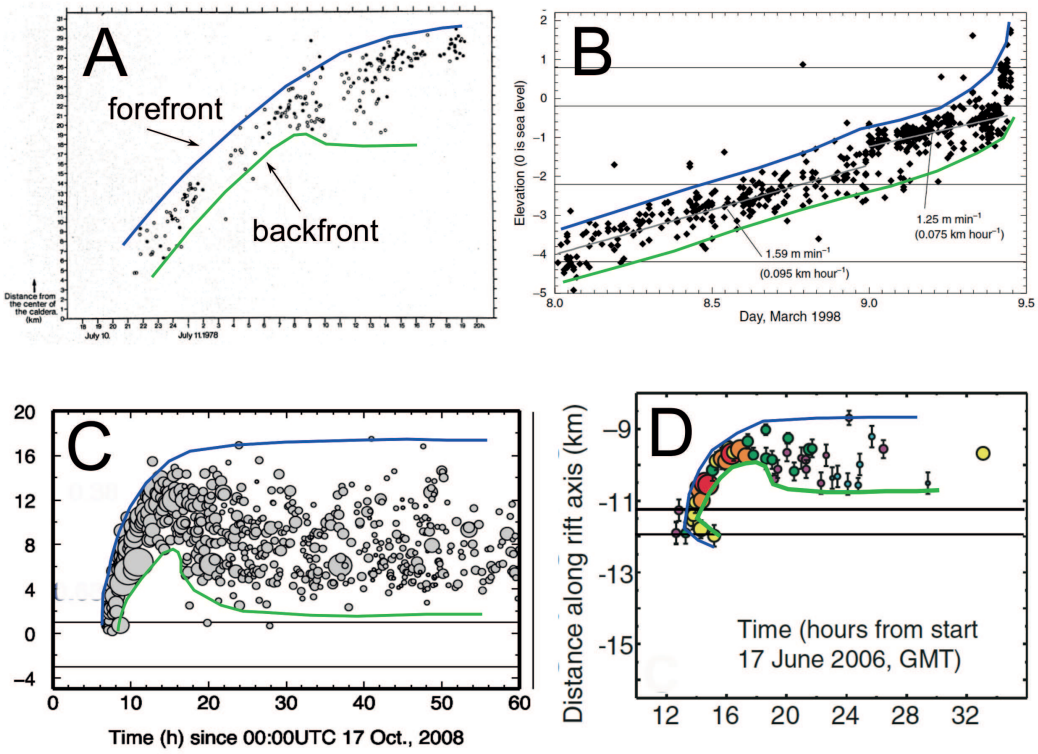

Figure 5: A) Seismicity induced by the 1978 lateral intrusion event at Krafla (Einarsson and Brandsdóttir, 1978, with permission), B) Seismicity induced by the 1998 vertical dike intrusion at Piton de la Fournaise, from Fig. 5, (Battaglia et al., 2005, with permission), C) Seismicity induced by the dike N. 11 of the rifting episode in the Manda-Harraro rift segment, Afar, Ethiopia, from Fig. 3, (Belachew et al., 2011, with permission) D) Seismicity induced by the 17 June 2006 dike of the rifting episode in the Manda-Harraro rift segment, Afar, Ethiopia, from Fig. 3, (Keir et al., 2009, with permission)

ponents, indicating faulting mechanisms deviating from pure shearing. Specifically for dikes, full stress inversions of induced seismicity returns puzzling results. Minson et al. (2007) found large non-DC components (both isotropic and CLVD) for the 2000 intrusion at Miyakejima and proposed a mixed shearing and opening mechanism of the faults. White et al. (2011) on the contrary found for the 2007–2008 dike below Mount Upptyppingar in the Kverkfjöll volcanic system (Iceland) insignificant non-DC components. In general, the origin and the significance of non-DC components in volcanic areas is still debated; independent evidence from crustal deformation and physics-based models is needed to shed light on this aspect.

3.2. Analogue laboratory experiments

Analogue laboratory experiments are an approach to understanding the kinematics and dynamics of diking that is complementary to natural observations. Although material properties differ drastically from natural systems, experimental conditions can be controlled rather precisely, and it is relatively easy to measure the three-dimensional propagation of an analogue dike in real time. Care is obviously required in scaling the experiments and in extrapolating results from analogue to natural systems, but insight gained in the laboratory can supply hypotheses and quantitative models to be tested against nature.

In order to observe fluid-filled cracks nucleating and propagating at laboratory scale, brittle solids with low stiffness, such as gelatin, need to be employed, because the absolute dimension of the fracture depends on the rigidity of the host medium (Weertman, 1971b). A sample of gelatin that is analogous of the brittle crust is obtained by dissolving gelatin powder into water and letting it set in a cold environment until it becomes a solid with Young modulus in the range of 100-50000 Pa (Takada, 1990, 1994a; Heimpel and Olson, 1994; Menand and Tait, 2002; Rivalta et al., 2005; Kavanagh et al., 2006; Di Giuseppe et al., 2009; Kavanagh et al., 2013). One of the difficulties in using gelatin as an analog material is that its rheological properties depend on the history of the cooling process. Kavanagh et al. (2013) presented a study of the rheology of gelatin. They also studied the evolution of gelatin parameters with time of curing, with the aim of defining the scaling conditions for experiments on magmatic intrusions. They conclude that to achieve appropriate geometric, kinematic, and dynamical scaling, experiments should be carried out in the temperature range 5-10°C (for the viscous component

to be negligible) and should employ gelatin concentrations in the range 2-5 wt%. Stable values of the elastic parameters are reached after about 1 or 2 days, depending on concentrations. Di Giuseppe et al. (2009) published a similar study on the use of gelatin for tectonic experiments.

Using a range of experimental techniques, fluids of different density and viscosity (for example air, water, glycerine, vegetable oils) are injected into gelatin, in a configuration that depends on scaling requirements to the natural system of interest. Air or water-filled cracks in gelatin will have a length and breadth of a few centimeters and a thickness of a few millimeters (Takada, 1990, 1994a; Heimpel and Olson, 1994). The geometry and kinetics of the developing fracture can be observed along with the response to the interaction with different external factors: rigidity layering (Rivalta et al., 2005; Kavanagh et al., 2006; Maccaferri et al., 2010), free surface (Rivalta and Dahm, 2006), density gradient (Lister and Kerr, 1991), external stress field (Watanabe et al., 2002; Acocella and Tibaldi, 2005; Kervyn et al., 2009; Menand et al., 2010; Corbi et al., 2014), dike-dike interaction (Takada, 1994a,b; Ito and Martel, 2002), dike-fault interaction (Le Corvec et al., 2013). The shape is affected significantly by the fluid viscosity. For example, a thicker tail is observed for more viscous liquids such as glycerine (Heimpel and Olson, 1994). In those cases, significant amounts of fluid mass are lost in the tail during propagation and a constant influx of fluid (or sustained pressure at the magma source) is necessary to maintain propagation (Fig. 6).

An example of an air-filled crack forming and propagating in gelatin is shown in the movie `http://www.youtube.com/watch?v=iD1h_2T75Jk` with a 5× speed-up over real time (Rivalta et al., 2013b). From a hole in the container, air is injected slowly with a syringe in solid gelatin. The resulting crack propagation is recorded with video cameras from two perpendicular perspectives (left: frontal view, right: cross-section). A crack of a few centimeters breadth and length (left), and a few mm thickness (right) opens and extends while being fed with air. Plumose lines, which show the 2D pattern of the propagating fracturing front, are visible in the movie as well. Gelatin blocks (such as this one) that are set in the refrigerators generally have hydrostatic stress conditions, so the crack picks a random vertical orientation. Here the crack develops tilted with respect to the vertical, probably due to how the injection needle was inserted. When the volume reaches a critical value (Weertman, 1971a,b), the crack begins to ascend by fracture propagation through the gelatine at the upper tip. If the viscosity of the fluid is sufficiently low, as in this case, the vast majority of the fluid can escape effi-

ciently from the crack tail and the crack pinches itself shut at the lower tip. Otherwise, some fluid volume will be retained in the elongating tail during propagation. The relatively high surface tension between water and air also helps an effective emptying of the crack's tail. Once the crack has formed in a particular orientation, it will continue on the same plane, even if the free surface is very close, as in the previous movie. This is also predicted by numerical models (Maccaferri et al., 2010); later we discuss in more detail the apparent sensitivity of the propagation direction to the initial orientation.

The aspect-ratio and the driving pressure of a crack containing a given volume of fluid may vary if the stiffness of the gelatin changes. In movie `http://www.youtube.com/watch?v=8y4U1vrk-gg` (Rivalta et al., 2013c), a layered gelatin block is composed of a stiffer layer and a more compliant layer superposed to it (gelatin of different stiffness can be obtained by using gelatin powder of different Bloom number or by varying the concentration of the same gelatin type). In this case the crack orients itself vertically, and once it reaches the critical volume of fluid, it proceeds at an approximately constant velocity until it comes close to the layer interface. There it accelerates upon crossing until it reaches a new constant velocity that persists until it accelerates again when approaching the free surface (Rivalta et al., 2005; Rivalta and Dahm, 2006). While the breadth of the fracture does not change much from one medium to another, the thickness increases, the crack shortens and the velocity increases by a factor of 20.

When the ordering of the layers is reversed, in movie `http://www.youtube.com/watch?v=MJHsl` (Rivalta et al., 2013c), the crack approaches a stiff interface. During propagation in the lower medium, an instability is visible that causes the crack tail to close in spurts rather than smoothly, as the upper tip propagates (Dahm, 2000b). When the crack approaches the interface, it decelerates and stops, because it does not carry enough volume to be overcritical also for the upper gelatin type (Rivalta et al., 2005, see also Section 4.2). With continued injections, the crack enlarges laterally until it exceeds the critical stress at the upper tip and breaks through the interface. Eventually it reaches the free surface, accelerating just before it.

Heterogeneities can disrupt the steady propagation of analogue dikes. In movie `http://www.youtube.com/watch?v=h7luTwuaG7s` (Rivalta et al., 2013a), the gelatin contains growths of fungi and gas bubbles. This gives a chance to observe what may happen when the medium has preexisting voids or fractures. Here we observe that when fluid-filled cracks propagate in non-intact gelatin, they do so in spurts, and the elastic energy is released

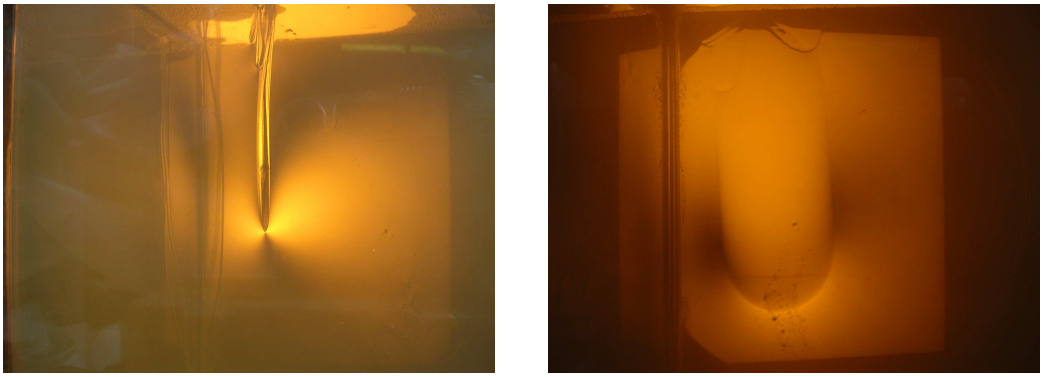

Figure 6: Stress field around a downward-propagating glycerin-filled crack in gelatin as evidenced by illuminating the tank through a polariser (left: cross-sectional view, right: frontal view).

in jerky leaps. These observations may be linked to seismicity during dike propagation: earthquakes may occur when the fluid-filled crack comes very close to preexisting fractures that concentrate stress leading to rock failure (see also Le Corvec et al., 2013).

Non-steady propagation can also result from coupling of propagation with solidification. Taisne and Tait (2011) injected, under constant volumetric flux condition, a hot, molten paraffin into a cold, brittle gelatin. They observe a step-wise mode of propagation, with duration and amplitude of each step a function of dimensionless flux and temperature. This unsteady behaviour could help to interpret the seismic burst observed during magma emplacement in cases such as Izu Peninsula, Japan (Hayashi and Morita, 2003; Morita et al., 2006) or Iceland (White et al., 2011).

4. Dike Propagation Modelling

4.1. Introduction

The field and laboratory observations of propagating dikes described in the previous section offer a basis for validation of existing numerical models or to construct new approaches. In this section, we review the technical developments from the last twenty years in modeling propagating dikes, with a particular focus on dike ascent.

Nakashima (1993) pointed out that there can be two types of fluid transport, which he labels types I and II. Type I involves the propagation of a

fluid-filled crack connected with a pressurized reservoir. The dynamic of the crack propagation is driven by the reservoir's excess pressure and the buoyancy of the fluid, either positive or negative. Type II involves the propagation of a fluid-filled crack isolated from any reservoir. This propagation is driven only by the buoyancy of the fluid confined in the crack. While useful for identifying end-member behavior, this classification itself does not address the implicit question of what are the conditions allowing a dike to become decoupled from its feeding source.

In the following, we describe two established methods or approaches that may be roughly linked to the two types of dike propagation. In the first section we describe the Weertman theory (Section 4.2) that (at least in its original formulation) addresses isolated, self-contained ascending fluid-filled cracks, driven only by buoyancy. Next, we address the lubrication theory (Section 4.3), that involves viscous flow of fluid into the ascending dike. Both approaches give rise to semi-analytical models when the geometry is simplified to 2D, taking advantage of the sheet-like shape of dikes. Both approaches are in principle extensible to more complicated geometries and three spatial dimensions, by using numerical methods. After the two approaches are discussed, we conclude with a review of current and emerging numerical methods that are applicable to either model type.

4.2. The Weertman school: buoyancy-driven magma-filled dikes

The Weertman approach for buoyancy-driven ascending dikes was first introduced by Weertman (1971a,b, 1973) to model water-filled crevasses in glaciers. Later it was applied to study magma-filled dikes at mid-ocean ridges and water-filled cracks in submerged materials. Weertman cracks are constant-volume batches of fluid propagating by breaking rock apart at their leading tip due to concentration of buoyancy-induced stresses. In Weertman models, the volume of fluid contained in the fracture is conserved during propagation by assuming that the fractures pinch themselves closed at the tail while they propagate. The dimension of the cracks must be large enough to make surface tension/surface energy effects associated with the magma unimportant, but small relative to the thickness of the crust (Weertman, 1971a). In their original formulation, Weertman fluid-filled fractures are restricted to a vertical crack plane, and are considered to be filled with an incompressible fluid; the viscous pressure drop within the fracture is alternately neglected or simplified as a constant gradient over the crack plane.

4.2.1. Formulation for static fractures

The Weertman theory predicts that if the fluid volume injected, V, is lower than a critical value V_c, the fracture will be static because there exists no configuration in which the stress intensity factor at the tips overcomes the fracture toughness of rock, K_c. If the injected volume increases, the fracture elongates. If $V = V_c$, the stress intensity factor at the upper tip (for a buoyant fracture that propagates upward), K^+, equals exactly K_c, so the fracture will tend to break apart the host material and ascend. As soon as propagation has started, the stress intensity factor at the lower tip, K^-, approaches zero; the fracture is assumed to close at the lower tip, forcing magma out of the tail when the stress intensity factor equals that for a broken medium, $K_c = 0$. The critical length of the fracture can be obtained from the two equations for the stress intensity factor at the tips of a fracture opening due to a linear pressure gradient (Secor and Pollard, 1975, e.g.):

$$K^+ = \sqrt{\pi a}\left(p_0 + \tfrac{a}{2}\,\tfrac{dp}{dz_{\mathrm{tot}}}\right) = K_c \tag{1}$$

$$K^- = \sqrt{\pi a}\left(p_0 - \tfrac{a}{2}\,\tfrac{dp}{dz_{\mathrm{tot}}}\right) = 0 \tag{2}$$

where p_0 is the overpressure at the mid-point of the fracture, a the fracture half-length and dp/dz_{tot} the total pressure gradient. For a liquid-filled fracture ascending in a hydrostatic/lithostatic stress field, $dp/dz_{\mathrm{tot}} = \Delta\rho g$, with g the acceleration due to gravity and $\Delta\rho$ the density difference between solid and liquid. If the stress field is more complicated, then the total tectonic gradient should be considered (for example, for dikes propagating longitudinally driven by topographic/tectonic gradients).

Eq. 1 gives $p_0 = a/2\, dp/dz_{\mathrm{tot}}$ and, once substituted in Eq. 1, leads to the critical length, a_c:

$$a_c = \left(\frac{K_c}{\sqrt{\pi}\frac{dp}{dz_{\mathrm{tot}}}}\right)^{2/3} \tag{3}$$

The opening of a fracture extending from $z = -a$ to $z = a$ is then given by (Weertman, 1980):

$$h(z) = \frac{(1-\nu)K_c}{2G}\sqrt{\frac{a}{\pi}}\sqrt{1-\left(\frac{z}{a}\right)^2}\left(1+\frac{z}{a}\right) \tag{4}$$

Note that Eq. 4 compares very well to air-filled fractures from laboratory experiments (see Heimpel and Olson (1994) and Dahm (2000b)), while for

liquid-filled fractures a slight modification is needed for the loss of fluid to a tail with a finite residual thickness (Heimpel and Olson, 1994).

4.2.2. Formulation for moving fractures

Nunn (1996) modified the Weertman formulation in order to take into account a simplified viscous stress drop and obtain the velocity of moving Weertman fractures. The formulation is based on the observation that for $V > V_c$ the fracture propagates, fluid flows in the direction of propagation, and a pressure drop will necessarily develop due to viscous resistance within the crack. If this viscous pressure drop is approximated as a constant gradient dp/dz_v over the whole length of the fracture, the basic formulation of the Weertman theory can be maintained. The thinner sections of the fracture (front tip and constriction to the tail) will in reality experience a higher viscous pressure drop, but a constant gradient is considered a good approximation over most of the crack plane, as shown in Taisne and Jaupart (2009), Fig. 7, Fig. 11 and Fig. 17, in Dahm (2000b), Fig. 6 and in Roper and Lister (2007), Fig. 2. The total pressure gradient can be separated into an external, static contribution, $\frac{dp}{dz}_{ext}$, and a dynamic contribution due to viscous motion:

$$\frac{dp}{dz}_{\mathrm{tot}} = \frac{dp}{dz}_{stat} - \frac{dp}{dz}_{v} \tag{5}$$

The propagating fracture in this model will be longer than a critical static fracture. In other words, if the viscous pressure drop is taken into account, the initial length of fracture that is required to attain a propagating state is larger than the critical length a_c by a finite amount ($\frac{dp}{dz}_{tot}$ is in the denominator of Eq. 3).

For example, for a dike ascending vertically in a lithostatic stress field (Nakashima, 1993; Nunn, 1996; Dahm, 2000b):

$$\frac{dp}{dz}_{v} = \frac{dp}{dz}_{stat} - \frac{dp}{dz}_{\mathrm{tot}} = \Delta\rho g - \frac{K_c}{a\sqrt{\pi a}} \tag{6}$$

Viscous resistance within the narrow fracture means flow of fluid to the crack tip is relatively slow, which limits the rate of fracture propagation. It is then appropriate to assume that the stress intensity factor at the propagating tip K is approximately equal to the critical value of that parameter, K_c.

Assuming laminar Poiseuille flow within the fracture, the pressure gradient associated with viscous resistance will be proportional to the mean

magma speed, v, the viscosity, μ, and inversely proportional to the square of the half-opening, h:

$$\frac{dp}{dz}_v = \frac{3\mu v}{h^2} \tag{7}$$

So, for a given volume of injection, a given fracture toughness and a given external, static gradient, the model predicts the propagation speed of the dike. The assumption of a simple Poiseuille flow is likely a significant over-simplification and has been argued to lead to speed predictions that are too large (Dahm, 2000b).

4.2.3. Recent extensions

The Weertman theory has been extended recently to include the effects of a free surface. Rivalta and Dahm (2006) observed air-filled cracks in gelatine experiments accelerated as they approached the free surface. To explain this they invoked a change associated with the free surface in the stress intensity factor at the upper tip of the fractures (Pollard and Holzhausen, 1979). Equivalently, this can be understood as the decreasing resistance to fracture opposed by the medium with the dike approaching the free surface, which makes the medium appear effectively weaker.

Rivalta and Dahm (2006) derived an approach incorporating into the formulation dynamic changes in the stress intensity factor (Nakashima, 1993; Nunn, 1996). The resulting modification of the Weertman theory was applied to explain the acceleration of the seismicity towards the free surface documented by Battaglia et al. (2005) for Piton de la Fournaise. By observing that the effect of the free surface should scale with the distance of the dike tip to the surface, Rivalta and Dahm (2006) also formulated an approach for inverting dike lengths on the basis of the hypocentral locations of the induced seismicity.

Dahm et al. (2010) extended the Weertman theory to model the bilateral migration of hypocenters sometimes observed in seismic data from hydraulic fracturing. Upon injections of fluids at high pressure, the induced seismicity is often found to migrate bilaterally at first, and then the migration continues in just one direction. They explain this with the presence of an external (i.e. tectonic) stress field driving the growth in competition with the injection pressure. Dahm et al. (2010) divide the growth process into four stages (Fig. 4.2.3):

1. Injection phase, when the excess pressure at the injection source is dominating, and therefore driving the growth. Generally the two tips of

the hydrofracture advance in opposite directions with different speeds. This phase ends when injection is stopped.

2. Post-injection phase during bidirectional growth, when the flow from the injection has dropped to zero. Now the external pressure gradient (due to buoyancy or of tectonic origin) takes over in driving the fracture into one particular direction, and the fracture must adjust to a new pressure balance by redistributing the volume of fluid it contains. The seismicity continues to propagate in two opposite directions for some time. This phase ends when, as evidenced by the migrating seismicity, the slower tip stops propagating.
3. Post-injection phase with unidirectional growth, when the fracture continues to elongate in one direction while it is still adjusting to the new pressure balance on the crack plane. This phase ends when the fracture toughness at the back tip becomes zero (the hydrofracture cannot elongate anymore and starts to close at the tail). The elongation of the fracture is now maximal.
4. The final phase, when the fracture has now become a Weertman-Nunn fracture. In this phase it is driven only by buoyancy or by tectonic stress. It is propagating as an isolated batch of fluid. This propagation will be very slow and can last for long periods of time.

Dahm et al. (2010) model the Coulomb stress change during propagation and show that such a model can explain not only the advancing front of the migrating seismicity, but also the retreating front (see Fig. 5), because after the passage of the propagating tip, rock volumes might fall under a stress shadow (a negative Coulomb Stress inhibiting seismicity) and therefore experience a sudden drop in seismic rate.

Non-symmetric growth, described by the model of Dahm et al. (2010), is consistent with other field (e.g. Maxwell et al., 2002; Reynolds et al., 2012) and microseismic (e.g. Fisher et al., 2004; Daniels et al., 2007; Walker et al., 2012; Reynolds et al., 2012) observations of hydraulic fractures. This model of successive phases may be applied with minor changes to explain the pattern of seismicity induced by a dike propagating from a magma chamber. For example, an initial bilateral migration of the seismicity was observed for several laterally propagating dikes during the Krafla and Manda Hararo rifting episodes (Keir et al. (2009); Wright et al. (2012), Fig. 5D). Tectonic stress taking over after the pressure gradient from the magma chamber has dropped to zero may then be the cause for the bilateral propagation of seis-

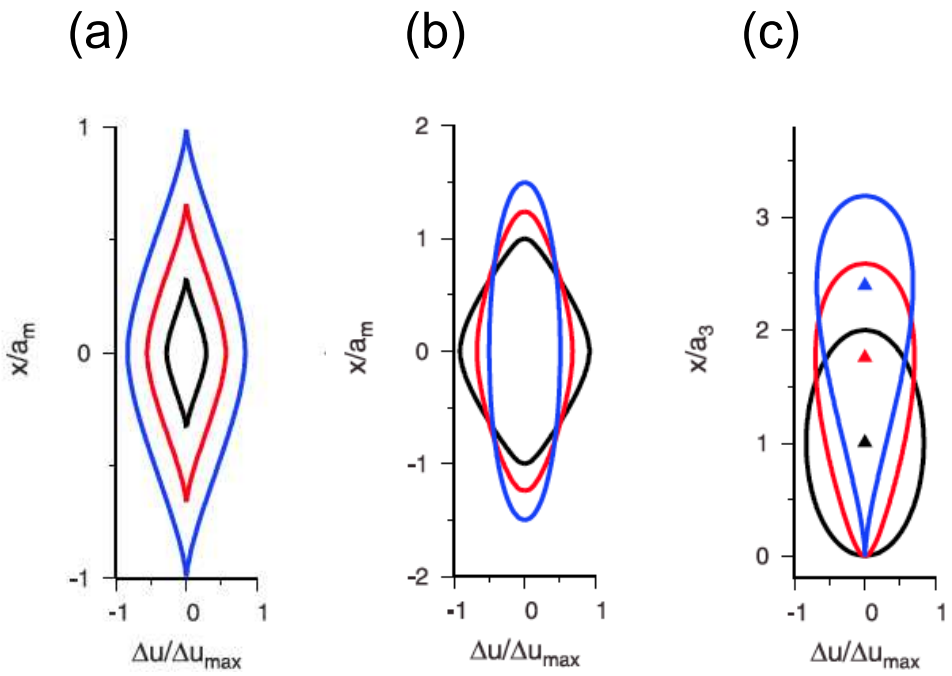

Figure 7: a) Injection phase: the fracture propagates bilaterally. The volume grows and the fracture elongates and propagates driven by the injection pressure. Here, the external (tectonic) gradient is zero. b) Bilateral post-injection propagation. The volume is now fixed. The stress intensity factor at the tips still overcomes the fracture toughness of the host rock and the fracture continues to elongate. c) Unilateral post-injection phase and solitary ascent phase: the fracture continues to elongate driven by its overpressure, until it becomes a Weertman fracture, driven only by buoyancy or by the tectonic gradient. From Dahm et al. (2010), with permission.

micity. Also, the discrimination of phases in the intrusion process might be relevant for dikes too: dikes are generally injected by a pressurized magma chamber.

4.2.4. Strengths and limitations

The Weertman model is a simple approach, and this represents both a strength and a limitation. The main advantage is that by neglecting or simplifying to a constant gradient the pressure gradient (and hence also the fluid flow within the dike), a large part of the analytical or numerical difficulties are avoided. This facilitates the inclusion and study of effects that are otherwise prohibitive (Sect. 5).

However, Lister and Kerr (1991) raise a number of issues regarding the

validity of the assumptions on which Weertman models are based.

1. They note that the model, in its original formulation, is inherently unstable: fractures are assumed to be exactly $a = a_c$ long so that $K^+ = K_c$, but as soon as they propagate they will be in fact longer ($a > a_c$). As described above (Sec. 4.2.2), this important point has been addressed by Nunn (1996), who introduced a constant viscous pressure gradient over the crack plane, making it possible to model supercritical, moving fractures and at the same time maintain the simple formulation.
2. They mention that for K_c of the order of 1 $\mathrm{MPa\,m^{1/2}}$, as in laboratory measurements, the resistance to fracture is negligible with respect to other contributions and it is unlikely that the size of propagating dikes is determined by the fracture toughness of rock. This point is very important and we discuss it at length in Sec. 4.4.2, where we show that there is evidence for field-based, effective fracture toughness measurements in the order $K_c^{\mathrm{eff}} \approx 100\,\mathrm{MPa\,m^{1/2}}$ or more. If such values are appropriate, fracture toughness is not negligible and becomes an important factor controlling dike size (Sec. 4.4.1). If we employ $K_c^{\mathrm{eff}} \approx 100\,\mathrm{MPa\,m^{1/2}}$ and keep the other parameters unchanged in the dike length and thickness estimate by (Lister and Kerr, 1991, p. 10055, Eq. 14a and 14b), we obtain a length in the order of 2 km and thickness 0.5 m instead of 100 m and 2 mm, respectively.
3. They stress that critically-long dikes ($a = a_c$) are very short and thin, and would freeze in a short time interval. This problem is solved by introducing higher values for effective fracture toughness, which will imply longer and thicker critical fractures (see point 2 above) and a constant pressure gradient as in Nunn (1996), because this also allows for longer fractures (point 1 above). However, the criticism that Weertman fractures need to move relatively fast in cold rock (shallow crust) for the approach to be valid still holds in general.
4. They point out that for dikes to pinch themselves closed at the trailing front, the viscosity of the fluid should theoretically vanish. This crude assumption may be justified only for low-viscosity magmas (we discuss this point in detail in Sect. 4.4.3). There is evidence that pure Weertman models work very well for low-viscosity fluids, and almost perfectly for gases. For example, they match observations of propagation of air-filled cracks in gelatin extremely well (Dahm, 2000b). This occurs because: a) the less viscous the fluid, the thinner the tail of the

crack, and the better the approximation of a constant volume ascent, b) the less viscous the fluid, the better is the approximation of negligible viscous stresses, c) air is a hydrophobic fluid and surface tension effects assist emptying the crack tail effectively.

No experiment or numerical model has addressed the issue of incorporating surface-tension effects as a modification to the effects of viscosity. A discussion of generalised trailing-front dynamics, based on numerical modeling, is included by Dahm (2000b).

The approximation of a vanishing fracture toughness at the trailing tip is also somewhat crude: stress concentrations at the trailing tip of the dike (the inlet from the tail) are visible, for example, from photoelastic images; see figure 3.9 of Tait and Taisne (2013).

Finally, Weertman models are 2D (as most models of dike propagation). This has to be kept in mind, especially when the conditions in the host medium change. For example, laboratory experiments with gelatin show that for density layering, fracture toughness or volume variations of the fracture, the breadth of the fracture might change with time.

4.3. The lubrication-theory school: dynamics controlled by magma flow

Simplifying the role of viscosity as in the Weertman approach (Weertman, 1971a,b) (Sect. 4.2) might not be an appropriate simplification of cases where viscosity is large. A better treatment of hydraulic fracturing in the oil and gas industry motivated the development of a theory for coupling elastic fracturing and fracture-hosted fluid flow (Khristianovic and Zheltov, 1955; Perkins and Kern, 1961; Barenblatt, 1962; Geertsma and de Klerk, 1969; Nordgren, 1972; Spence and Sharp, 1985). The flow model was simplified using the lubrication approximation, which is appropriate for a flow with an aspect ratio much greater than unity in the direction of flow. Building on this literature, Spence et al. (1987) modelled the effect of viscous flow on a buoyancy-driven dike in 2D, assuming a steady state regime of propagation. Their model considered only one particular value for the ratio of fracture toughness to fluid viscosity. A generalization for relatively small fracture toughness was carried out by Lister (1990b,a) and the theory was fully generalized by Roper and Lister (2007). Even in these more recent papers, a stationary solution is obtained for physical properties that are constant in time and space; in other words, these models neglect variations of the fluid injection and of stratification of the host rock. These limitations are ad-

dress by Taisne and Jaupart (2009) and Taisne and Jaupart (2011) who develop a semi-implicit numerical scheme that allows for the study of spatial and temporal changes of host-rock and/or magma properties. Furthermore, most of the theoretical papers cited above focus on incompressible magma (Spence et al., 1987; Lister, 1991; Lister and Kerr, 1991; Roper and Lister, 2007; Taisne and Jaupart, 2009). Only a few of them consider a pressure-dependent density for the magma or the presence of a gas precursor (Lister, 1990b; Taisne and Jaupart, 2011; Maimon et al., 2012), this will be detailed in Section 5.15. We discuss some results and future directions regarding magma properties including compressibility and phase transitions in Sects. 4.4.3, 5.10 and 5.15.

4.3.1. Model formulation: Magma Flow

The theory as formulated by (e.g. Lister, 1990a) begins by expressing the magma pressure P as

$$P = P_{\text{Lith}} + P_e \,, \tag{8}$$

where P_{Lith} is the lithostatic pressure, and P_e is the over-pressure that drives deformation of the fracture walls. For small Reynolds numbers, the flow of a viscous fluid within a thin fracture is laminar and one can use lubrication theory (Batchelor, 2000); in that case the Navier-Stokes equations reduce to

$$0 = -\frac{\partial P}{\partial z} + \mu \frac{\partial^2 w}{\partial x^2} - \rho_m g \,, \tag{9}$$

where w is the vertical velocity profile of the magma within the dike (see Fig. 8c), ρ_m and μ the magma density and viscosity.

Solution to Eq. (9) follows by first noting that the volume flux ϕ of magma at depth z is given by

$$\phi(z) = \int_{-h}^{h} w(z,x) dx, \tag{10}$$

where the dike width is $2h$. Combination of equations 9 and 10 leads to:

$$\phi = -\frac{2}{3\mu} h^3 \left(\frac{\partial P}{\partial z} + \rho_m g \right). \tag{11}$$

Finally, substituting for P into the flux equation (11), we obtain the Poiseuille equation

$$\phi = -\frac{2}{3\mu} h^3 \left(\frac{\partial P_e}{\partial z} - \Delta\rho g \right), \tag{12}$$

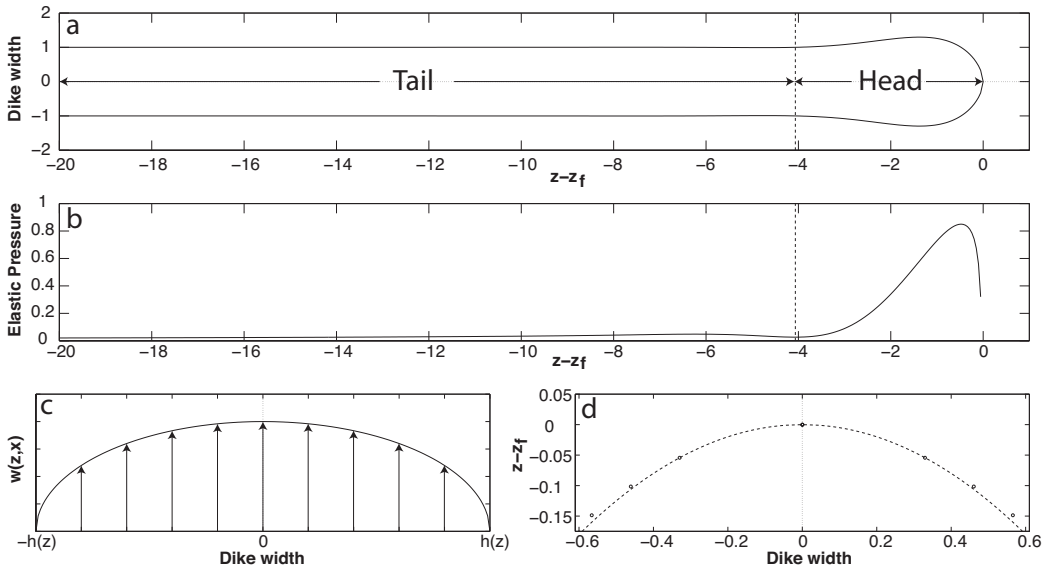

Figure 8: Panels a and b: typical dimensionless width and elastic pressure profile within a propagating dike. Panel c: arbitrary velocity profile for a laminar viscous flow used in equation 10. Panel d: Cross-section of the tip of the dike. The condition defined by Eq. 20 is respected (dashed line shows Eq. 20, and the dots the output of the numerical simulation). Dike width, depth and pressure have been normalized using scaling argument leading to equations 22, 24 and 25.

where $\Delta\rho = \rho_s - \rho_m$ is the magma buoyancy.

The formulation of the fluid flow equations is completed by enforcing mass conservation according to the equation

$$2\frac{\partial \rho_m h}{\partial t} = -\frac{\partial \rho_m \phi}{\partial z}. \tag{13}$$

When limiting consideration to an incompressible fluid filling the crack, Eq. 13 reduces to volume conservation

$$2\frac{\partial h}{\partial t} = -\frac{\partial \phi}{\partial z}. \tag{14}$$

4.3.2. Elastic Deformation

For a dike extending from a distant source ($z \to -\infty$) to a tip located at $z = z_f$, half-width h and overpressure P_e are related to one another through the following equation (Muskhelishvili, 1953; Weertman, 1971a):

$$P_e(z) = -\frac{G}{1-\nu}\frac{1}{\pi}\int_{-\infty}^{z_f}\frac{\partial h}{\partial \xi}\frac{d\xi}{\xi - z}, \tag{15}$$

where G is the shear modulus and ν is Poisson's ratio. One can invert this equation to solve for the dike width as a function of P_e. Integrating by parts leads to the following equation for h (Spence et al., 1987):

$$h(z) = \frac{1-\nu}{G}\frac{1}{\pi}\int_{-\infty}^{z_f} k(z_f, z, \xi) P_e(\xi) d\xi, \tag{16}$$

where kernel $k(z_f, z, \xi)$ is such that:

$$k(z_f, z, \xi) = \ln\left|\frac{\sqrt{z_f - z} + \sqrt{z_f - \xi}}{\sqrt{z_f - z} - \sqrt{z_f - \xi}}\right|. \tag{17}$$

4.3.3. Propagation Condition

The shape of the dike's tip is imposed in the region where $z \to z_f$ to ensure that sufficient energy is available to fracture rock. It is also possible to employ this known asymptotic solution to regularize the pressure near the tip in computational algorithms. Just ahead of the dike tip, the singularity is expressed as

$$P_e(z) \sim -\frac{K}{2\sqrt{z - z_f}} \text{ for } z > z_f\,, \tag{18}$$

where K is the stress intensity factor. In the case of a propagating dike, the stress intensity factor, K, is equal to the fracture toughness, K_c, implying that the shape of the dike near the tip (Fig. 8), is defined as (Muskhelishvili, 1953; Weertman, 1971a):

$$h \sim \frac{1-\nu}{G} K_c \sqrt{2(z_f - z)} \ \text{, for } z \to z_f \,. \tag{19}$$

Combining equations (16-19) leads to the following boundary condition for the dike tip (Lister, 1990a):

$$K_c \sqrt{2} = \frac{2}{\pi} \int_{-\infty}^{z_f} \frac{P_e(\xi)}{\sqrt{z_f - \xi}} d\xi. \tag{20}$$

4.3.4. Boundary Conditions

The system of equations requires three boundary conditions. Firstly, a steady state solution is made possible by assuming that magma is injected at a constant rate Q at $z \to -\infty$. Secondly, the near-tip region is assumed to be filled with vapor and so the pressure at the fluid front is equal to the saturated vapor pressure for the magma. Finally we have the asymtotic solution for h at the leading edge of the dike defined in eq. 19.

Note that the analytical results derived by Lister (1990a) are possible only provided the steady state solution associated with a constant-flux condition at the dike source. However, this assumption is neither necessary in a general sense nor is it universally valid. Alternately, a time-dependent input flux can be introduced with a semi-implicit method used by Taisne and Jaupart (2009, 2011) by appropriately modifying the mass conservation equation

$$\int_{z_1}^{z_f^{t+1}} (\rho_m h)^{t+1}(\xi)\ d\xi = \frac{Q^{t+1} + Q^t}{2} \Delta t + \int_{z_1}^{z_f^t} (\rho_m h)^t(\xi)\ d\xi \ , \tag{21}$$

with Q describing the mass flux at the source. This enables modelling of the temporal evolution of an injection of a constant mass of magma, assuming $Q = 0$.

4.3.5. Strengths and Limitations

The main strength of lubrication theory model is the accuracy of the solution of the viscous motion within the dike and, with it, the accuracy of predictions regarding the velocity of the dike (which is a central problem in magma propagation) and the shape of the dike. The weaknesses are related to

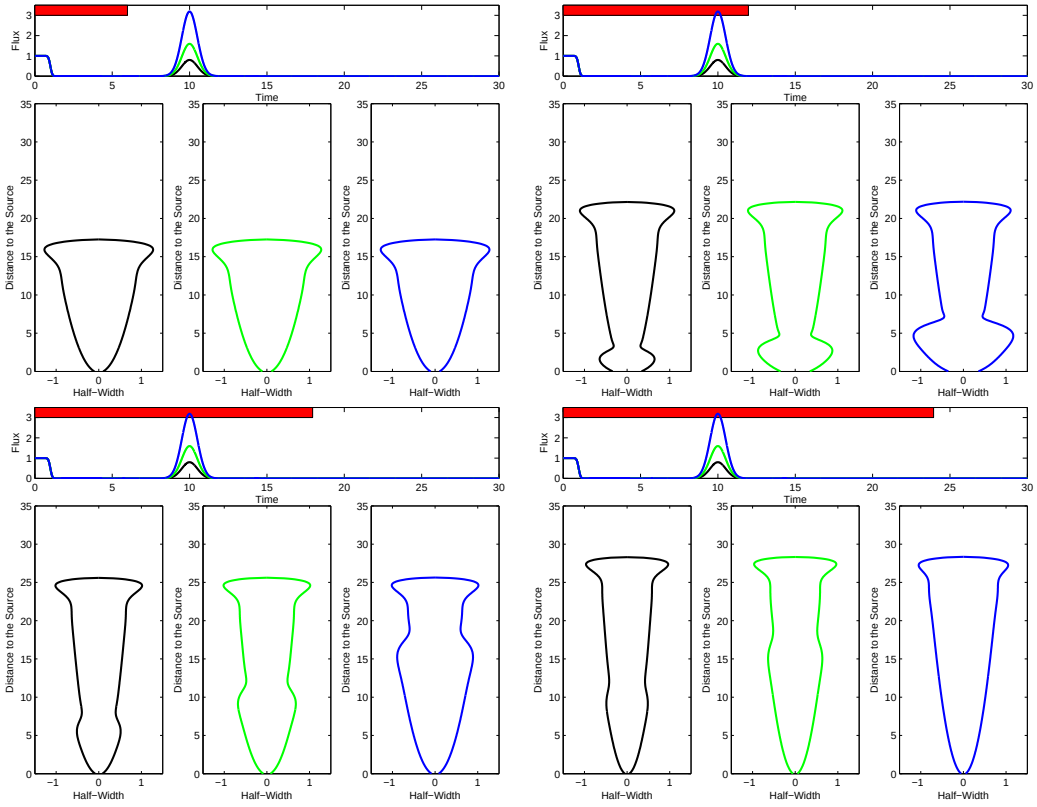

Figure 9: Example of variation of the flux at the source. Four snapshots showing the time evolution of a dike subject to a pulse of magma being injected at the source, the normalized volume of the pulses are 1, 2 and 4, respectively, for black, green and blue curves. The top curve represents the normalized flux at the source, the red bar represent the time at which the profiles are drawn.

1. The difficulty of including external influences such as inhomogeneous stress fields. This could be included in the future through the use of an apparent buoyancy.
2. In order to resolve the dynamic of dike propagation much effort has been done on the 2D problem, neglecting the 3D effect. This introduces large epistemic uncertainties: it is difficult to know what would change in the results if the fluid could also flow along the third dimension. From a mathematical point of view, any change in the third dimension will drastically impact the dynamic obtain in 2D, since the 2D flux is derived from the 3D flux divided by b.
3. Available lubrication theory models do not provide information on potential change in the direction of propagation, but assume either purely vertical or purely horizontal propagation.

4.4. Critical analysis of the two approaches

The approaches described in Sections 4.2 and 4.3 were seen for some time as being in conflict with each other. The conflict can ultimately be cast as a debate about the importance of viscous resistance to flow of the magma versus fracture toughness of the hostrock. To help guide the choice of the most appropriate model for a specific application, we next compare Weertman and lubrication theory models through dimensional analysis, review laboratory and field measurements of rock fracture toughness, and discuss the appropriateness of common assumptions and individual dike propagation models.

4.4.1. Dimensional Analysis

As shown by Lister (1990a) and Lister and Kerr (1991), a simple method to evaluate dike behavior is to consider the main force balance in the tail and nose regions (see Fig. 8a). In both regions, the driving force is magma buoyancy and one must determine the dominant resistance to propagation. There are two relevant sources of resistance, or dissipation, in the system: 1) viscous flow of the magma, and 2) fracture of the rock. We may thus consider two different force balances in the nose, depending on the dominant resistance to propagation. The characteristic dimensions of the system are the scales for the half-width of the dike tail, h, and for the length of the dike head, L.

In the case where viscous dissipation is dominant, h^* is derived by balancing buoyancy and viscous pressure drop (elastic overpressure can be neglected

in the tail region, Fig. 8b) leading to (Lister and Kerr, 1991):

$$h^* = \left(\frac{3\mu Q}{2\Delta\rho g}\right)^{1/3}, \tag{22}$$

where Q represents the 2D volumetric flux of magma injected into the propagating dike. Combination of Q and h^* defines the velocity scale

$$c^* = \frac{Q}{2h^*}. \tag{23}$$

L^* is derived from the balance between the driving force from buoyancy and viscous resistance to flow (which is coupled with elastic deformation of the rock). This leads to

$$L^* = \left[\frac{Gh^*}{(1-\nu)\Delta\rho g}\right]^{1/2} = \left(\frac{3\mu Q}{2\Delta\rho^4 g^4}\right)^{1/6}\left(\frac{G}{1-\nu}\right)^{1/2}. \tag{24}$$

Finally the pressure scale is defined as

$$P^* = \Delta\rho g L^* = \left(\frac{G}{1-\nu}\right)^{1/2}\left(\frac{3Q\mu\Delta\rho^2 g^2}{2}\right)^{1/6}. \tag{25}$$

If fracture is the limiting process, the fluid does not provide any resistance to closure in the tail region and hence according to Eq. 22, which describes the balance of force in the tail region regardless of the relative importance of the toughness, the thickness of the tail goes to zero when viscosity and/or influx goes to zero. Balancing the driving force of magma buoyancy with resistance to fracturing defines a scaling length for the head of the dike, L_f, such that:

$$K_c = \Delta P\sqrt{L_f} = \Delta\rho g L_f^{3/2}, \tag{26}$$

where K_c is the toughness and ΔP is the magma overpressure in the nose. Solving for L_f, we find that:

$$L_f = \left(\frac{K_c}{\Delta\rho g}\right)^{2/3}. \tag{27}$$

Comparison with Eq. 3 confirms that this approach recovers the Weertman solution. It is also apparent that there is no means by which to estimate

velocity of the dike. By using Eqs. 25 and 27, the pressure scale can be expressed as

$$P_f = \left(\Delta\rho g K_c^2\right)^{1/3}. \tag{28}$$

The ratio between the two different length-scales or, equivalently, the ratio between the two pressure scales quantifies the relative importance of viscous flow versus rock fracture. It is therefore useful as a proxy for the regime of dike propagation. This ratio is given by:

$$\frac{P_f}{P^*} = \frac{L_f}{L^*} = \left(\frac{2}{3}\right)^{1/6} \left(\frac{(1-\nu)^3 K_c^4}{G^3 Q \mu}\right)^{1/6}. \tag{29}$$

This can also be written as a function of a dimensionless toughness ratio such that:

$$\frac{L_f}{L^*} = \left(\frac{K_c}{K^*}\right)^{2/3}, \tag{30}$$

where K^* is a toughness scale associated with viscous flow requirements. Combining Eqs. 29 and 30 lead to:

$$K^* = \Delta\rho g (L^*)^{3/2} = \left(\frac{G^3}{(1-\nu)^3}\frac{3\mu Q}{2}\right)^{1/4}. \tag{31}$$

This toughness scale does not depend on the buoyancy of magma.

The dominant resistance to propagation dictates the magnitude of the buoyancy force in the nose region and hence the length of that region. In turn, this sets the relevant length-scale for the equations of motion. If $L_f/L^* \gg 1$, or if $K_c/K^* \gg 1$, corresponding to large rock toughness, then viscous dissipation is not limiting and hence sufficient buoyancy-induced driving force must be accumulated over the length L_f to overcome the resistance to fracture. In this case, the proper length-scale is L_f. In the other limit, for $L_f/L^* \ll 1$, or $K_c/K^* \ll 1$, it is the elastic opening of the fracture that requires the largest stresses, and one should scaling lengths with L^*. Roper and Lister (2007) have demonstrated that for $K_c/K^* < 2$ the length of the nose region scales with the viscous length-scale, L^*, and its width is comparable to h^* (see Fig. 8a in which $K_c/K^* = 1$). As shown in Fig. 2 of Roper and Lister (2007), the nose extends over a length of $\approx 4L^*$ in this regime, independent of the toughness ratio and hence independent of the fracture toughness of encasing rocks. For $K_c/K^* \gtrsim 2$, the length of the nose region is much larger, as expected. The asymptotic limit such that the nose length scales with L_f

is reached for $K_c/K^* \gtrsim 8$. In this limit, the width of the nose region deviates markedly from that of the tail, as shown in Fig. 3 of Roper and Lister (2007).

In both cases, the tail region is in the same dynamical regime characterized by a balance between buoyancy and viscous forces, which emphasizes the fundamental role played by the nose region. Hence, there arises a second criterion for the validity of the constant-volume, zero-viscosity Weertman model. This criterion requires that the volume of residual fluid in the tail must be small relative to the volume of fluid in the head of the dike. By using Eq. 22 for the half-width of the viscous-dominated dike tail, and Eqs. 3 and 4 to obtain the volume of a Wertmann crack, we obtain:

$$L_t \ll \left(\frac{(1-\nu)^3 K_c^6}{G^3 Q \mu \Delta\rho^2 g^2} \right)^{1/3}, \tag{32}$$

where L_t is the length of the tail, i.e. the difference between the depth of the head region and the depth of the magma source.

In summary, the lubrication model under the zero-toughness assumption is valid for $L_f/L^* \ll 1$. On the other hand, the Weertman model applies for $L_f/L^* \gg 1$ as long as the dike tail (which is not formally treated within the Weertman model) satisfies Eq. 32. The case $L_f/L^* \gg 1$ with Eq. 32 not satisfied, i.e. a K_c-dominated dike with decreasing volume, is not covered by the classic Weertman theory but needs a taylored approach. The applicability of the individual models is therefore closely linked to the value of the rock fracture toughness, as discussed in the next section.

4.4.2. Fracture Toughness and Dike Propagation Regime

There is a long debate in the literature regarding estimates of rock fracture toughness relevant for km-sized dikes. In theory, the fracture toughness is a material property and should not vary with crack dimensions. However, non-elastic processes at the crack tip such as plastic deformation or microcracking are not necessarily invariant with respect to fracture size; in fact there is ample evidence to the contrary. The question is not whether the toughness depends on fracture size but rather how to translate the dependence into estimates of toughness at the scale of dikes and other large structures.

In laboratory studies, K_c for rocks is typically of the order of 1 MPa $m^{1/2}$ (Atkinson, 1984; Atkinson and Meredith, 1987). For example, Balme et al. (2004) measured the fracture toughness of basalt samples from Iceland, Vesuvius and Etna at up to 600° temperature and 30 MPa pressure, obtaining

values from 1.4 to 3.8 MPa $m^{1/2}$. They observe an influence of both pressure and temperature on K_c but values remain in the same order of magnitude at the scale of the experiments. However, even at laboratory scale, the size of the initial notch or ligament size has been empirically shown to give a power-law variation of K_c, supporting the idea of a size effect on the fracture toughness (e.g. Carpinteri, 1994; Shlyapobersky et al., 1998). These observations have inspired a number of theoretical treatments based on the statistical mechanics of crack propagation in disordered media and/or on the interaction of the near-tip stresses with the plastic zone ahead of the crack tip (e.g. Borodich, 1999; Bažant, 1997; Dyskin, 1997), but without direct experimental evidence at very large scale, even the theoretical treatments are difficult to trust as tools for extrapolation.

One important line of research for resolving this issue is based on detailed observations of dikes in the field. Klein et al. (1987) observed that areas along Kilauea's East Rift where seismicity is persistent appear to act as barriers for propagation. Rubin et al. (1998) remarked that in general the seismicity induced by dikes constitutes a sink of inelastic energy: it provides evidence of a release of fracture energy beyond what needed to create new surface for the propagating dike alone. Given that K_c is related to strain energy through the relation:

$$K_c^2 = 2\frac{G}{1-\nu}\frac{\Delta E}{\delta l}, \tag{33}$$

where ΔE is the variation of strain energy for an incremental fracture extension δl, any dissipation of elastic energy will be mirrored into an effective (also called apparent) value of K_c, K_c^{eff}. Slip on pre-existing fractures, and the correspondent energy release during propagation, scale with the dimension of the dike supporting the hypothesis of a fracture-size scaling of fracture toughness.

A variety of other work has considered the relation between the dimension of cracks and fracture toughness. Field studies (for example Delaney and Pollard, 1981; Delaney et al., 1986; Pollard, 1987; Vermilye and Scholz, 1995) have shown that the size of the tip process zone scales with the dimension of the crack (Heimpel and Olson, 1994). Olson (2003) studied the scaling relationship between fracture opening and length of three sets of fractures from Vermilye and Scholz (1995) and Delaney and Pollard (1981) and conclude that for those data sets, the fracture aperture scales with the squared length of the fractures. By assuming that the growth of those fractures was controlled by the fracture toughness of the medium, Olson (2003) calculates the

relevant "in-situ" K_c^{eff} and finds values in the range 8 to 25 MPa $m^{1/2}$ for fractures between 2 cm and 20 m length, and 40–4000 MPa $m^{1/2}$ for 100 meter-scale dike segments around the Ship Rock volcanic plug in NW New Mexico (Delaney and Pollard, 1981).

K_c^{eff} can also be estimated using inverse methods and associated numerical models. Jin and Johnson (2008) developed a model for the propagation of multiple parallel dikes. The model incorporates viscous flow within the dike and solves the resulting non-linear (integral) equation through a perturbative approach. They assume constant dike velocities of the order of 0.01 – 0.1 m/s and an overpressure of about 3 MPa, and obtain compatible stress intensity factors of about 100 to 200 MPa $m^{1/2}$. Rivalta and Dahm (2006) also found a value of about 100 MPa $m^{1/2}$ by considering the effects of the free surface on the migration of hypocenters for an ascending dike. Similarly, Bunger and Cruden (2011) found that K_c in the range of 500–1300 MPa $m^{1/2}$ provides the best match between a model of laccolith emplacement and aspect ratio data. A possible scale-dependance of K_c^{eff} has never been taken into account in any model so far.

These values of K_c exceed laboratory values by as much as 3 orders of magnitude and the scaling they imply between K_c and the dike length remains a matter of discussion (Scholtz, 2010; Olson and Schultz, 2011). The data is probably too limited to resolve these debates at present. There is also a lack of fracture toughness data at confining pressures relevant for dikes (mid to shallow crustal levels). Most measurements (Balme et al., 2004; Schmidt and Huddle, 1977) have been carried out at confining pressures relevant for the upper crustal layers (<3 km depth) and there is poor constraint on the influence of the confining pressure on K_c, when the effect is probably significant (Rubin, 1993c), in particular when combined with the effect of increased temperature (Funatsu et al., 2004). Furthermore, all of these discussions, including the present one, must bear in mind that field measurements are made on solidified structures that do not necessarily reflect dynamics of the dike during the propagation phase. This will influence the value estimated for K_c^{eff} since these measurements may overestimate the ratio of the thickness to the length, especially if there was additional inflation following the arrest of the dike tip.

What is clear, though, is that the issue is central to appropriately modeling dike growth. If we focus on dykes driven by basaltic magmas, we can take typical values of the relevant physical properties and control variables as $\mu = 10^2$ Pa s and $Q = 2$ $m^3 s^{-1} m^{-1}$ (Thordarson and Self, 1993). As-

suming a reasonable value of $G \approx 10^{10}$ Pa and $\nu = 0.25$ for the rock, we find that the toughness scale coming from viscous dissipation (Eq. 31 and Lister (1990a)) lead to $K^* \approx 160$ MPa m$^{1/2}$. One should note that this estimate does not depend on magma buoyancy at all and is weakly sensitive to the various inputs because of the small power-law exponent involved. Therefore, for lower-end viscosity magmas such as Kimberlite (0.1 Pa s), it only decreases sightly to $K^* \approx 30$ MPa m$^{1/2}$ and for lower magma fluxes ≈ 0.02 m^{3}s^{-1}m^{-1} (appropriate for Piton de la Fournaise volcano on Réunion Island, (Traversa et al., 2010)) it decreases to $K^* \approx 50$ MPa m$^{1/2}$. We therefore conclude that if $K_c^{eff} \lesssim O(100)$ MPa m$^{1/2}$ at the scale of dikes, then the zero toughness lubrication model is valid, while the Weertman model would be more appropriate from $K_c^{eff} \sim O(1000)$ MPa m$^{1/2}$.

In general, Weertman and lubrication theory models in their original formulation (no viscous flow and zero fracture toughness, respectively) are therefore end-member models for dike propagation: 1) Viscous magma flows slowly into the dike and the dike tip does not propagate a very long distance from the chamber ($\lesssim 1$ km, so that the effective fracture toughness should not significantly exceed 100 MPa m$^{1/2}$). These dikes may best modeled with the lubrication theory approach. 2) Magma viscosity is very low (see for example long carbonatite or kimberlite-filled dikes in the range 5 to 10 km long and for which viscosity is in the range 0.1 to 1 Pa·s, Sparks et al. (2006)), with magma-filled pockets detaching effectively from the magma reservoir where they originated and traveling long distances (even through 200 km thick cratons) in a few hours or days (as demonstrated by the degree of preservation of diamonds in kimberlite deposits). These may be better modeled as Weertman fractures.

The case of interest may be intermediate, so the modeling approach should be chosen according to an assessment of the approximations or assumptions that are appropriate for a specific application (Fig. 10). Moreover, as discussed above, for km-sized dikes K_c^{eff} may be in the range $O(100)$ to $O(1000)$ MPa m$^{1/2}$ (corresponding to $L_f = [1\text{–}5]$ km). Perhaps unsurprisingly, these values overlap with the limits of validity reported above. Given this overlap, we conclude that recent extensions aimed at relaxing the strong assumptions of no viscous flow on one hand and zero fracture toughness on the other should be preferred (Sects. 4.2.2, 4.3 and 4.4.4).

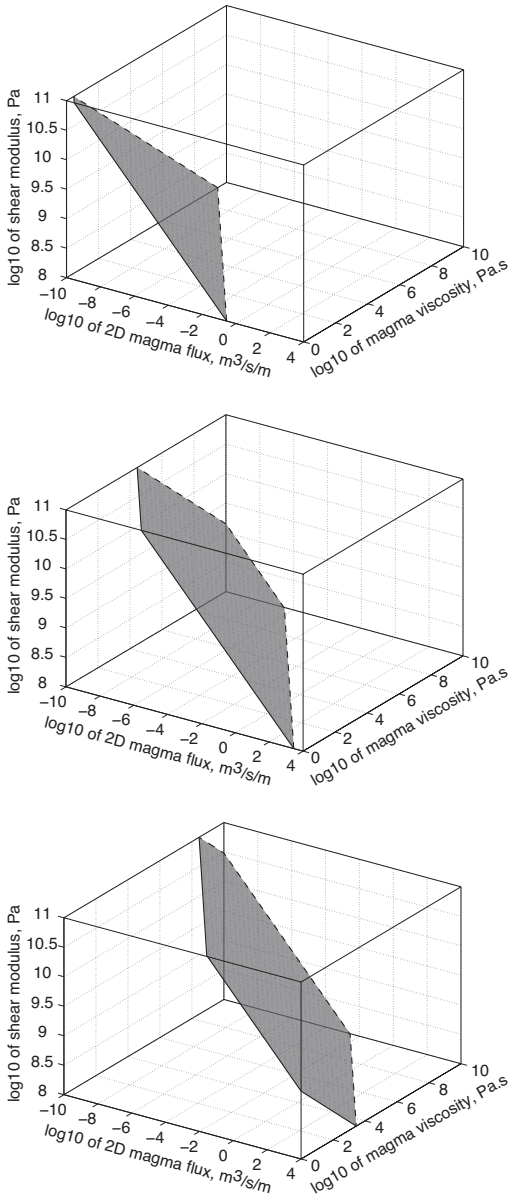

Figure 10: Surface representing $K_c/K^* = 1$. Above the surface, $K_c/K^* < 1$, represents the "lubrication" domain, below the surface, $K_c/K^* > 1$, represents the "Weertman" domain. Each panel is associated with a different value of the fracture toughness, $K_c = 1MPa\, m^{1/2}$, $10MPa\ m^{1/2}$ and $100MPa\ m^{1/2}$

4.4.3. Magma influx from the reservoir and the dike tail

Beside the strong assumptions just discussed (no viscous flow for Weertman models, zero fracture toughness for lubrication models), either model types rely on further simplifications to make the problem tractable. Weertman models are conceptualised as propagating, isolated constant-volume batches of magma; Lubrication models are often implemented with simplified boundary conditions such as constant influx from below or constant pressure at the magma reservoir. In this paragraph we will discuss these assumptions and their broader implications.

Three main issues are hidden behind those conceptualisations, related to magma transfer from a reservoir into a dike and within the dike tail, that have never been properly addressed. 1) What conditions allow an effective emptying of the tail (magma retained completely within the head of the propagating fracture)? 2) Under what conditions does the head separate hydraulically from the feeding magma source? 3) How does the state of magma reservoirs change during feeding?

Magma is retained effectively in the head of the fracture if the volume contained in the tail is small compared to the head volume. This condition is respected if Eq. (32) holds. Therefore, if the length of the tail is smaller than the quantity L_t, the constant-volume assumption is approximately valid, and Weertman models can be applied safely. Using the parameter values above along with $\Delta\rho = 300$ kg/m^3 and $g = 9.81$ m/s^2 we obtain $L_t = 0.06, 600, 66000$ m for $K_c = 1, 100, 1000$ MPa m$^{1/2}$, respectively. Again, we find that Weertman models require large fracture toughness values, and obtain that they can be safely applied to model dikes propagating over large distances if the fracture toughness is large, because a small portion of magma mass is lost within the tail. It is possible that the rate of loss of magma to the tail may also be compensated by volume increases caused by decompression. Volume compensation may be very effective since gas bubbles in magma grow in dimension and number during ascent, although this has never been checked quantitatively. Moreover, magma viscosity and compressibility are factors that could moderate the issue of magma loss to the tail. Lower viscosity (which can be as low as 0.1 Pa s for kimberlitic, ultrabasic, low-silica melts) means a smaller viscous pressure drop over the length of the dike. This, in turn, implies that less magma is needed to maintain the same propagation speed or shape.

The issue of hydraulic connectivity between magma reservoir and dike is

vastly ignored or sometimes simplified to a cylindrical channel transferring the magma from a higher pressure reservoir to a lower pressure dike inlet. In models where the pressure at the reservoirs and dike are solved for dynamically, the shape and thickness of such a channel may have a significant effect. We discuss how this issue has been addressed in recent models further below (Sect. 5.10).

Most lubrication theory models rely for simplicity on the assumption of a constant pressure at the inlet. However, even if the initial volume of the magma chamber is much larger than the total volume of magma injected in the dike, it may be a poor approximation to consider the pressure of the chamber as constant. In fact, significant pressure decreases at magma chambers feeding dikes have been observed for lateral dike propagation events around the world (Segall et al., 2001; Buck et al., 2006; Rivalta, 2010). The pressure drop due to the extraction of magma from a reservoir can be calculated as follows:

$$\frac{\Delta M/M}{\Delta p} = \frac{(\rho\Delta V + V\Delta\rho)/(\rho V)}{\Delta p} = \frac{1}{V}\frac{\Delta V}{\Delta p} + \frac{1}{\rho}\frac{\Delta\rho}{\Delta p} = \beta_c + \beta_m \qquad (34)$$

where p, V, β_c, are the pressure, volume and elastic compressibility of the magma chamber and ρ, and β_m are the density and compressibility of the magma, respectively. The compressibility of degassed basaltic magma at crustal depths is in the range $\beta_m = 0.4\text{–}2\times10^{-10}\,\mathrm{Pa}^{-1}$ (Spera, 2000), while β_c depends on the shape of the chamber and on the rigidity of the host medium (Segall et al., 2001; Rivalta and Segall, 2008; Amoruso and Crescentini, 2009; Rivalta, 2010). For spherical chambers and $G = 3\,\mathrm{GPa}$ to $25\,\mathrm{GPa}$, $\beta_c = 0.3\text{–}3{\cdot}10^{-10}\,\mathrm{Pa}^{-1}$. This implies that extracting just 0.1% of the magma resident in a chamber may result in a pressure drop $\Delta p = \Delta M/M \cdot 1/(\beta_c+\beta_m)$ of several MPa or more. Hence, similar to hydraulic fracturing where the fluid influx is mechanically controlled and the pressure varies (most often decreasing) in response to fracture growth, the pressure at the magma chamber feeding a dike will tend to decrease during injection.

Alternatively, some models assume a constant magma influx into the dike. The relation between source pressure and magma influx is influenced by the force balance that drives dike propagation (Menand and Tait, 2002; Roper and Lister, 2005). Traversa et al. (2010) showed that a finite-sized magma chamber experiencing a pressure decrease as it feeds a dike may lead to propagation with nearly-constant volumetric flux. However, inversions from crustal deformation data indicate that real cases may show some

complexity. For example, the estimated time dependent volumetric flux into the 1997 and 2007 dike at Kilauea (Segall et al., 2001, Fig. 4) and (Montgomery-Brown et al., 2011, Fig. 7) was maximum during the first hours of propagation and then decreased with time. Models assuming a constant total mass for coupled magma chamber(s) and dike(s) systems have obtained an exponentially decreasing volumetric influx into the dike (Rivalta, 2010). That model however does not include fracturing. A further extension of the model including a time-dependent K_c might help us interpreting observations during dike arrest.

4.4.4. Where the Two Schools Reconcile

Recently developed models provide a path to reconciliation between the Weertman and lubrication classes of dike model. They do this by relaxing the assumptions that create key differences. Two papers, one from each side of the debate (Dahm, 2000b; Roper and Lister, 2007), are particularly relevant to understand how the two approaches reconcile and in what cases the end-member approaches are valid.

Dahm (2000b), representing the Weertman school, developed a numerical boundary element model (see also Sec. 4.5 below for other boundary element studies of dike propagation) for constant-mass, buoyancy-driven, fluid-filled fractures (hence in principle Weertman fractures, with no magma influx from below). However, he also included 2D magmatic flow within the crack and the consequent viscous stress drop on the crack plane. In particular, the model is of a Hagen-Poiseuille flow through a piecewise constant-width fracture (h is discontinuous along the crack) with a moving boundary (Fig. 11a). The sophistication of the model for the fluid flow is somewhere between the constant pressure gradient normally considered in extended Weertman models (Sec. 4.2.2) and solving the equations governing the flow, as in the lubrication theory approach. If the fracture propagates with constant mass (if none of the fluid is left in the channel behind the fracture) the pressure gradient is singular at the link between head and the tail of the crack, as noticed before by Spence and Turcotte (1990); Nakashima (1993); Rubin (1995). This occurs because buoyancy-propelled ascent of a magma pocket requires the magma-filled fracture to retain effectively all the enclosed magma during propagation; in contrast, lubrication theory states that in a finite time interval, it is impossible to fully expel viscous fluid out of a closing gap. Dahm (2000b) addresses this problem by requiring that a small quantity of fluid is left in the channel during propagation. In this way, the viscous pressure

gradient is no longer singular, it is just very large at the tail (Fig. 11b). This suggests that most of the energy during propagation is dissipated within the tail region or, in other words, that the constriction at the tail controls the velocity of the fracture, consistent with a result from the lubrication theory. Dahm (2000b) links the numerical instability at the tail to a physical instability observed during experimental injections in gelatin, where the tail of air-filled cracks is observed to shut closed in jerky movements (see movie at `http://www.youtube.com/watch?v=hHqUwHRvilU`, Rivalta et al. (2013a)). In the approach by Dahm (2000b), it is not possible to predict from theory how much fluid gets lost in the tail.

Roper and Lister (2007), representing the lubrication school, develop a lubrication-based model with a finite fracture toughness and solve the problem for a crack containing a constant volume of fluid (Fig. 12c). They find that viscous effects still control how quickly the cracks propagate. They also find that a large fracture toughness implies a teardrop-shaped crack, whose length and width scale with $k^{2/3}$ and $k^{4/3}$, respectively, fed by a narrow tail. They define

$$k = K_c/K^* = \left(\frac{2K_c^4}{3\mu Q m^3}\right)^{1/4}, \tag{35}$$

where Q is the magma influx into the dike and $m = G/(1-\nu)$. They show that the head and tail are connected through a constriction of length and width scaling with $k^{-2/5}$ and $k^{-4/15}$, respectively. These results obtained through modeling and scaling analysis match very well with the geometry of a Weertman fracture in general and with the results by Dahm (2000b) in particular (compare Figs. 11 and 12).

Both models were developed with the aim of extending the applicability of the original approaches. Furthermore, Dahm (2000b) applied his model to fluid-filled fractures in nature. He estimated a velocity of ≈ 0.1 m yr^{-1} for water-filled fractures in pressurized sediments and 0.1 m s^{-1} for magma-filled dikes in the upper mantle (Fig. 13). The model also predicts that water- and oil- filled fractures in sediments have a thickness of the order of 10^{-5} m and begin to ascend spontaneously when their length exceeds about 1.2 m. For $K_c \approx 1$ GPa m$^{-1/2}$, magma-filled fractures in the upper mantle would start to ascend spontaneously when they accumulate enough volume to reach a length of 5 km. Their average thickness during propagation of such a dike would be about 0.3 m. Dahm (2000b) includes a thorough comparison of his estimates with previous models. Additionally, he finds good agreement

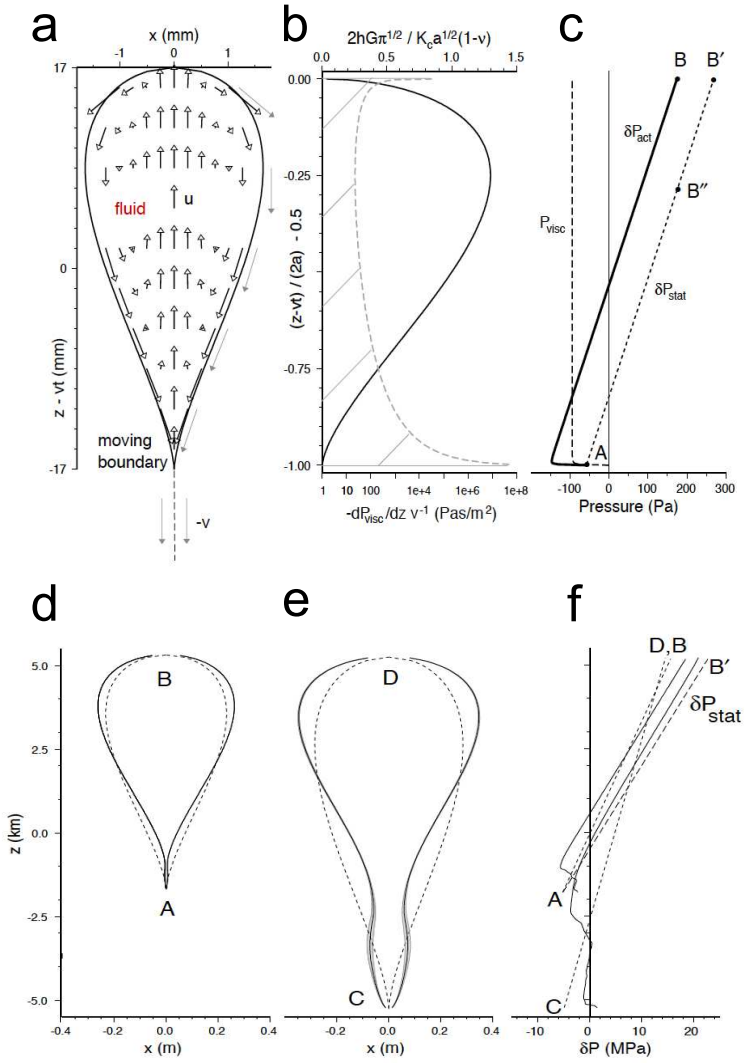

Figure 11: Fig. 3 and 6 from Dahm (2000b), with permission. a) Crack cross-section and velocity field of the fluid within the fracture. b) Solid line: crack half-width (solid line), dashed line: viscous pressure gradient. c) Total overpressure in the fracture, sum of the static overpressure and viscous pressure drop. (d) Average shapes (solid lines) derived from the first 500 iterations of the model. The dyke lengths are 1.3 (left) and 1.9 (right) times the critical length for fracture propagation. Dashed line: initial opening of the fracture at iteration 1. (e) Average (solid lines) and initial (dashed) overpressure in the fluid. The hypothetical static overpressure is indicated for the shorter fracture by a long-dashed line (A to B').

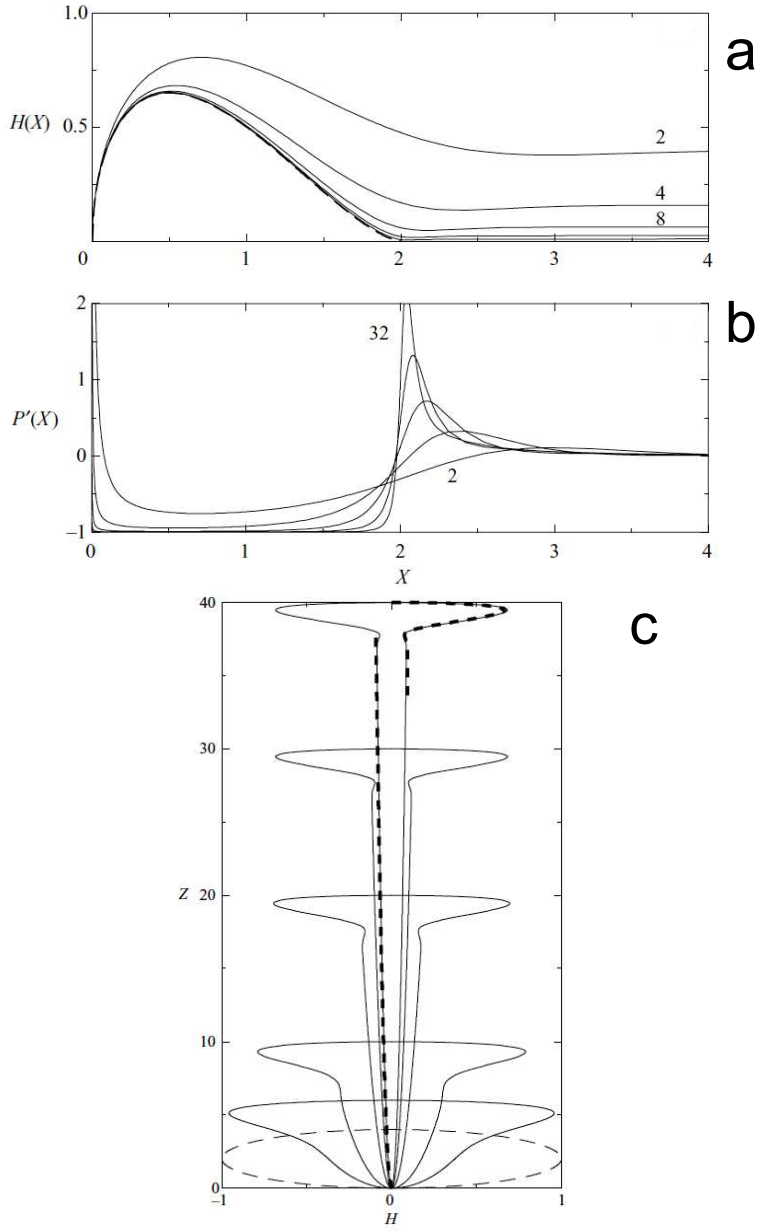

Figure 12: a) Normalized opening of fracture for different ratios between fracture toughness and viscous resistance (k=2, 4, 8, 16 and 32). b) Normalized pressure gradient. c) Evolution of the scaled crack width from an initial shape (long-dashed) shown at 6, 10, 20, 30 and 40 iterations. Figs. 3 and 8 from Roper and Lister (2007), with permission.

with some field data from both water-filled fractures in sediments and dikes in the upper mantle. A wider comparison with estimates from nature would be desirable, especially now that the physical understanding of propagation of fluid-filled fractures in brittle materials and the role played by magma and rock parameters has advanced, and that industrial operations can provide a much wider dataset for a comparison.

Roper and Lister (2007) apply their model to discuss the validity and applicability of analog experiments using gelatin (Sect. 3.2). They observe that laboratory experiments are in the regime $K >> 1$ (fracture toughness dominated). They compare their theoretical results to experimental studies by Takada (1990) and Heimpel and Olson (1994). As they notice, in laboratory experiments using large viscosity fluids, head-and-tail structures are clearly visible. The viscous control of propagation rate can be deduced from the increasing propagation rates in a given gel with decreasing-viscosity fluids. They also discuss the fracture criterion in gelatin, observing that there is no analytical solution for a three-dimensional Weertman pulse (with stress intensity equal to K_c along its upper boundary and 0 on the point of closing along its lower boundary). They observe that a numerical solution would be expected to have the same scalings as their equation (6.5) with vertical and lateral extent $O((K_c/\Delta\rho g)^{2/3})$ and width $O((K_c/\Delta\rho g)^{1/3}K_c/m)$, thus giving a critical volume $V_c = O((K_c/\Delta\rho g)^{5/3}Kc/m)$. They observe that 1) a buoyant crack with volume less than V_0 should not propagate and, 2) a crack with low viscosity and large toughness should propagate with a head of approximately the fixed shape and volume of such a pulse. They seem not to find confirmation of this in the data by Takada (1990) and Heimpel and Olson (1994) and conclude that the failure mechanisms in gelatin are significantly different from those of more rigid brittle solids such as ceramics or rock. In particular, they suggest a rate-dependent fracture resistance. While the correctness of points 1) and 2) for gelatin experiments have been indeed confirmed in numerous other experiments (see Sect. 3.2), further investigations of scaling relationships and fracture processes in gelatin and comparison to theory would help our understanding of the applicability of laboratory analogs to water- and magma-filled fractures in the Earth's crust and mantle.

The studies by Dahm (2000b) and Roper and Lister (2007) testify how predictions from the Weertman and the lubrication schools converge when restrictive assumptions are relaxed. Both approaches remain limited in that they consider only dikes propagating straight and they lack flexibility in including external effects because of the large computational effort necessary

to obtain a very detailed modeling of the fluid motion in the fracture. For the purpose of addressing questions regarding the interaction of dikes with external factors and studying the behavior of dikes in different tectonic settings, numerical models simplifying strongly the motion of fluid within the fracture have instead proved very flexible, as described in the next section.

4.5. Numerical Models

As presented above, semi-analytical solutions from the classical presentations by Weertman (1971a,b) and lubrication models (Spence et al., 1987; Lister, 1990a) are appropriate in the limits of: 1) negligible fluid viscosity or fracture toughness, respectively, and, for both types of models, 2) simple geometries typically limited to homogeneous, infinite media subjected to a relatively simple (i.e. locally uniform) lithostatic stress. Additional contributions to both confining and internal pressure due, for example, to gradients in the topography or bubble nucleation within the dike will lead to more complicated geometries and propagation behavior and cannot be easily treated with the semi-analytical approaches. Furthermore, a growing consensus in the debate on effective fracture toughness (Sect. 4.4) suggests that both viscous flow and rock fracture toughness must be included to produce a broadly applicable dike model. In this context, two hybrid styles of models are particularly promising: 1) Weertman-type models that relax the constant volume assumption and include fluid flow, and 2) Lubrication-theory based models that allow for a non-zero fracture toughness. These "mixed" models require numerical solutions even for simple geometries.

Probably the most common numerical approach to solving dike propagation models is based on the boundary element method (BEM), see Crouch and Starfield (1983). This method is designed to incorporate the coupling between magma pressure and rock deformation; it requires discretization of the dike boundary and any other non-analytical boundary in the medium. Such models are built by taking advantage of analytical solutions for elementary dislocations; these are appropriately superposed to represent a pressurized, opening crack. The most important advantage of this method relative to others that require meshing of the entire domain, such as the classical Finite Element Method, is that re-meshing as the dike propagates is relatively simple and computationally inexpensive. This is because re-meshing simply requires that new elements are added at the dike tip.

Early dike propagation models of this type include Dahm (2000a) and Muller et al. (2001). Both methods are used to derive dike trajectories re-

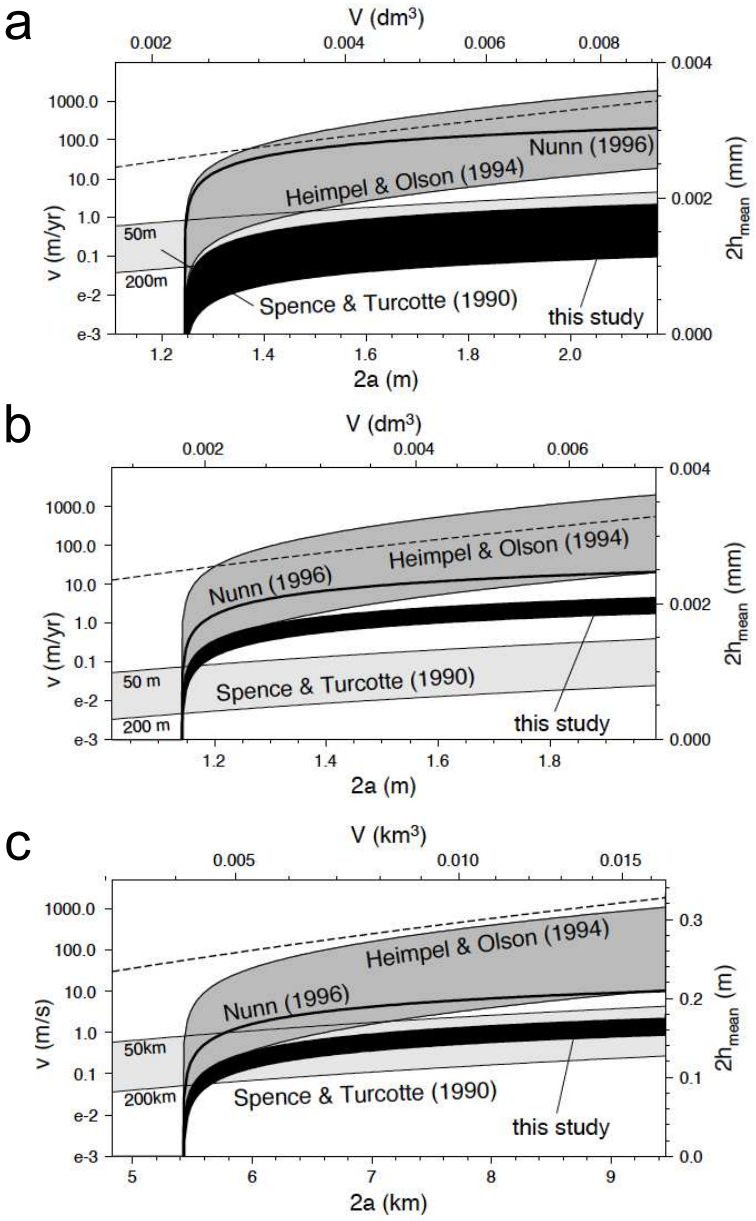

Figure 13: a) Predicted propagation velocities of water-filled fractures in pressurized sediments by Dahm (2000b) (see paper for details). Model estimates are compared with results by Nunn (1996), Spence and Turcotte (1990) (using propagation distances between 50 and 200 m) and Heimpel and Olson (1994) (assuming a yield strength between 100 and 1000 MPa). The average thickness is plotted as a dashed line. Fig. 8 from Dahm (2000b), with permission. b) Predicted propagation velocities for oil-filled fractures in pressurized sediments. Fig. 9 from Dahm (2000b), with permission. c) Predicted propagation velocities for magma-filled fractures in upper mantle rocks. Fig. 10 from Dahm (2000b), with permission.

sulting from the interaction of dikes with heterogeneous stress fields. Under this method, several interacting tensile and dip-slip dislocations are combined to model an inclined dike; boundary conditions on the dike plane are prescribed for the dike overpressure and for a total release of shear stress. The models differ in how the dike trajectories are selected: Dahm (2000a) uses an energy-release criterion in which the energy release is calculated for virtual elongations in several directions and the direction leading to the maximum release is chosen (Nuismer, 1975); in contrast, Muller et al. (2001) select the direction minimising the shear stress, because this will be perpendicular to the direction of maximum hoop stress around the tip of the dike (Erdogan and Sih, 1963). Only if the dike tip is highly resolved on the numerical mesh, the minimum-shear stress criterion gives results very similar to the maximum strain energy release (this because the former is based on the shape of the dike tip, which must be calculated very precisely). The energy release criterion works for coarser discretizations because it takes into account the shape of the entire fracture and is less sensitive to details in the tip. In both models, the dike aperture at the trailing dislocation is checked for negative values, which can occur due to closing associated with propagation of a confined pocket of fluid. If the aperture is negative, the dislocation at the tail is deleted or, alternatively, the aperture is set to zero and the linear system for the set of dislocations is re-solved to find the equilibrium configuration. This approach allows for a quasi-static model of dike propagation. External stress fields can be easily introduced in such a numerical scheme (see Sec. 5).

The numerical models provide a framework for other generalizations. For example, the model by Dahm (2000a) includes compressibility of the magma and imposes a conservation of mass rather than of volume. Maccaferri et al. (2010) and Maccaferri et al. (2011) improve on models of Dahm (2000a) by including gravitational potential energy in the energy balance equation (see also Sec. 5 below). However, current models do not yet provide the ability to consider dike curving and growth with a finite fracture toughness and fluid viscosity at the same time. Recent models by Maccaferri et al. (2010) and Maccaferri et al. (2011) do not include fluid viscosity, while the semi-implicit models by Taisne and Tait (2009) and do not include dike curving.

In a field that is related to modeling of dike propagation, the hydraulic fracturing techniques that have advanced unconventional oil and gas production have led to a proliferation of novel numerical models (see Sec. 6). These consider the growth of fluid-filled, pressure-driven cracks and, up to the point

where buoyancy forces or the cooling/solidification of the magma are invoked, they are essentially identical to elasto-hydrodynamic dike propagation models. Advances in modeling of hydrofracture represent a resource for new and more powerful approaches to modeling dike propagation. The power of Boundary Element and Boundary Integral Methods have been harnessed to simulate hydraulic fracture growth since the 1980s (e.g. A. H.-D. Cheng, 1984; Vandamme and Curran, 1989). However, there are some significant challenges. These include devising efficient computational schemes so that solutions can be obtained in practically-relevant time frames, bridging the gap between the mostly 2D simulations and the mostly 3D physical phenomena, and accounting for complexity that is ubiquitous in geological environments. These are partially overcome by:

- Design-motivated modeling of network growth of hydraulic fractures by integrating so-called pseudo-three-dimensional (P3D) modeling with Discrete Fracture Networks (Meyer and Bazan, 2011; Kresse et al., 2013). This approach uses a drastically-simplified, local elasticity relationship that is valid when the hydraulic fracture is very long relative to its height, i.e. blade-like in shape. This simplification induces orders of magnitude reduction in computational time but the applicability is limited to relatively blade-like hydraulic fractures.

- Boundary Element Models that consider hydraulic fracture interaction with pre-existing fractures (Zhang et al., 2009; Dahi-Taleghani and Olson, 2011). These allow consideration of one of the most important sources of complexity, but are limited to relatively few natural fracture interactions in a two-dimensional framework.

- Simulators that overcome the limitations of P3D and 2D models by accounting for planar hydraulic fracture growth in a 3D medium (Peirce and Detournay, 2008). The computational cost is partially offset by implicit time stepping, thus allowing coarser discretization of time, and embedding appropriate asymptotic behavior of the near-tip opening, thus allowing coarser discretization of space.

- The eXtended Finite Element Method (XFEM), that overcomes the need to re-mesh a traditional FEM model as the hydraulic fracture grows. These models are capable of simulating growth in complex geological settings and are, in principle, extensible to three dimensions

(Lecampion, 2009; Dahi-Taleghani and Olson, 2011; Gordeliy and Peirce, 2013; Chen, 2013; Weber et al., 2013; Ru et al., 2013). In some cases, XFEM includes specific functions to enrich the finite element basis that ensure accurate and efficient computation when under strong fluid-solid coupling (Lecampion, 2009; Gordeliy and Peirce, 2013; Chen, 2013).

- Damage mechanics-FEM based models for three-dimensional growth of hydraulic fractures including the impact of stochastically heterogeneous rocks (Wangen, 2011; Li et al., 2012; Guest and Settari, 2012).

- Distinct Element Models (DEM) capable of modeling highly complex, three-dimensional growth patterns including interaction with Discrete Fracture Networks (Damjanac et al., 2010; Nagel et al., 2013). The main limitation of these models is the need for very fine discretization in order to accurately match benchmarks (an A. P. Peirce et al., 2013).

While all of these approaches provide steps toward 3D modeling, the overall challenge is that the most thoroughly benchmarked models are 2D or 3D models that constrain growth to one or more planes. This is very limiting because dikes have been inferred to bend and twist at some volcanoes (Bagnardi et al., 2013; Xu and Jónsson, 2014) while adjusting from one stress domain to the next, so that a fully 3D approach would be required to predict the dynamics of such dikes. Currently, it is out of reach to model this behavior with workable computational times and with benchmarking that demonstrates suitable confidence that the model is providing a correct solution to the basic, underlying mechanical problem.

5. Results including interaction of dikes with the surroundings

The challenges associated with modelling dike propagation go beyond the issue of the relative importance of magma viscosity and rock fracture toughness. Dikes almost invariably grow in environments that draw into question the simplifications that make the modelling problems tractable. Here we review a range of complications associated with the interaction between dikes and their surroundings, how they have been addressed, and the associated progress in understanding the dynamics of dikes.

5.1. External stress field

As described above (Sect. 2), the trajectory of a dike is controlled by the orientation of the principal stresses. Spatial variation of that orientation will

force a propagating dike to change its direction. However, drastic turns of dikes during their propagation (e.g. from dike to sill orientation) are not instantaneous but occur over a finite distance. This arises because dikes do not propagate in perfect alignment with the stress field, but rather are continuously adjusting toward alignment. This is particularly true when the stress field is heterogeneous or the dike driving pressure is very high (Dahm, 2000a; Watanabe et al., 2002). Menand et al. (2010) study experimentally the characteristic length scales over which a horizontal compressive stress field exerts a steering effect on ascending, air-filled cracks in gelatin. Their dimensional analysis shows that this distance varies exponentially with the ratio of crack effective buoyancy to horizontal compressive stress. Up-scaled to natural systems, these results imply a spatial scale of a few hundreds meters to a few kilometers for a dike-to-sill rotation to occur, so that this mechanism should be important for crustal-scale processes. Dike bending and twisting has been inferred to occur also at the volcano edifice scale Bonaccorso et al. (2010); Bagnardi et al. (2013); Xu and Jónsson (2014); material heterogeneities may however also play a dominant role (see Sec. 5.5 below).

Numerical models (Dahm, 2000a; Maccaferri et al., 2010, 2011) return the general result that the rotation of a dike in a heterogeneous stress field occurs over spatial scales that are of the same order of magnitude as the dimension of the crack. Maccaferri et al. (2011) analyze different scenarios for an external stress field: compression, extension and the load of a volcanic edifice (Sec. 5.2). They find for example that a kilometric spatial scale is needed to turn a dike into a sill or a sill into a vertical dike. The spatial scale is influenced by the ratio between overpressure within the dike (which can be estimated with the equation $\Delta p = \rho g L/4$) and compressive/extensional/loading/unloading stresses, as shown experimentally by Watanabe et al. (2002) (Sections 5.2 and 5.3).

5.2. Load of a volcanic edifice

The load of a volcanic edifice modifies the local stress field and therefore exerts a control on the trajectory of dikes ascending nearby. Gudmundsson (2002), for example, reports observations of inclined sheets and dikes dipping toward central volcanoes. The theoretical problem of how ascending dikes are influenced by the stress field associated with a volcanic edifice has been studied with several approaches.

Dahm (2000a) used a boundary element approach (Sec. 4.5) to model expected trajectories in such a stress field. He finds that gravitational loads

attract ascending dikes, which tend to focus at the base of the volcano, erupt and reinforce the process by piling up more material in the same location, adding to the overburden. Also, he highlights how dikes are not driven exclusively by the principal stresses, but also by the gradient of tectonic/local stresses and magma buoyancy, and the trajectories might be more complicated than what is simply suggested by the principal stresses.

Maccaferri et al. (2011) extended the results of Dahm (2000a) by calculating the trajectories of dikes ascending at various initial angles, directly below the volcanic edifice or offset from it. No external stress field was added in this case. Most of the trajectories stream into the base of the volcanic edifice, but occasionally a dike may escape from the trap and erupt at a considerable distance from it (Fig. 14F1–4). If the buoyancy is not sufficient (if the dikes are not very large), the dikes will stop just below the base of the load (Fig. 14F1), extending laterally and erupting, or creating/feeding a shallow crustal magma reservoir.

Muller et al. (2001) carried out laboratory experiments to investigate the effect on analog dikes of a mass lying on top of a brittle gelatin block (Fig. 14D). Watanabe et al. (2002) performed similar analog experiments with gelatin. They calculated how much dike trajectories are deflected as a function of the ratio between dike driving pressure and gravitational loading. They also noticed that ascending, fluid-filled cracks decelerate in proximity of the load and eventually stop, with the deceleration proportional to the size of the load. Bonaccorso et al. (2010) observed that the 2001 dike at Etna tilted towards the volcano summit during ascent, consistent with the theoretical and experimental predictions just outlined (Fig. 14E). They used results from analog modeling by Watanabe et al. (2002) to infer the overpressure of the dike and the overpressure at the magma chamber at breakout.

Kervyn et al. (2009) used air-filled cracks in gelatin and golden syrup in sand-plaster to explore how volcano load controls magma ascent and vent locations. They found rising dikes approaching the conic stress field are arrested by the compressive stress of the load and begin extending laterally. Pinel and Jaupart (2004) studied the influence of volcano loads on the lateral extension of shallow dikes and considered how this influences the location of eruptive vents (Sec. 5.12).

Taken together, these results also indicate that the stress field caused by gravitational loading may be the reasons why large volcanic edifices such as Etna, for example, develop a stable magma reservoir (which can be detected by measurements of crustal deformation).

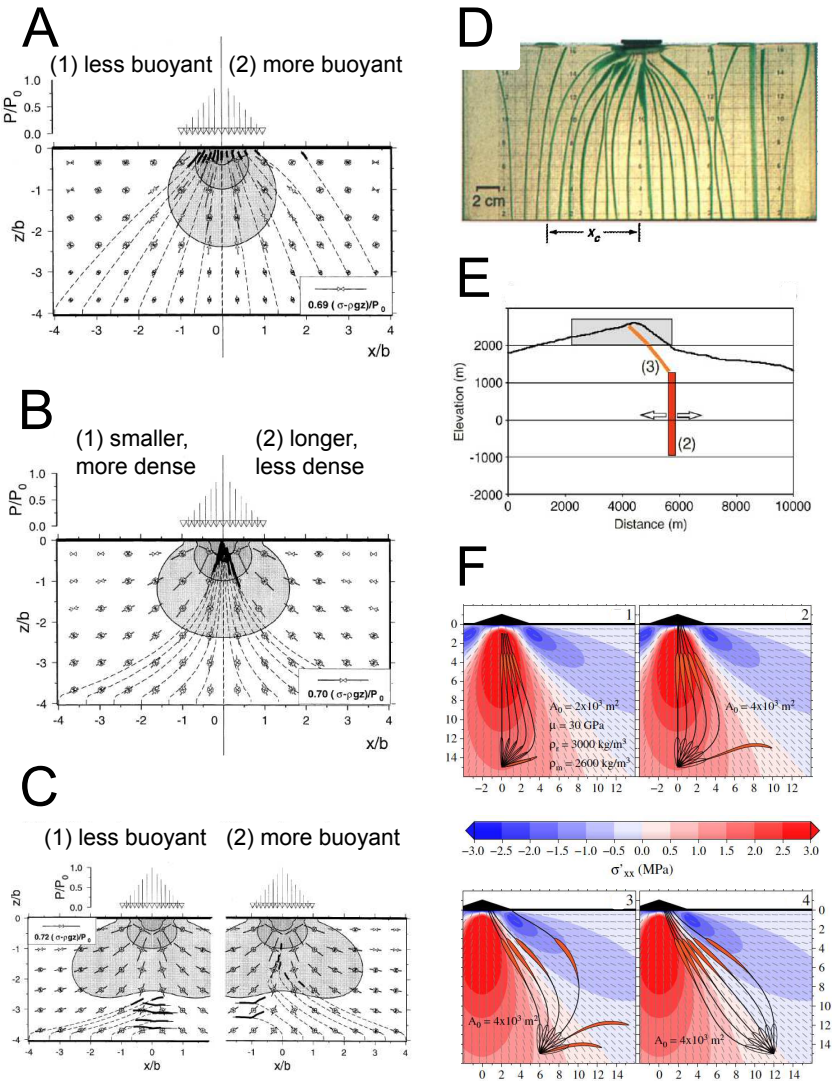

Figure 14: Experimental and numerical models of dike ascent in a stress field modified by loading of volcanic edifices. A) Boundary element model of dike trajectories under the influence of a triangle-shaped volcanic load. The principal stresses rotate and promote ascent towards the volcano. The individual dikes are not interacting with each other. Less buoyant dikes follow the trajectories closely (1), more buoyant dikes need more space to rotate (2). Fig. 7 from Dahm (2000a), with permission. B) Same as A), but with an additional tectonic compressive stress equal to $P_L/12$, where P_L is the pressure caused by the volcanic edifice. Fig. 8 from Dahm (2000a), with permission. C) If the compressive tectonic stress is higher ($P_L/6$) some of the trajectories turn horizontal, and sill emplacement is favoured. Fig. 9 from Dahm (2000a), with permission. D) Trajectories of analog dikes in gelatin under the influence of a load applied to the surface. Fig. 1a from Muller et al. (2001), with permission. E) Dike rotation observed for the 2001 dike intrusion at Etna. The rotation was interpreted as originating from the load of the volcano edifice and summit. From Bonaccorso et al. (2010), with permission. F) Influence of a triangle-shaped volcano load on the trajectories of dikes departing with different orientations from an axial (top) or a off-axis (bottom) magma chamber. The compressive stress induces dike arrest at depth, promoting the creation of a magma chamber. Fig. 5 from Maccaferri et al. (2011), with permission.

5.3. Unloading

Seasonal loading/unloading conditions may occur at high latitudes or altitudes due to cyclic icecap melting and formation. Albino et al. (2010) studies how this causes variations in magma pressure and therefore influences the likelihood of dike initiation. They find that unloading favors dike nucleation and the occurrence of seismicity.

Loading due to a topographic weight (Sec. 5.2) causes a rotation of the principal stresses in the crust, steering ascending dikes into the base of a volcano. Similarly, unloading due to mass removal influences dike propagation, and has the opposite effect of defocusing ascending dikes to the side of a region which has been unloaded. Significant unloading may occur over various time scales during volcano flank collapse, deglaciation, or crustal thinning. Hooper et al. (2011) calculated the unloading effect caused by icecap melting at Kverkfjöll, Iceland. They found that the orientation of the ascending dike, inferred from inversion of InSAR data, is not consistent with the tectonic stress state modified by the current icecap melting. However, it would would fit with the more intense modification induced by icecap melting after deglaciation (Fig. 15A). They inferred that deglaciation modifies the capacity to store magma in the crust.

Corbi et al. (2014) developed an axially symmetric finite element model for the unloading effect due to a massive withdrawal of magma from a volcano reservoir and the associated caldera formation. The unloading was modeled as a decompression over the caldera area, amounting to the missing topography from the most recent caldera collapse, superposed to an isotropically stresses volcano. The latter assumption is justified by observing that volcanic edifices form over long time scales; multiple dike intrusions and anelastic release of deviatoric stresses compensate over such long time scales any deviations from an isotropic state of stress. Therefore, only recent sub-surface mass changes (caldera collapses) would be uncompensated for. The model was applied to Fernandina volcano, Galàpagos: under those assumptions, σ_3 is oriented vertically below the caldera, favoring the creation of horizontal sill-shaped magma chambers. On the flanks, close to the surface, σ_3 is out of plane: the pattern of the principal stresses is consistent with the bending and twisting of the recent dikes inferred from crustal deformation data and from the pattern of the surface fissures at Fernandina (Bagnardi et al., 2013).

Maccaferri et al. (2014) studied the trajectories of dikes in rift environments by coupling the gravitational unloading due to crustal thinning and the creation of a topographic depression with an extensional stress field (see

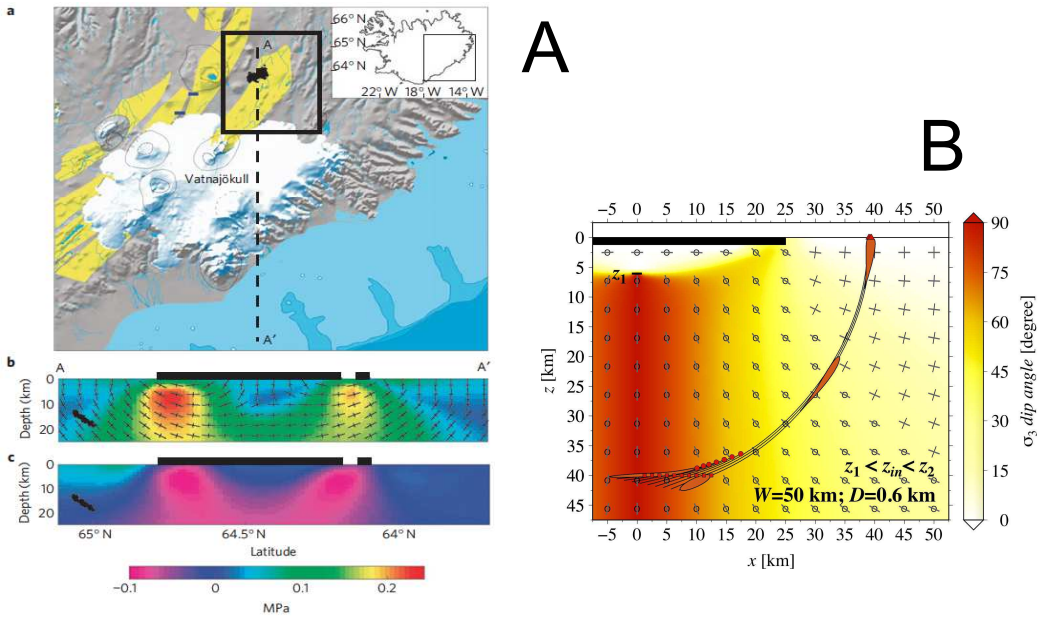

Figure 15: Numerical models of diagonal dike ascent in a stress field caused by unloading. A) The unloading at is caused by icecap melting during the last deglaciation. From Hooper et al. (2011), with permission. B) The stress field is the sum of tectonic extension and unloading due to crustal thinning. From Maccaferri et al. (2014), with permission.

also Sect. 5.4). The unloading resulting from crustal thinning induces decompression melting in the mantle, so that magma will pond at the crust-mantle boundary and release magma-filled dikes. Consistent with the focusing effect that is obtained by studies on gravitational loading, Maccaferri et al. (2014) found that the principal stresses in the crust are rotated by the effect of the unloading forces, and that ascending dikes will follow diagonal trajectories that steer them away from the rift axis towards the shoulders of the rift. This model is applied to explain the distribution of volcanism in rifts and the existence of off-rift volcanoes, offset of tens of kilometers with respect to the source of volcanism below the rift (Fig. 15B).

5.4. Extensional and compressional tectonics

Great potential lies in applications of dike modeling to magmatic tectonic environments. These models open the possibility to reveal the mechanisms of formation of large scale volcanotectonic features, such as the morphology of slow or fast spreading ridges, rifts, volcano chains in subduction zones.

Kühn and Dahm (2004) employ a viscoelastic version of the model by Dahm (2000a) to study dike ascent at mid-ocean ridges. Their model includes the passive motion of the mantle through a 2D isothermal corner flow. They conclude that the observed focussing of melt beneath mid-ocean spreading axes cannot be explained by corner flow models and additional mechanisms are needed, such as large magma reservoirs or permeability barriers. Kühn and Dahm (2008) includes dike-dike interaction (Sec. 5.7) to study the formation of shallow magma reservoirs at fast or slow spreading MOR.

Choi and Buck (2010) discuss the influence of upper mantle viscosity on the topography profile of fast-spreading mid ocean ridges. They develop a numerical model based on Qin and Buck (2008) including mechanical coupling between tectonic extension and diking. The model has two layers, a crust with viscosity evolving with time overlaying a mantle with constant viscosity. Amagmatic periods, where extension is loading the system, are modeled through a finite differences scheme. They are punctuated by sudden dike intrusions, modeled by means of a BEM code, where the vertical extent of the dikes is optimized to compensate for the residual tectonic stretching (difference between residual stress from the last diking period cumulated with the extension added during the amagmatic period). Choi and Buck (2010) find that the topography profile has a strong dependence on the viscosity of the mantle, with an axis high or a valley forming for low- or high-viscosity

mantle rocks, respectively. Moreover, very high viscosity below mid-ocean ridges could lead to dikes that intrude into the mantle.

Parsons et al. (1992) focuses on the paradox of magma ponding and horizontal intrusion of basaltic magma at various depths, common in various tectonic environments, including extensional ones where vertical ascent is theoretically expected to dominate. The paradox is that the stress conditions favoring horizontal intrusions (σ_3 vertical) are expected to block the opening of vertical feeder conduits necessary for their formation. Parsons et al. (1992) discuss a number of mechanisms, mainly of rheological nature (alternation between very rigid to viscoelastic layers, density layering) but also the effect of previous intrusions on the next: many vertical intrusions compensate extension and may cause stress rotations. This may be behind dikes turning into sills.

Maccaferri et al. (2014) offers an alternative explanation for the deep horizontal sheet intrusions found in extensional settings. The decompression caused by the decrease of weight on the lower crustal sheets and mantle due to crustal thinning may be responsible for a vertical σ_3 and therefore favor horizontal intrusions. Vertical feeder dikes may then be driven, as suggested by Parsons et al. (1992), by rheological differences between layers or by the local stress field due to the pressurization of the horizontal sills: locally σ_3 may become horizontal again, leading to nucleation of a vertical dike, that would turn as a sill as soon as its tip reaches an area outside of the influence of the sill-induced stresses.

Some studies consider the effect of extensional or compressional tectonics coupled with loading/unloading due to modifications of the mass distribution on the surface, for example crustal thickening or thinning. Dahm (2000a) includes a compressive tectonic stress in addition to the stress caused by the load of a volcanic edifice. The dike trajectories become closer to each other, and for a particularly intense compressive stress, the dikes turn into sills and build a system of stacked intrusions that may generate a stratified magma reservoir (Fig. 14B and C). Muller et al. (2001) also study the trajectories of dikes in the stress field of a volcanic load, with application to intervolcanic spacing in the Cascade volcano province.

5.5. Rigidity layering

Dikes hosted in layered rocks that have associated variations in material parameters can be strongly affected by those variations. As predicted by numerical models (Bonafede and Rivalta, 1999a; Gudmundsson, 2002, 2003;

Rivalta and Dahm, 2004), host-rock anisotropy and heterogeneity is recognised as the main control on the observed local (fine scale) variations in the thickness of a dike. Dikes are often observed to be arrested at or to intersect several layers with strong contrasts in the elastic parameters. Geshi et al. (2012) predicted with finite element models the geometries of dikes from the caldera walls of Miyakejima and Piton de la Fournaise.

Maccaferri et al. (2010) investigated the effect of layering on the travel path of ascending magma-filled dikes. Propagation across the layer interface is modelled using published analytical solutions for tensile and dip-slip dislocations in a medium made up of two welded half-spaces with different elastic parameters (Bonafede and Rivalta, 1999b; Rivalta et al., 2002). Maccaferri et al. (2010) find that the rigidity change at the interface causes a deviation of fluid-filled fractures crossing it: if the fractures pass from a high-rigidity layer to a low-rigidity one, they will be deflected towards the vertical direction, while the opposite holds if the fractures pass from a low-rigidity to a high-rigidity medium (see Fig. 16a and b, respectively). Above some critical incidence angle that depends on the rigidity ratio at the interface, the ascending dikes may deviate to become horizontal sills. Maccaferri et al. (2010) validated their numerical model with gelatin experiments. An inclined air-filled crack was created at the bottom of the container by injecting air through an inclined hole. The empirical angle of 'refraction' at the interface was compared with the results of the numerical model run with experimental parameters; the two were found to be in perfect agreement, within uncertainties.

An analysis of energy release during dike propagation can be used to predict the velocity of the dike and where it might be stopped by material variations. Drawing a horizontal line in Fig. 16c and d to represent the energy needed to create new crack surface (or, in other words, to break the medium), and observing when this line crosses the curve of the energy release, we can deduce that a dike moving from a high-rigidity medium will accelerate until it reaches the interface and then suddenly decelerate; however, it will maintain a larger velocity in the weaker medium than in the stiffer medium. Dike stopping is not predicted in this case. These theoretical deductions are consistent with observations of gelatin experiments (Sec. 3.2) (Rivalta et al., 2005). On the other hand, for a crack traveling from a low-rigidity medium to a high-rigidity one, it is plausible that for the crack tip at the interface between the media the energy released by propagation is lower than the energy needed to create new crack surface. In such a situation a

dike is predicted to stop before reaching the interface or at the interface (for example, for $\Delta E = 15\,\mathrm{MPa\ m}$, Fig. 16c and d). If the crack does manage to cross the interface (for example for $\Delta E = 10\,\mathrm{MPa\ m}$), depending on the rigidity ratio it may continue propagating (r<1.66) or not (r>2.5). One must, however, bear in mind that in natural systems (and more complicated models), the third dimension may also accomodate dike extension, and that this may be energetically preferred over ascending in unfavored conditions. Vertical ascent may become favored after lateral extension; see movie at `http://youtu.be/MJHslWoMXoI`, Rivalta et al. (2013b,c).

5.6. Density layering

The level of neutral buoyancy (LNB), where the density of the material within a dike becomes equal to the density of the wall rock, affects the dynamics of propagation of a dike. The LNB is not a physical barrier to the propagation of a rising magma. The total hydrostatic pressure, which is obtained by integrating the hydrostatic pressure gradient $\Delta\rho g$ from the level of melt production or from the lower tip of the dike (Takada, 1989; Lister, 1991, Fig. 3), is maximum at a LNB. Therefore the magma will preferentially spread at this level, but may still penetrate into layers of rocks of lesser density than the magma. This will modify the upward velocity of the dike, as explained below.

Taisne and Jaupart (2009) solved for the time-dependent propagation of a crack through a medium with vertical stratification of density. Previous work using a similar methodology (see Sec. 4.3) obtained only stationary solutions for constant physical conditions. For example, Lister (1990a) considered a viscous fluid propagating in a homogeneous elastic medium under constant source conditions. The results provided a basic state solution used to validate the formulation and code of Taisne and Jaupart (2009). They then went further, quantifying the effect of spatially variable material properties on the speed of propagation of a dike. For decreasing but positive buoyancy, the dimension of the dike adjust to the new properties of the surrounding medium; dike width increases while upward speed decreases. If the dike penetrates a layer where it has a negative buoyancy, pressure will build up at the interface and a sharp deceleration occurs Taisne and Jaupart (2009). Furthermore, Taisne and Jaupart (2009) show this pressure increase may, in turn, initiate a sill, especially at a discontinuous decrease in density (Fig. 17A).

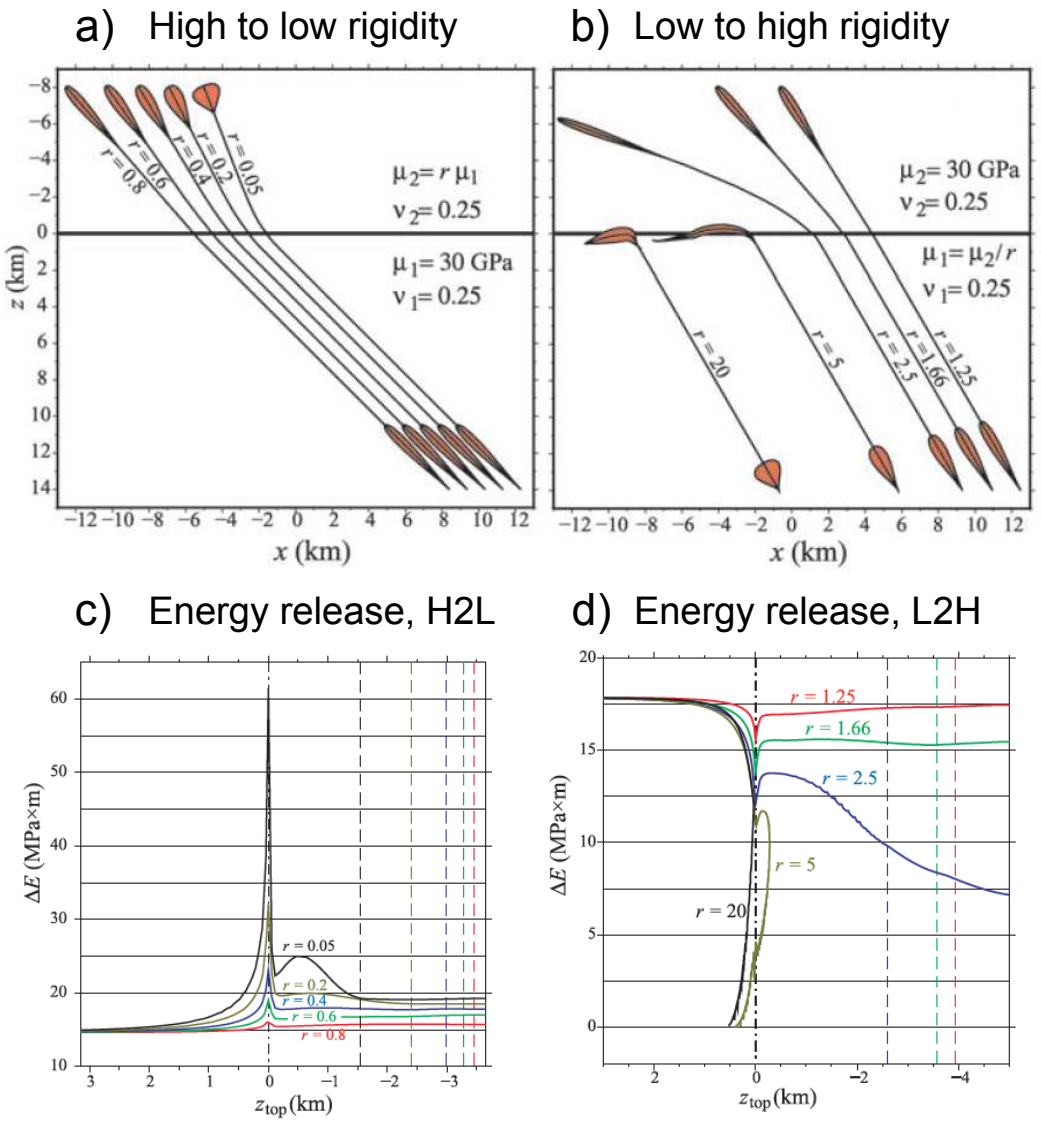

Figure 16: Dike trajectories deviate when dikes cross interfaces separating material with different rigidity. The angle of deviation depends on the rigidity ratio and on the angle of incidence, similarly to light in optics, but also on buoyancy and driving pressure. Maccaferri et al. (2010) calculated the trajectories with a boundary element code (Sec. 4.5). a) Trajectories for dikes transiting from high to low rigidity, paths are relative to varying rigidity ratios, as declared in figure. b) Same as (a), but the dikes transit from a low to a high rigidity layer. c) Total (elastic + gravitational) energy released during propagation from high to low rigidity rock (panel a). d) Same as (c), but relative to panel b). Figure modified from Figs. 7, 8, 10, 12 in Maccaferri et al. (2010), with permission

Maccaferri et al. (2011) studies the trajectories of inclined dikes under different stratification scenarios by allowing for density layering that is independent of rigidity layering. Deflections similar to what described in Par. 5.5 are obtained only if there is a discontinuity in the rigidity. If only the density is discontinuous across a horizontal interface, the dike will continue in the same direction as it crosses the interface between the two layers of different density (Fig. 17B). The dike may stop if it experiences a state of negative buoyancy, but its leading tip will still penetrate significantly into the medium of low density (Fig. 17B, C.3). In this case, the typical inverse tadpole shape assumed during vertical ascent is replaced by a pointy profile.

It should be noted that the dikes are not allowed to extend in the third dimension in either of the models described above. The increasing pressure in the upper part of the dike will favor lateral, rather than vertical, propagation and thus instead of leading to sill inception the results by Taisne and Jaupart (2009) and Maccaferri et al. (2011) may feed results obtain by Pinel and Jaupart (2004) or Lister (1990a) dealing with horizontal migration of dikes.

5.7. Dike–dike interaction

Focusing of ascending, magma-filled dikes by dike–dike interaction was modelled numerically and experimentally by Ito and Martel (2002). In particular, Ito and Martel (2002) consider the deviation expected when an ascending dike feels the stress field due to a pre-existing, stalled dike. They find dikes will, in general, tend to interstect or merge to previously ascended dikes. In their numerical model, the contribution of external stresses and other parameters such as buoyancy and driving pressure is also included and is related to how effectively dikes focus and merge.

Building on this research, Kühn and Dahm (2008) combines the simulation of fracture propagation with dike interaction (Sec. 5.1). Dikes interact by adapting to the stress field caused by preceding dikes that arrested in the crust, which leads to focussing and crossing of dykes. The method is applied to study how magma chambers and sheeted dyke complexes may form at mid-ocean ridges. They find that interaction between dykes can have significant consequences under certain conditions: the interaction is small under lateral tension that is large compared to the pressure in the dike head; otherwise, dikes tend to attract each other and form large, magma-filled bodies or sill layers.

A

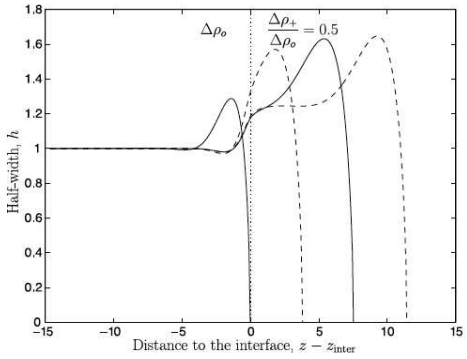

B

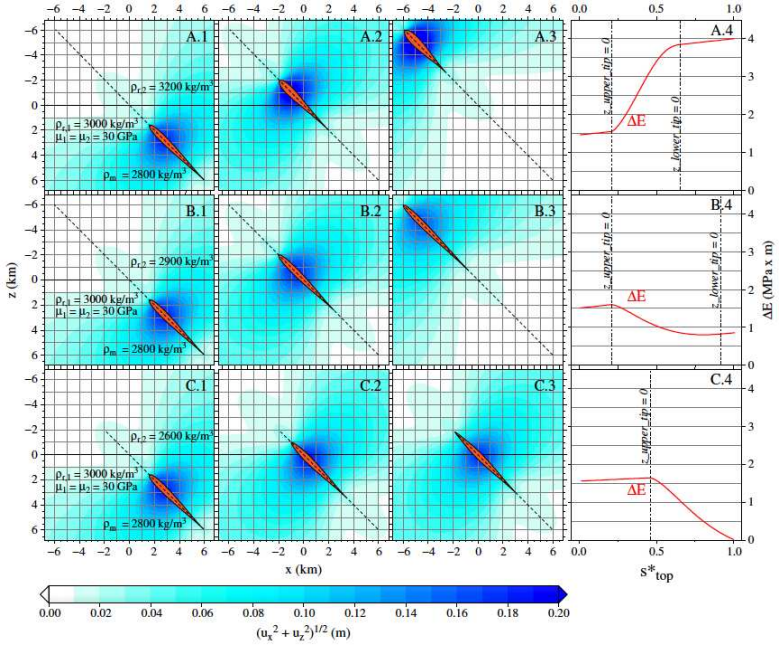

Figure 17: A) Results from a lubrication theory approach on dike propagation in a density-layered medium. The shape of a dike penetrating into a layer with reduced buoyancy is shown. The interface lies at $z = z_{\text{inter}}$ (vertical dotted line). Results are shown for various snapshots at fixed time interval. The nose region rapidly adjusts to new dimensions in the upper layer. Calculations are made for a dimensionless stress-intensity factor equal to 1, i.e., Kc/K* = 1. From Taisne and Jaupart (2009), with permission. B) In each row, successive snapshots are shown of a dike propagating in a medium made up of two welded half-spaces with different density. From Maccaferri et al. (2011), with permission. The viscous flow of magma within the dike is neglected, as in Weertman theory. Density of rock and magma are declared in the images, where ρ_{r1} and ρ_{r2} are the densities of the lower and upper half-space, respectively, μ_1 and μ_2 are the rigidities, ρ_m is magma density. The modulus of the displacement vector induced in the medium is shaded in the background. The dashed line represents the energetically-preferred path and the opening of the dike is exaggerated by a factor 1400. The final column shows the specific total energy release, plotted as function of a spatial coordinate along the dike path.

Dike–dike interaction has also been studied in relation to rifting episodes, where sequences of dike intrusions compensate the strain accumulated over centuries at divergent plate boundaries (see Section 5.8). For example, emplacement location of the dikes in the Manda-Hararo segment (Afar, Ethiopia) is found to be influenced by the location of previously emplaced dikes. In particular, dikes tend to emplace in locations where tectonic tension has either not yet been compensated by previous dikes (local opening minima) or has accumulated at their tips (Hamling, 2010; Grandin et al., 2010b). In this respect, dikes behave much like earthquakes: they occur in fault areas where stress has not been relieved by previous, recent earthquakes, or occur as aftershocks where stress has increased due to inhomogeneous slip or at the edge of faults (see also Sect. 5.8 below).

5.8. Scaling and dike sequences in rifting episodes

The scaling laws of earthquakes and main shock–aftershocks sequences have been the subject of great interest in literature. Dike sequences in rifting episodes offer a chance to compare earthquake sequences with a process similar in that it relieves accumulated tectonic stresses, but different in that a source of magma needs to be available to compensate for the volume of tectonic extension.

Buck et al. (2006) developed a numerical model to study main-dikes/after-dikes sequences in rifting episodes. The model includes the following features: (a) the relative tension associated with tectonic extension (the tensile stress gradient drives the dikes away from the magma chamber); (b) a compressive stress compensation produced by each emplaced dike (this has the role/effect of reducing the tectonic stress difference after each dike has been emplaced); (c) a magma chamber that undergoes a pressure drop during diking (this is responsible, together with the level of pre-existing tensile stress, for stopping the dikes); and (d) the existence of some threshold values of driving pressure required to initiate diking from the magma chamber (i.e. for the pressure in incipient dikes to be sufficient to overcome the fracture toughness of rock and continue propagation). Under these assumptions, the model predicts sequences of dikes that mimic many of the characteristics observed during rifting episodes, as observed during the 1975–1984 Krafla sequence, and the sequence in the Manda-Harraro segment of the East African Rift that started in 2005 (Wright et al., 2012).

Passarelli et al. (2014b) analyzed the statistics of rifting episodes at divergent plate boundaries and found that they have scaling characteristics that

are similar to mainshock–aftershocks sequences. The volumes of the dikes from rifting episodes are distributed according to a power law that mimics the Gutenberg-Richter magnitude–frequency relation found for earthquakes worldwide (Fig. 18), and the seismic moment released by the dikes as a function of time is consistent with the release rate of seismic moment through aftershocks (Omori law). The strong control from tectonic extension (for divergent plate boundaries this is likely dominant with respect to magma overpressure) and dike–dike interactions (see also Sec. 5.7) are inferred to be an important process controlling these scaling laws.

5.9. Fracturing, faulting, induced seismicity

Dikes and earthquakes interact in two main ways: (i) dikes induce faulting and earthquakes during propagation, and (ii) earthquakes on pre-existing faults or fractures influence propagating dikes. Here we review the main studies that link propagating dikes with faulting and fracturing. We discuss results specific to hydraulic fracturing in Sec. 6. In Sec. 3.1.3 we presented an overview of the main observations on dike-induced seismicity. From a modelling perspective, the mechanisms behind the generation of seismicity by propagating dikes has been investigated using a range of analytical, numerical, statistical and experimental approaches.

Buck et al. (2005) model numerically the generation of faulting by diking at mid-ocean ridges with the purpose of explaining the formation of abyssal-hill-bounding faults pervading the surface of the oceanic crust. As Buck et al. (2005) observe, given that dike intrusions occur at lower stress than is needed for faulting, many authors assume that faults at mid-ocean ridges form only during the time intervals between diking events when no magma is available for dike intrusion (Carbotte and Macdonald, 1990). However, this simple model does not fit more detailed observations related to the dip direction of the faults, their development as a function of distance from the axis and the presence of complex structures at the intersection of ridges and transforms. In the model by Buck et al. (2005) faults develop where the stress overcomes brittle yielding. Elastic, viscous and brittle-plastic deformation accompanying isostatic balancing due to density changes is taken into account. The role played by dikes in the models is central but it can be simplified to columns of magma intruding at the axis at regular time intervals. The models examines end-members (buoyancy- vs. stretching-dominated ridges, leading to axial highs and valleys, respectively) and the proportion of extension accommodated by diking.

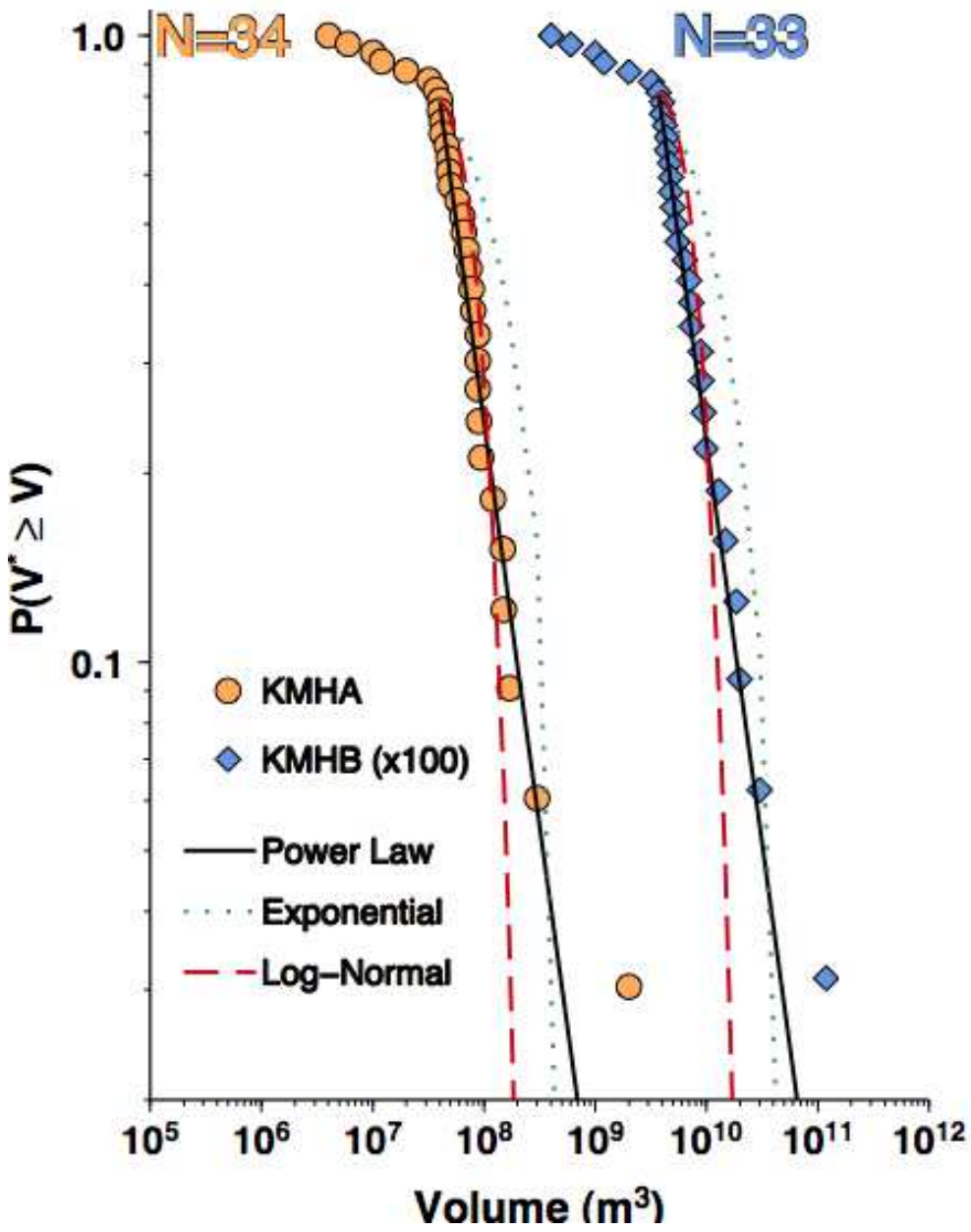

Figure 18: The frequency–total volume distribution of dikes from the Krafla and Manda-Hararo rifting episodes follow a power law, analogous to the Gutenberg-Richter relation for aftershock sequences. From Passarelli et al. (2014b), with permission.

The seismicity linked to dike intrusions is known to be related to advance of the crack tip, but it is also known to mirror the response of the surrounding rock to the deformation and stresses induced by the magma intrusion (see e.g. Rubin and Gillard, 1998; Traversa et al., 2010). Rubin and Gillard (1998) examine the stress field induced by a propagating dike in a bid to explain the origin of dike-induced seismicity. They include a dike-tip cavity in their model and study the stress field in its proximity. The tip cavity is a low pressure zone where magma cannot penetrate quickly and may attract fluids from rock pores. Seismicity is found to be most likely around this area, provided that pre-existing, favorably oriented fractures exist. Rubin et al. (1998) studied the seismicity induced by the 1978 and 1984 dikes at Kilauea. They observe that the spatial distribution of dike-induced earthquakes reflects areas where the differential stress is high and does not necessarily reflect the real extent of the dike. They also observe repeating seismic events coming from the same fault patch. This observation has recently been confirmed by Jakobsdóttir et al. (2008) and White et al. (2011), who observed earthquakes of inverse polarity coming from the same patch, meaning that the same fault patch (or two patches very close spatially) experienced slip in opposite directions within short time intervals (seconds or minutes).

Rivalta and Dahm (2004) develop a boundary element model for a dike embedded in a fractured medium. In this model a pressurized dike interacts with randomly distributed fractures that are also interacting with each other. The dike opening is calculated as a function of the density of fractures. The weakening and inhomogeneities represented by the fractures cause an increased, irregular opening profile in the dike, as described qualitatively by Ida (1992) (Sec. 5.12). The average dike opening from the numerical model agrees with predictions from effective media theory, which assumes a fractured medium to be homogeneous but with modified, effective elastic parameters (Davis and Knopoff, 1995; Dahm and Becker, 1998). These can be obtained as a function of fracture density by solving a differential equation. The model is applied to explain post-intrusion seismicity and deformation for the 2000 dike intrusion at Miyakejima. The deformation and the seismicity are found to be linked through an exponential law during the post-intrusion phase. Rivalta and Dahm (2004) conclude that progressive weakening of a medium due to diffuse seismicity may induce additional opening in the dike, if more magma is available. This, in turn, feeds back to the generation of more seismicity. A different relation was found for the aftershocks and deformation following earthquakes. Savage and Yu (2007) found a linear relation

between the number of aftershocks and amount of post-seismic relaxation for the first 160 days following the Chengkung earthquake and for the first 560 days following the Parkfield earthquake. The difference between the response of rock to diking and faulting may be due to the presence of friction on faults. On the contrary, dikes are frictionless fractures and the dike walls are free to deform for some time after the intrusion. The model by Rivalta and Dahm (2004) is static; no attempt has yet been made to model numerically dike propagation in a fractured medium (but see Le Corvec et al. (2013) for an experimental study of fluid-filled fracture propagation in a faulted medium).

Our understanding of the source-physics of earthquakes has informed the development of theories for how dikes induce seismicity. The rate-and-state theory of friction on a fault (Dieterich, 1994) links a local Coulomb stress change (defined as the shear stress diminished by the friction times the normal compressive stress) to a change in the seismicity rate. This theory provides a link between models of dike shape evolution during propagation and observables related to seismicity. It has been used to make inferences on the correlation between the amount of seismic energy release during dike-induced earthquake swarms and the rate and volume of propagating magma: (Pedersen et al., 2007) show how the relationship between volume change and earthquake rate varies greatly between different intrusions and is strongly linked to the background stress state or background seismicity rate. The equations of the theory are solved for time-dependent stressing (which is what occurs during dike injections) by many authors (see e.g. Dieterich et al., 2000; Segall et al., 2006; Hainzl et al., 2010; Maccaferri et al., 2014). The calculation of Coulomb Stress changes and of changes in the seismicity rate with the rate-state theory are rich with details that are beyond the scope of the present review (see instead Harris (1998); Stein (1999); Cocco et al. (2000); Hainzl et al. (2010); Toda et al. (2012) for Coulomb stress studies and tools and Dieterich et al. (2000); Toda and Stein (2002); Segall et al. (2006); Maccaferri et al. (2013); Segall (2013) for dike-related applications of the rate-state theory). The 2D nature of most numerical models of propagating dikes restricts applications of Coulomb stress studies and rate-state theory to 2D, with the resulting uncertainty that adding a third dimension may change the results in a significant way. A promising application is described by Segall et al. (2013), who shows how inversions of crustal deformation data can be combined with rate-state earthquake nucleation theory (Dieterich, 1994) to get an improved picture of the shape of a propagating dike.

Using data from the 2000 intrusion at Miyakejima, Passarelli et al. (2014a) studied the relation between double-couple fault plane solutions of induced earthquakes, the Coulomb stress induced by the dike and the statistics of the earthquakes. They find that the focal mechanisms match well with the optimally-oriented planes for the 3D Coulomb stress change around an elliptical penny-shaped dike, resulting in a strong correlation between rake, strike and dip of the earthquakes, smoothly varying around the dike edges. They also find that earthquakes with a predominantly strike-slip mechanism follow the usual Gutenberg-Richter statistics for tectonic earthquakes, while predominantly normal faulting mechanisms lack in proportion large magnitude events. According to the pattern of the Coulomb stresses, such normal faulting earthquakes are expected to occur mainly in the crustal layer above the dike. A lack of large magnitude events may occur because of a limited thickness of such a layer, limiting the physical dimension of the faults, or, alternatively, because of the decreased strength of the rock in shallow layers, so that the ability to sustain large stress accumulation is limited.

A new seismological approach has been applied at Piton de la Fournaise volcano to track magma motion during an intense seismic swarm. It is based on seismic wave attenuation, and on the theory that ratio of radiated energy between 2 stations is a function of the location of the source. Any time evolution of this ratio can be confidently interpreted in terms of migration of the source, namely the propagating dike. Application of this method to Piton de la Fournaise shows that the dynamics of propagation is complex, with variation in upward velocities punctuated by phases of arrest (Taisne et al., 2011a).

5.10. Coupling of magma chambers and dikes, connectivity, induced deformation

The behaviour of dikes is controlled by their hydraulic connectivity to a magma reservoir. This control is so important it was the basis for a classification of dikes into two types Nakashima (1993): dikes fed by a magma chamber versus propagating, isolated magma pockets. To understand why these two categories exist, we must ask what are the conditions under which a dike nucleated from a magma reservoir may hydraulically separate from it? Key factors include the rheology of the host medium, the temperature difference between magma and host rock, the viscosity of the magma, and the distance between the dike tip and the chamber. We know that shallow dikes nucleated from magma reservoirs in the elastic crust will be coupled to the

magma reservoir for at least some of the propagation distance. For example, the 2000 intrusion at Miyakejima continued to thicken for weeks after being arrested at several km distance from the magma chamber (Nishimura et al., 2001), implying that connectivity may be large even in cases where magma chamber and dike tip are widely separated. Quantitative evidence of the coupling between magma reservoir and dike was presented by Tryggvason (1984), who made a careful comparison of dike widening-related volume increase and magma chamber volume loss for the first dikes from the 19875–1984 Krafla rifting episode. An early model about chamber-dike coupling is by Mériaux and Jaupart (1995). The model includes a pressurised reservoir shaped as a funnel with elliptical opening connected to a fissure. Rock fracturing is neglected in the model and the governing equations are solved for the pressure and the fluid flux as functions of reservoir size and magma supply rate to the reservoir. High supply rates and small chamber sizes lead to small amounts of magma flowing into the fissure and therefore to larger reservoir pressurization and magma volume stored. The delay time between the onset of reservoir inflation and the opening of the fissure decreases with increasing reservoir size. Rapid deflation of the reservoir occurs if the supply rate decreases with time.

Inverting measurements of surface deformation associated with dike intrusion has provided useful insight into the characteristics of the dike. Mostly, such studies have offered only a static picture of the emplacement process. Crustal deformation data can sometimes be used to constrain the dynamics of dike propagation, but models attempting to invert time-dependent deformation are rare. Even less common are inversions that employ physics-based models, which can be used for a better understanding of dike dynamics and of the interaction with other deformation-inducing sources such as major faults and magma chambers.

Segall et al. (2001) develops a time-dependent dike growth model to explain the decreasing rate of volume change of the dike during the 1997 intrusion at Kilauea. Simple models of dikes fed at constant pressure or constant inflow from magma chambers do not predict a decreasing volume rate and could not be applied to the intrusion. Segall et al. (2001) observe that the rate of volume decrease at the magma chamber mirrored the volume increase at the dike, suggesting that the growth was limited by the ability of the chamber to sustain pressure during the intrusion. Their model suggests that eruptions during intrusion are favored by compressive stress regimes, large, compressible reservoirs, and high connectivity between chamber and

dikes. Magma level changes at Pu'u O'o lava lake, hydraulically connected to the magma chamber, were also used to give an estimate for its total volume, around 20 km^3. Rivalta and Segall (2008) collected evidence of large mismatches between observed volume changes at magma chambers and dike volumes during intrusion events. Dikes are often observed as having a much larger volume than the volume change at the feeding reservoir. They suggested that magma compressibility and the different elastic compression of the host medium for different magma chamber shapes are responsible for this discrepancy. Blake (1981), Sigmundsson et al. (1992), Johnson et al. (2000) had already recognized that volume changes at spherical magma chambers do not correspond to the true volume of magma injected or extracted, because the compression/decompression of the much larger volume of magma residing in the chamber compensates some of the volume injected/extracted.

Further studies focused on solving the flow of magma between coupled magma-filled structures. Rivalta (2010) developed a model of the pressure drop during mass transfer from a chamber to a dike and found evidence for such a coupling for several lateral dike propagations, as demonstrated by the pressure drop at the magma chamber and the synchronous volume gain by the dike. The coupling was probably active for the total propagation time for two of the after-dikes of the sequence at the Manda Harraro segment, Afar, Ethiopia, (propagation time in the range of about 3–16 hours), for the 1997 dike intrusion at Kilauea volcano, Hawaii, (about two days) and for the 1978 dike intrusion at Krafla volcano, Iceland. As for the 2000 intrusion at Miyakejima, Japan, the dike was pressurised by the chamber at least for the first 12 hours of propagation but it is unclear whether it continued for the total propagation time of about a week. It is possible that other driving forces, such as the topographic load, assumed a greater role in the later stages of the propagation so that the coupling, although still present, lost its importance.

Tarasewicz et al. (2012) develop a model for how the connectivity between magma storage zones at different depth may evolve during volcanic activity. During the 2010 Eyjafjallajökull eruption in Iceland, seismic activity was observed to counterintuitively propagate downwards over about 30 km depth and ten weeks time of volcanic unrest. Systematic changes in the petrology of the magma suggest a multilayered plumbing system. Tapping of each of the individual storage zones preceded an explosive surge in eruption rate. Tarasewicz et al. (2012) explain these systematics in terms of a decompression wave that triggers magma release from progressively deeper

sills in the crust.

Segall et al. (2013) present a method to combine the information from crustal deformation and from the seismicity linked to a propagating dike in order to obtain the time-dependent distributed opening of the dike. The method is based on linking deformation (and thus stress changes) to the induced seismicity rate through the rate-state earthquake nucleation model (Dieterich, 1994). The dike is modeled as a horizontally extending rectangular crack in an elastic half-space, subject to spatially uniform but time-dependent overpressure. Some forward models are presented with the expected hypocenters of induced earthquakes (Fig. 19). These forward models show that time-dependent seismicity rate behaves differently for rock volumes above or below the dike or at intermediate depth (adjacent to the dike). Similar space-time patterns have been observed in nature (Sect. 3.1.3) and in industrial operations, see also model by Dahm et al. (2010). The method is then applied to the 2007 Fathers Day lateral intrusion in Kilauea Volcano. Segall et al. (2013) find that it is difficult to fit both deformation and seismicity with a simple dike model with a horizontal propagation and a vertical tip line. In particular, the location of the dike's bottom edge relative to the deep part of the migrating seismicity cloud is difficult to constrain. The approach is very promising in that it integrates physics-based knowledge with observations.

5.11. Dike arrest

Why and how a dike ceases to propagate is a central question in volcanology. In this manuscript we have already explored the case of arrest due to a stress barrier caused by a volcanic load (Sec. 5.2) or by layering (Sec. 5.5). Magma solidification within the dike (Sec. 5.14) and faulting on pre-existing or dike-created structures (Sec. 5.9) are also thought to be potential causes of dike arrest. Furthermore, pressure decrease at the magma chamber has been shown to cause dike arrest (Rivalta, 2010). This issue merits some attention from numerical modeling in the future, as there are many unanswered questions.

Qin and Buck (2008) discuss partial stress release during diking. This can originate from limited magma supply when the dike is coupled to a magma chamber and results in an upper limit on the width of dikes. Multiple dike intrusions may then be required to release the entire accumulated stress (Sec. 5.8).

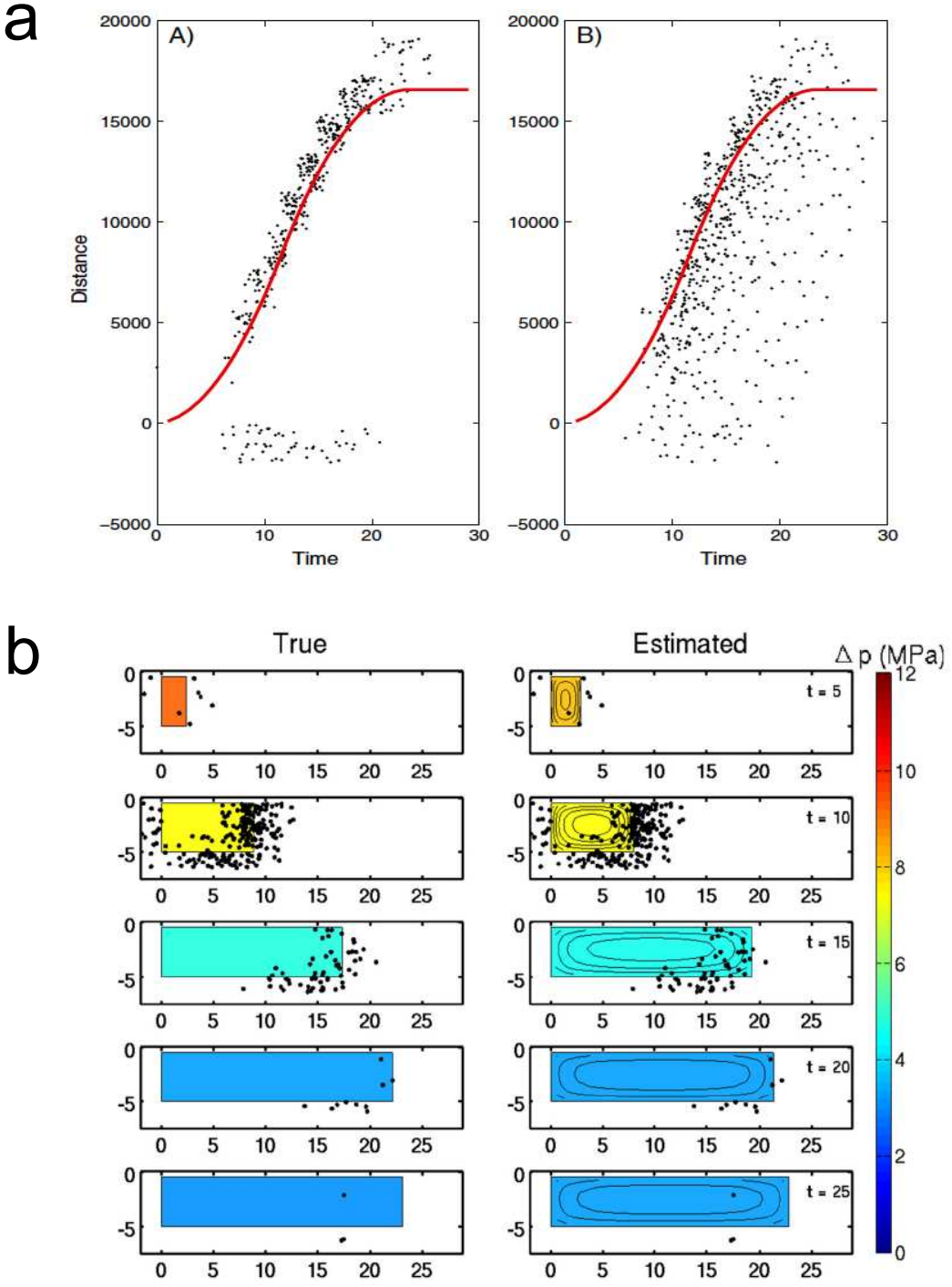

Figure 19: a) Predicted space-time hypocenter distribution (A) adjacent to dike and (b) below the dike. Red curve represents position of propagating dike tip. Fig. 5 from Segall et al. (2013), with permission. b) Side view of simulation results: comparison between (left) input dike model and (right) that estimated from inversion. Color maps dike overpressure; contours in right column are curves of constant dike opening. Fig. 8 from Segall et al. (2013), with permission.

Baer (1991) examines dike exposures in the Ramon area of Israel and calculates the stress intensity factor for an extension crack approaching a mechanical interface. He concludes that dike segmentation and arrest are controlled mainly by local stresses, shear moduli differences between adjacent layers, and, partly, by bedding plane slippage. Taisne et al. (2011b) explore 3-dimensional effects using laboratory experiments on a constant-volume, vertically propagating dike and consider the conditions under which to expect dike arrest and/or horizontal extension. They also investigate the behavior of a dike penetrating into a low density layer using numerical analysis. From both analyses they predict the minimum volume of magma that must be injected into the dike for an eruption to take place. A more complicated situation occurs in the intrusion of dikes into sedimentary, porous rocks, where fluidization of rock is induced by pore pressure increase, causing fingering in the shape of the dike (Sec. 5.13).

5.12. Predicting vent locations and times of intrusions and eruptions

Even if volcanoes often give notice of unrest through seismic activity, deformation or unusual degassing, knowing when and where an eruption could occur has not been an easy task in volcanic hazard. Significant effort has been devoted in identifying the temporal and spatial pattern of eruptions and understanding the physical mechanisms controlling the creation of eruptive vents. One of the topics currently under investigations is monogenetic volcanism, where volcanic fields are composed of tens of volcanic vents created and occupied by only one eruption.

Ida (1992) presents a model for the variation in opening width along a magma-filled fracture, assuming laminar flow of an incompressible fluid. He correlates the formation of fissures, polygenetic volcanic edifices or monogenetic vents to the changes induced in the width of the dike by the specific tectonic settings. A variable width along dike length leads to preferred locations for magma erupting at the surface. He also observes that various degrees of inhomogeneity in the crust lead to a non-uniform increase in width that may evolve in separated vents. Ida (1999) models dike growth by assuming a fissure with opening constant over length but not constant in time. The dike is coupled to a magma chamber (see Sec. 5.10) and the opening is affected by elasticity and the external tectonic stress. Tip processes are neglected completely but discussed thoroughly. The model is used to evaluate the effect of the external stress field on whether the dike will erupt or form and intrusion. He finds that extensional stress conditions favor growth only until

a limited length, while compressive or moderately extensional stresses favor 'unlimited' growth until the dike erupts. The model is applied to explain trends in deformation data from Izu-Tobu and Izu-Oshima, Japan.

Pinel and Jaupart (2004) study the influence of volcano loads on the extension of shallow dikes, distinguishing three regimes: (1) eruption through the summit, occurring when the load is not very significant and magma is buoyant, (2) storage beneath the edifice, occurring when the load is large and magma buoyancy is not very high, (3) horizontal propagation to feed a distal eruptive vent, which can only be achieved if the load by an edifice prevents eruption in the dike nucleation area and if magma is negatively buoyant at shallow depth. The model explains the distribution of erupted products which show decreasing magma evolution with increasing distance from the focal area.

Segall (2013) reviews the conditions under which dike intrusions may be predicted from inflation–deflation patterns at the magma chamber. He concludes that in general, it is not possible to define a threshold in the amount of inflation that would immediately lead to the rupture of the magma chamber's walls and the initiation of an intrusion. The main reason for this is that the stress conditions in the host medium are likely to be changed by each intrusion, which will relieve some of the tectonic tensile stress (see also Sec. 5.8). Indeed, the level of inflation related to dike initiation differed for each intrusion during the 1975–1984 Krafla rifting episode (Sturkell et al., 2006).

5.13. Segmentation

While models typically assume stable propagation of a dike's leading edge, segmentation and fingering instabilities are predicted by theory and observed in the field and laboratory. Segmentation, which here refers to out-of-plane bifurcation of the dike front and which can lead to observed en-echelon dikes, is commonly interpreted to result from rotation of the stresses or, equivalently, from a mixed mode of fracture, opening (Mode I) and tearing (Mode III) of the dike tip (Pollard et al., 1975, 1982). This interpretation draws its original inspiration from the laboratory experiments performed in glass by Sommer (1969), who showed that under mixed-mode mechanical loading the segmentation occurred when the stress rotation angle was greater than a threshold value of about 3.3 degrees which, according to the formulae presented by Pollard et al. (1982), corresponds to a ratio of the Mode III stress

intensity factor K_{III} to the Mode I stress intensity factor K_I of $\approx$ 0.05–0.10, depending on the ratio of the extensional to the shear stresses. However, more recent experiments wherein fluid-driven cracks were subjected to mixed Modes I–III loading have shown that segmentation can occur at even lower ratios, i.e. with $K_{III}/K_I \approx 0.01$ (Wu et al., 2009). Furthermore, it can be shown that the angle of the segments relative to the overall strike of the array of en echelon dikes is related to the stress rotation angle and extensional to shear stress ratio (Pollard et al., 1982). As a consequence, the morphology of en echelon dikes can be used to aid in the interpretation of paleostresses; however, experiments have demonstrated that the twist angle of the segments is overestimated by theory (Cooke and Pollard, 1996). Well known examples of segmented dikes include the petal-like morphology of the dikes near Ship Rock, New Mexico, USA (Figure 20a) (Delaney and Pollard, 1981; Delaney et al., 1986).

Another mechanism, which is potentially applicable to a similarly wide range of settings, has been identified through recent analysis and experimentation (Figure 20b). That work shows that an emergent finger-like morphology can also be related to an instability to transverse perturbations of a buoyancy-driven ascending dike front (Touvet et al., 2011). Such perturbations can naturally arise from heterogeneity in the rock properties at a scale comparable with the dike thickness, and therefore should be ubiquitous in natural host rocks. For California's Inyo dike, it has been argued that segmentation is driven by variations in the host-rock rheology and fracturing style (Reches and Fink, 1988).

5.14. Heat exchange, cooling

Heat transfer between magma in dykes and the host rock is interesting for a number of reasons. First, cooling of the magma in propagating dykes is thought to be one of the factors inducing deceleration and arrest (Fialko and Rubin, 1998). Second, dyke intrusions heat and weaken the crust or lithosphere (Havlin et al., 2013), influencing processes ranging from the accumulation of cooled intrusions below volcanic edifices to crustal thinning in continental rifts.

Solidification of magma flowing in an open conduit has been studied by Delaney and Pollard (1982); Bruce and Huppert (1990); Lister (1994a,b). Lister and Kerr (1991) state that solidification, or a step in viscosity, of the magma would have comparable effect on the propagation as an increase of fracture toughness. Rubin (1993b) and later Bolchover and Lister (1999)

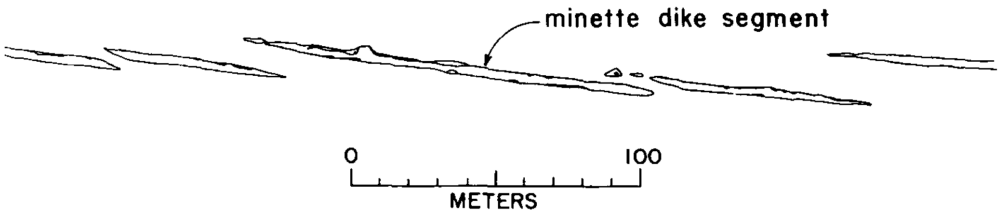

a)

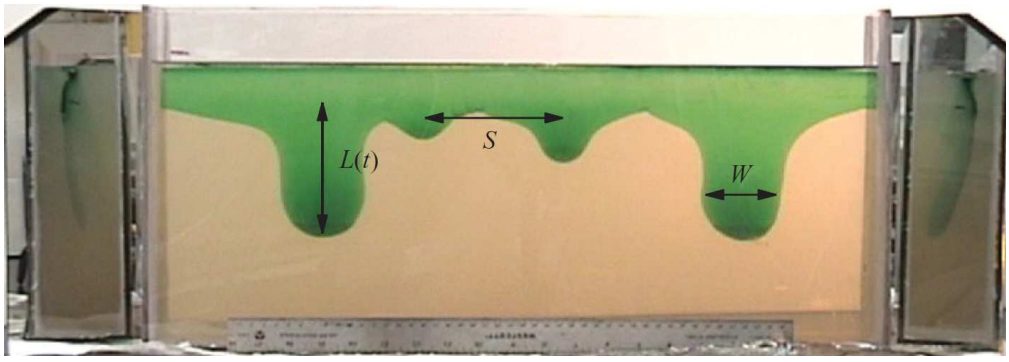

b)

Figure 20: Two types of segmentation. a) Map of part of minette dike near Ship Rock, New Mexico, from Delaney and Pollard (1981), b) Fingering instability of negatively buoyant analogue dike in gelatine, from Touvet et al. (2011).

study the early stage of a propagating magma subject to solidification and derive a critical length below which solidification prevents propagation. Taisne and Tait (2011) conducted experiments involving magma solidification during migration. They found that despite a constant flux of injection, the propagation occurred in successive steps alternating with a phase of arrest associated with inflation. In those experiments the average behavior of the propagation could be captured through the surface-creation rate, rather than the upward propagation rate. The authors compare the surface-creation rate to the rate of seismicity associated with magmatic intrusion and show how this approach may lead to early estimation of the physical conditions driving the injection, such as the volumetric flow of magma injected.

Heat transfer is an important process during the evolution of continental rifts. Bialas et al. (2010) developed a 2D numerical approach to investigate the relation between the volume of magma intruded into dikes and the amount of lithospheric weakening. The simulations consider the available rifting force and the lithospheric structure (including a depth- and temperature-dependent rheology) and a boundary element model for the dikes based on Crouch and Starfield (1983) and Weertman (1971a). The amount of magma (and total dike thickness) needed to weaken the lithosphere is discussed in terms of model parameters as well as the conditions under which magmatic or amagmatic rifts develop on Earth.

Daniels et al. (2014) obtained numerical solutions to the conservation of energy equation to quantify the transfer of heat from dikes to the continental crust during rifting. The thermal models are benchmarked against a priori constraints on crustal structure and dike intrusion episodes in Ethiopia. The study finds that through sequences of dike intrusions, the crust heats and weakens rapidly (in less than 1 Ma). The model is applied to the Main Ethiopian Rift (MER) and to the Red Sea rift (RSR) in Afar, which show a different elastic thickness and seismogenic depths. By applying the heat transfer models to these constraints, converted into constraints for crustal temperatures, Daniels et al. (2014) calculate that no more than half of the MER extension since ≈2Ma has been accommodated by dike intrusion.

5.15. Volatile exsolution and fragmentation in dikes

In recent years there has been significant progress in modelling the evolution of the physical properties of magma with changing pressure in a reservoir Mastin and Ghiorso (2000); Dobran (2001); Huppert and Woods (2002); Sahagian (2005). However, models of dike propagation that include such

systematics are rare and, in particular, the effect of gas exsolution on a propagating dike remains poorly understood. In general, three directions have been taken: modeling the bulk effects on compressibility of bubble formation, without entering in the details of phase transitions; modeling the dynamics or the effects of a gas pocket at the top of the dike; coupling gas exsolution laws with the equations of flow for the magma.

Pioneering work by Lister (1990b) shows how the accumulation of gas at the tip of the dike affects its shape. These results were obtained by assuming a stationary solution and therefore do not account for the effect of decompression as the dike ascends. Following the experimental work done by Menand and Tait (2001), Maimon et al. (2012) model a gas pocket at the top of a propagating dike. They find that any gas pocket forming by ascent and accumulation of bubbles within the dike will propagate at a faster speed than the magma below, and will escape the dike by fracturing the rock ahead.

For viscous magma, and neglecting the motion of the bubbles into the magma, Taisne and Jaupart (2011) shows that compressibility and fragmentation processes lead to counterintuitive results. The mass conservation in the system can be written as $\rho_m W \Sigma = Q$, where ρ_m represents magma density, W the mean upward velocity, Σ the cross section of the dike and Q the mass flux. This could be re-written as a volume conservation, such as $Q/\rho_m = W\Sigma$. This way, it is easy to see that a decreasing density will induce either an increasing velocity with thinning of the dike, or a decreasing velocity with fattening of the dike. In order to understand this behavior we can write the modified Navier-Stokes equation as follows:

$$\frac{\partial P_e}{\partial z} = -\frac{3\mu}{2h^3}\phi + (\rho_s - \rho_m)g\,, \tag{36}$$

where the two terms on the right-hand side represent the viscous pressure drop and the buoyancy. This equation shows that the viscous pressure drop tends to decrease the elastic pressure gradient and that this gradient is maximized when viscosity is negligible, while buoyancy tends to increase it. Assuming a viscous mixture of magma and gas, the continuous increase of the buoyancy induced by the decompression of the rising magma will induce a thinning and increasing velocity of the propagating dike. While approaching the surface, the gas volume fraction will increase and fragmentation may occur within the propagating dike. In this case a sudden drop in viscosity occurs because the mixture will change from magma bearing bubbles to gas bearing droplet of magma, inducing an increase of the elastic pressure

gradient.

This gradient is maximized when viscosity is negligible, thus the elastic pressure gradient in the fragmented region is greater than the one in the viscous region. This explains why we have an inflation of the fragmented region with respect to the viscous region, and why deceleration in the propagation is induced by the fragmentation. In other words that increase of elastic pressure within the fragmented region induce inflation that allow magma accumulation without involving thinning and acceleration.

5.16. Coupling to the asthenosphere

In many settings where magma traverses the lithosphere and crust in dikes, the magmatic source is located in the asthenosphere. Magma transport within the asthenosphere is thought to be by flow through the permeable network of pores between mantle grains (e.g. McKenzie, 1984; Scott and Stevenson, 1986; Spiegelman and McKenzie, 1987); under this theory, magma ascends by porous flow to the base of the lithospheric cold thermal boundary layer. The behaviour of the magma at the base of the lithosphere remains an open question. Sparks and Parmentier (1991) considered magmatic interaction with the bottom of the lithosphere, where the conductive geotherm above intersects the geotherm of the approximately adiabatic mantle below. Here the temperature of the magma/mantle system drops below the melting temperature, creating a barrier to porous flow that has typically been considered as impermeable. This barrier is thought to stall the ascent of melts, creating a boundary layer where magma accumulates with an overpressure due to its buoyancy. If the boundary is sloping, the gradient of this overpressure has a horizontal component that drives magma to migrate laterally (Sparks and Parmentier, 1991). A thermo-mechanical instability (Katz, 2008) or mantle heterogeneity (Katz and Weatherley, 2012) can interrupt this lateral transport and cause melt to pool at the base of the lithosphere, where magmatic overpressure may become large.

Magmatic overpressure in this setting should lead to dike propagation into the lithosphere above. Until recently, however, models of diking and brittle failure were distinct from models of porous melt migration. Work by Havlin et al. (2013) and Keller et al. (2013), taking two different approaches, addresses this disconnect and seeks to quantify the magmatic interaction between the asthenosphere and the lithosphere. Havlin et al. (2013) consider a model in which a one-dimensional asthenospheric column feeds

magma upward by porous flow to an impermeable boundary, where a decompacting boundary layer develops with increasing porosity and overpressure. Dike initiation and propagation from this boundary layer are modelled by theory simplified from Lister (1990b), Meriaux and Jaupart (1998), and Roper and Lister (2005). Magma accumulates until the overpressure reaches a critical value given by $P_{\text{crit}} = K_c/\sqrt{h} - \sigma$, where $K_c = 1$ MPa is the critical stress intensity factor, h is the height of an incipient dike, and $\sigma = 5$ or 10 MPa is the ambient tectonic stress normal to the dike (tension positive). Havlin et al. (2013) assume the pressure gradient within a propagating dike is balanced by buoyancy forces and viscous resistance to flow; they then compute the magmatic flux Q that satisfies this balance and also matches the reservoir overpressure P_d and dike-tip criterion for propagation. The overpressure in the decompaction layer evolves with time according to a pressure diffusion equation for a compressible, poroelastic material (e.g. Brace et al., 1968; Wong et al., 1997). The dike and the decompaction layer are coupled by matching Q and P_d, giving a consistent model that predicts the growth of dike height based on magmatic flux and volume conservation. Dike growth ceases when the dike freezes across or when the dike-magma flux goes to zero. The reservoir overpressure then grows steadily until it again reaches the critical value; the duration of the complete cycle is used to define a dike-reccurance time interval as a function of system parameters. Havlin et al. (2013) then use the recurrence interval, predicted dike spacing, and total dike volume to compute a volumetric flow rate out of the asthenosphere and into the lithosphere. This, in turn, implies a heat flux that they use to predict the thermal erosion of the lithosphere.

The strength of the approach of Havlin et al. (2013) is that it uses symmetry assumptions, analytical methods, and approximations to bridge scales of magmatic accumulation in the asthenosphere (10^3–10^4 m, 10^4–10^5 yr) to scales of transport through dikes in the lithosphere (10^{-2}–10^2 m, 10^{-3}–10^{-2} yr). However these idealisations also give rise to an important weakness: an inability to model the heterogeneous conditions present in a more realistic view of the lithosphere/asthenosphere system. These strengths and weaknesses are reversed in the approach taken by Keller et al. (2013), who extend the formulation of McKenzie (1984) and Bercovici et al. (2001) to incorporate a visco-elasto-plastic rheology with an effective stress principle (Terzaghi, 1943; Skempton, 1960). Here the idea is to capture a broad range of magma/mantle interaction, from viscous deformation to brittle/elastic diking and faulting, within a single, continuum formulation. Solutions to the

nonlinear system of governing equations are obtained numerically. Model behaviour is studied through a series of test-cases where a pool of magma is injected at the bottom boundary of a ∼4×6 km domain filled with homogeneous solid that is subject to an imposed extensional strain rate of 10^{-15} sec^{-1}. These calculations show three categories of roughly distinct behaviour depending on the imposed viscosity of the host rock. The first of these corresponds to distributed, viscous deformation of low-viscosity asthenospheric mantle (10^{18} Pa s), which has been previously modelled. At moderate host-rock viscosity (10^{21} Pa s), magmatic transport becomes localised into channels caused by large magma overpressure at small shear stress. This may be considered an intermediate regime before dikes emerge in the case of the high host-rock viscosity representing mantle lithosphere (10^{22} Pa s, resulting in extensional stress of ∼10 MPa). In this latter case, elasto-plastic deformation associated with tensile failure is dominant, and a sub-vertical, melt-rich crack propagates upward at low magmatic overpressure. At the highest imposed viscosity (10^{23} Pa s), tensile and shear failure combine to localise deformation onto a system of dikes and normal faults. Keller et al. (2013) go on to consider lithospheric models with depth-dependent strength profiles of the crust and lithosphere that produce complex patterns of deformation and melt transport from the asthenosphere into dikes and faults.

Due to limitations of model resolution, dikes in the models of Keller et al. (2013) actually have a porosity of ∼25% and a width that is one or two grid cells (∼40 m); the viscous resistance to flow within them arises from the Darcy drag term in the governing equations. Hence these dikes behave differently from classical models of dikes as fluid-filled cracks. In particular, they are much wider and grow much slower than those modelled semi-analytically by Havlin et al. (2013), despite the fact that both studies consider the same range of extensional tectonic stress. And because Keller et al. (2013) do not consider thermal evolution in their formulation, their dikes cannot freeze, and hence do not have a recurrence interval, making it difficult to compare with the long-term behaviour predicted by Havlin et al. (2013). However, numerical simulations provide the flexibility to model complex lithospheric architecture and spatially variable magmatic sources. Finally, both approaches neglect the (thermo)dynamics of the narrow, transitional zone between pore-hosted and dike-hosted melt transport, where temperatures remain on or near the solidus; Havlin et al. (2013) formally neglect this transion while Keller et al. (2013) do not resolve it. The consequences of this deficiency

are unknown because there is little (if any) understanding of the dynamics localised in this zone.

Despite their shortcomings, these two studies represent complementary approaches to coupling magma transport through the asthenosphere and lithosphere. They seem to initiate two avenues of research leading toward models of (for example) off-axis volcanism at mid-ocean ridges, batholith emplacement, continental rifting, and the seismic character of the lithosphere–asthenosphere boundary.

6. Investigation along with industrial hydraulic fractures

Although hydraulic fracture can provide a useful analogue for diking, it is worth emphasising that dikes and industrial hydraulic fractures differ in a variety of ways. Magma can solidify during dike propagation so that a complete model should consider the coupling between these processes. Buoyancy forces typically drive dike propagation and but not hydraulic fractures. Industrial hydraulic fractures are driven by fluids that are orders of magnitude less viscous; leak-off of fluid into the surrounding formation is typically important for industrial hydraulic fractures and expected to be negligible for dikes; industrial hydraulic fractures attain maximum volumes that are orders of magnitude smaller than dikes.

Still, there are many similarities between the mechanisms driving dike propagation and industrial hydraulic fractures. Both processes are fundamentally fluid-driven cracks and are typically modeled by the coupled equations of elasto-hydro-dynamic crack propagation, described in Section 4.3. Both processes result in induced seismicity and microseismicity. Both processes can result in the formation of essentially single features, i.e. a localized dike or hydraulic fracture, or they can result in a swarm or network of fluid-driven cracks. Both dikes and hydraulic fractures can be altered in their propagation when they encounter barrier layers or faults. These issues are explored in more detail in the subsections that follow.

There is a broad synergy between the study of dikes and hydraulic fractures. Not only are the mechanisms similar, these studies are naturally complementary because dikes provide detailed, mappable data regarding the final configuration attained by fluid-driven cracks, albeit with relatively little known about the boundary conditions associated with the system that resulted in the observed geometry. And while the boundary conditions are

well known for industrial hydraulic fractures, the final geometry is never directly observable (with the exception of experiments in which hydraulic fractures are placed ahead of the advance of a mine and then directly mapped (Elder, 1977; Lambert et al., 1980; Warpinski et al., 1982; Warpinski, 1985; Warpinski and Teufel, 1987; Diamond and Oyler, 1987; Steidl, 1991; Jeffrey et al., 1992, 1995; van As and Jeffrey, 2002; Jeffrey et al., 2009)). Hence, dike and hydraulic fracture studies are complementary because the quality of data and data gaps for each case are the complement of the other.

6.1. Growth barriers

Growth barriers are of great interest both to dike propagation and hydraulic fracturing. In dike propagation, layers that serve as growth barriers control the potential for arrest of ascending dikes and therefore are among the most important considerations in predicting volcanic hazards (Gudmundsson et al., 1999; Gudmundsson, 2005). Furthermore, growth barriers are essential for understanding the transition of dikes to sills (Rivalta et al., 2005; Kavanagh et al., 2006; Maccaferri et al., 2011; Taisne et al., 2011b) and the concomitant potential for magma-chamber formation (Gudmundsson, 2011a).

In industry, the issue of vertical propagation of hydraulic fractures is referred to as "height growth" because it deals with the limitations to the vertical extent, or height, of vertically oriented but laterally propagating blade-like hydraulic fractures in the presence of bounding layers that serve as partial impediments to vertical propagation. In this context, ascertaining the presence, or lack thereof, of barriers to vertical hydraulic fracture growth is paramount for design of hydraulic fractures that grow in productive strata and avoid growth into layers that will not positively contribute to the economics of the well ("growth out of zone"). Microseismic mapping of thousands of hydraulic fracturing stages from shale reservoirs in North America has shown that the separation between underground water sources and shale reservoirs is so great relative to the height growth that it is probably of little relevance to the overall environmental risk profile of shale gas/oil production (Fisher and Warpinski, 2012; Warpinski, 2013). However, the ability to predict height growth could be useful for understanding the potential for contamination of ground water associated with stimulating much shallower coal-seam gas wells (EPA, 2004).

The geometrical similarities between observed dikes and hydraulic fractures associated with a growth barrier are striking. Dikes have been observed

to cross, arrest, or deflect when they encounter potential barriers (Fig. 21) (Gudmundsson et al., 1999; Gudmundsson and Loetveit, 2005; Gudmundsson, 2011a). Inspired by these contrasting behaviors, experiments in gelatine have obtained analogues to each case based on variation of the relative material properties, especially the stiffness, in a two-layered system (Fig. 22) (Rivalta et al., 2005; Kavanagh et al., 2006). Similarly, mine-through mapping of hydraulic fractures in coal seams shows both arrest and deflection to the horizontal when the hydraulic fracture encounters a relatively stiffer and stronger rock layer (Figure 23a-b) (Elder, 1977; Lambert et al., 1980; Diamond and Oyler, 1987; Jeffrey et al., 1992). Furthermore, mine-through experiments in coal demonstrate meters to tens-of-meter scale examples of more complex geometries that can arise in the presence of multiple layers. Notably there is a tendency for hydraulic fractures to cross stiff/strong layers if they are thin and bounded by relatively thick soft/weak coal layers and, intriguingly, to grow on the contact above a thin stiff layer that is separated from a thick stiff layer by a thin soft layer (Fig. 23c) (Lambert et al., 1980; Diamond and Oyler, 1987; Jeffrey et al., 1992, 1995).

Although the observations are similar, there are nuanced but important differences in the interpretations made by research communities studying dike and hydraulic fracturing. The starting point is actually similar, with both communities recognizing the fundamental importance of variations in the in-situ stresses and the mechanical properties of the layers (Simonson et al., 1978; Teufel and Clark, 1984; Warpinski and Teufel, 1987; Gudmundsson et al., 1999; Economides and Nolte, 2000; Rivalta et al., 2005; Kavanagh et al., 2006; Gudmundsson, 2011a; Maccaferri et al., 2011). However, the dike research community has tended to consider the role of stresses in terms of the impact of rotation of the orientation of the least compressive stress direction in the vicinity of a magma chamber, the surface, or a volcanic edifice (Gudmundsson et al., 1999; Gudmundsson, 2011a; Maccaferri et al., 2011); it has placed a relatively strong emphasis on the importance of the contrast in mechanical properties between the layers, most notably the relative stiffness (Rivalta et al., 2005; Kavanagh et al., 2006). In contrast, the hydraulic fracturing research community considers height growth to be primarily driven by the relative magnitude of the minimum in-situ compressive stress among the layers; contrasts in strength are considered to play a relatively minor role and the stiffness contrasts among layers are considered to be of key importance — but this is primarily via their impact on stress variation among the layers when they are subjected to remote tectonic

Figure 21: Dykes meeting contacts. a) A vertical, 6-m-thick dyke penetrates all the basaltic lava flows in North Iceland. b) A vertical, 0.3-m-thick dyke becomes arrested at the contact between a pyroclastic layer and a basaltic lava flow in Tenerife, Canary Islands. C) The dyke becomes singly deflected along the contact to form a sill between a basaltic sheet and a lava flow, Southwest Iceland. From Gudmundsson (2011a), with permission.

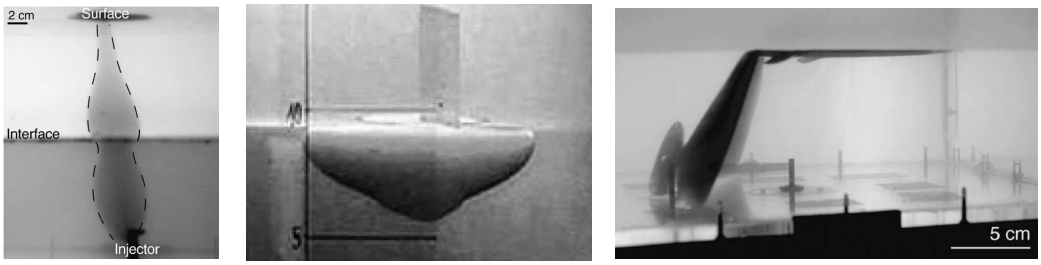

Figure 22: Experiments in gelatine showing: a) Analogue dike crossing into a less dense and less rigid upper layer, from Kavanagh et al. (2006), with permission, b) Arrest when an ascending analogue dike encounters a relatively stiff layer ($G_U/G_L = 5.5$ for shear modulus G) and lacks sufficient buoyant driving force to propagate in the upper layer, after Rivalta et al. (2005), with permission Fig 5a, c) Formation of an analogue sill along the contact between a lower soft layer and an upper stiff layer in a case with $E_U/E_L = 6.6$ for Young's modulus E, from Kavanagh et al. (2006), with permission.

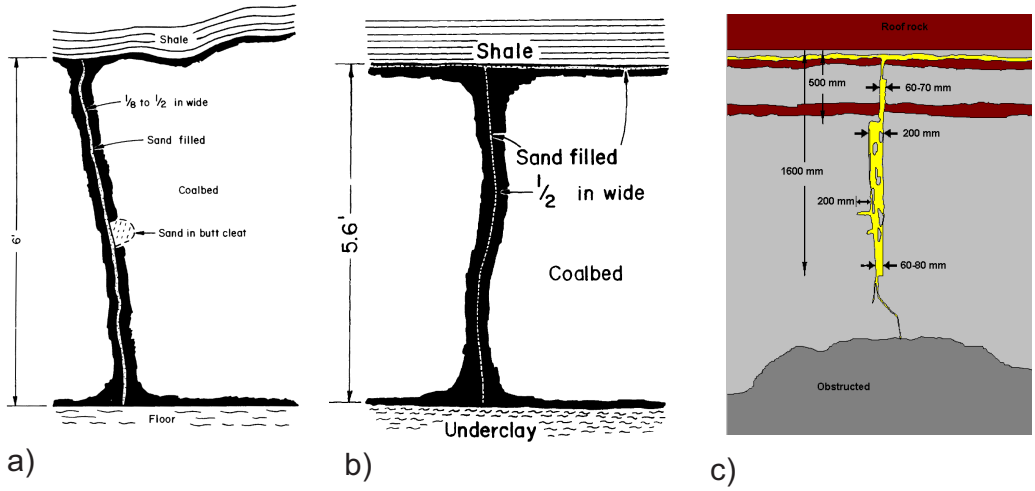

Figure 23: Examples from mine through mapping of hydraulic fractures in coal showing: a) Arrest of height growth at relatively stiff/strong roof and floor layers, from Diamond and Oyler (1987), with permission, b) Formation of horizontal growth component along the contact between the coal seam and a relatively stiff/strong roof rock, from Diamond and Oyler (1987), with permission, c) Direct crossing of the stiff/strong but thin layer between two coal layers and growth of a horizontal component above a relatively stiff/strong layer that is separated from the stiff/strong roof rock by a relatively thin layer of soft/weak coal, redrawn after Jeffrey et al. (1992), with permission.

loading (Teufel and Clark, 1984; Warpinski and Teufel, 1987; Naceur et al., 1990; Gu and Siebrits, 2008). Put another way, both communities agree that stiff/strong layers serve as barriers to growth, however the hydraulic fracturing community typically understands this to be because stiff layers tend to have higher stresses than neighboring lower stiffness layers, while the dike research community tends to interpret the contrasts in material properties themselves to be more directly responsible for dike arrest.

6.2. Induced seismicity

Seismic energy is released during both hydraulic fracturing and dike propagation. The timing and location of seismic events provide valuable information on fracture growth. For dike propagation, monitoring typically focuses on events with magnitudes larger than 1; stress transfer associated with dike intrusion has been suggested to be associated with magnitude 6 and larger earthquakes (Julian, 1983; Savage and Cockerham, 1984; Toda et al., 2002). In contrast, hydraulic fractures for the petroleum industry produce microseismicity of magnitude lower than 1, with the vast majority of events smaller than magnitude zero (Warpinski et al., 2012a; Warpinski, 2013). Note that here we limit our discussion to microseismicity associated with the hydraulic fracturing itself and do not consider the regional increase in seismicity with observed magnitudes up to 5.7 that have been inferred to result from or be exacerbated by deep wastewater injection (e.g. Council, 2012; van der Elst et al., 2013). Deep wastewater injection, although it is associated with disposal of a waste stream generated by unconventional oil and gas production including hydraulic fracturing, takes place at greater depth, larger time scales, and lower pressures, which is to say that it is a substantively different process. Note also that hydraulic stimulation of geothermal wells located in deep, hot, low permeability crystalline rocks in some cases are associated with microseismicity in a similar range to what is observed for oil and gas hydraulic fracturing (Pearson, 1981; Evans et al., 2005), but has been observed to exceed magnitude 3 in both Basel, Switzerland and the Cooper Basin, Australia (Deichmann and Giardini, 2009; Mukuhira et al., 2010).

The difference in magnitude range attests to the difference in scale between the two processes. Still, in both dike propagation and hydraulic fracturing there is an observed prevalence of shear (strike-slip) events that is taken to indicate that the most important mechanism for generating seismicity is slippage of nearby faults (Hill, 1977; Pearson, 1981; Savage and Cockerham,

1984; Shapiro et al., 1997; Toda et al., 2002; Rutledge and Phillips, 2003; Shapiro et al., 2006; Warpinski et al., 2012b). For dikes, the activation of nearby faults is thought to be directly induced by the stress surrounding the intrusion (Toda et al., 2002) or from fault pressurization due to stress or thermally-induced fluid migration (Hill, 1977; Sibson, 1996). For hydraulic fractures, the main source mechanism is commonly taken to be slippage of critically-oriented natural fractures and faults that are pressurized by fluid which diffuses out of the hydraulic fracture and through the formation (Pearson, 1981; Rutledge and Phillips, 2003; Warpinski et al., 2012b). The parabolic shape of the seismic leading and trailing fronts associated with hydraulic fractures is taken as support for this mechanism (Parotidis et al., 2004; Shapiro et al., 2006) and, conversely, it has been proposed that the spatial evolution of microseismicity can be used to deduce the reservoir permeability (Shapiro et al., 1997, 2002). This parabolic shape of the microseismic leading and trailing fronts (Fig. 24) stands in contrast to the shape of the seismic fronts observed for dikes (Fig. 5) and attests to the relative importance of fluid diffusion in the generation of microseismicity associated with hydraulic fracturing. This difference may also be associated with the relative importance of direct fault activation from deformation-induced stress changes propagating at the rate of propagation for dikes.

6.3. Networks and swarms

While models often limit consideration to simple propagation geometries, there is field evidence from the petroleum industry that certain conditions lead to complex, network-like growth. The generation of complex hydraulic fracture networks in the Barnett shale in Texas, USA, was first inferred from microseismic data in the early 2000s (Maxwell et al., 2002; Fisher et al., 2004). It is one of the modern petroleum industry's most influential discoveries because it is believed that this network growth is an important contributor to the economical production of gas from the Barnett formation and it therefore significantly shaped the stimulation strategies that have been employed as shale gas production has expanded to commercial scale to several other formations in North America (King, 2010).

Meanwhile, numerical analysis has demonstrated that the relative difference between the least principal stress, which is invariably horizontally-directed in shale reservoirs, and the other horizontal principal stress component is a determining factor in whether hydraulic fractures grow as networks or localized features (Olson and Dahi-Taleghani, 2009; Kresse et al., 2013).

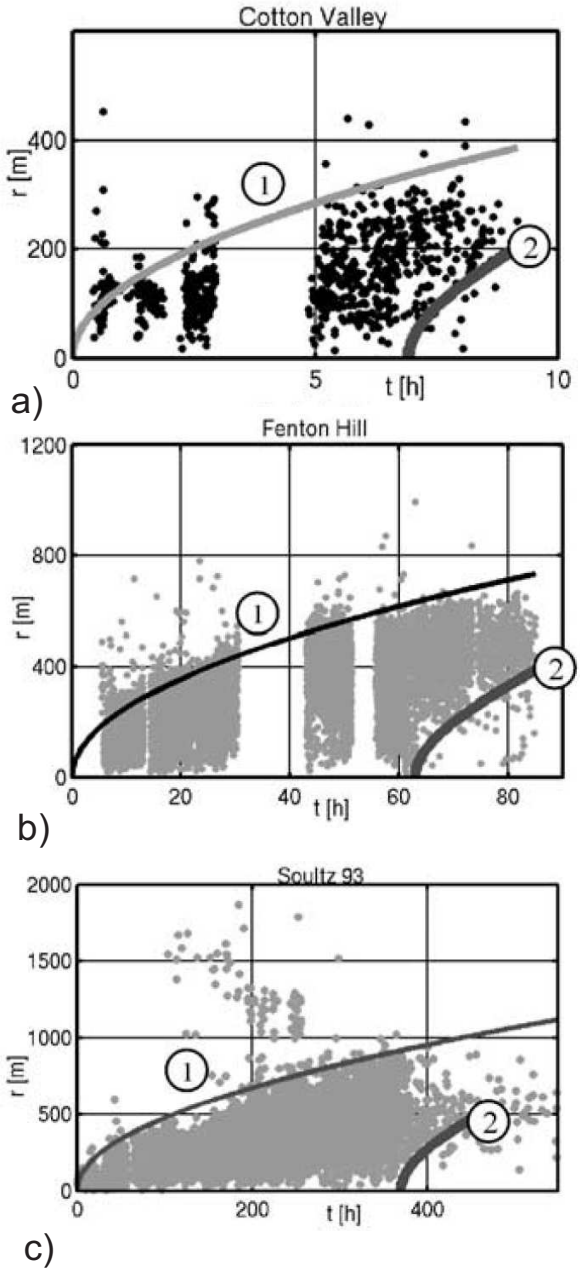

Figure 24: Distance r between the microseismic event and the injection point as a function of time, where the seismic back fronts (curve 2) and parabolic envelopes (curve 1) are computed using the same diffusivity for each case study according to the methods in Parotidis et al. (2004). Examples are: a) Cotton Valley gas field, Texas, USA; b) Fenton Hill hot rock geothermal site, New Mexico, USA; c) Soultz-sous-Forêts hot rock geothermal site, France. From Parotidis et al. (2004), with permission.

For the Barnett shale, the two horizontal stresses are thought to be very nearly equal (e.g. Abbas et al., 2013), and according to numerical models this scenario is ideally suited to network-like growth. Additionally, an analytical model (Bunger et al., In Press) has shown that injection from multiple entry points will tend to result in a fracture spacing that is about 1.5 times the vertical extent of hydraulic fractures which are limited in height by barrier layers (see Section 6.1); this explains the observed tendency of hydraulic fractures to attain a spacing of the main well-transverse network branches of around 150 m in the Barnett where their vertical extent is limited to about 100 m (Fisher et al., 2004).

In summary, the experience so far of the petroleum industry, when combined with numerical and analytical modeling, has identified at least two ingredients for network growth: 1) limited height growth and 2) relatively similar horizontal principal stresses. While there are almost certainly other important factors in network growth of hydraulic fractures, the two that have been identified so far can also give useful insights for other applications. Firstly, these factors explain why Engineered Geothermal System (EGS) trials have rarely, if ever, achieved a complex, interconnected growth of hydraulic fractures (Jung, 2013) in spite of a stimulation strategy that is designed with that goal (Tester et al., 2006). EGS sites have typically had relatively substantial differences between the minimum and intermediate principal stress magnitudes (e.g. Barton et al., 1988; Valley and Evans, 2007) and the massive nature of the formations means they do not provide height-limiting growth barriers (or similarly, one of the lateral extents when hydraulic fractures are oriented in a horizontal plane). Without these ingredients it is not surprising that observations over the past decades point to a strong tendency to generate localized growth.

Beyond engineering applications, the ingredients for network growth can also give insights into the mechanisms leading to growth of giant radiating dike swarms, of which there are 199 documented on Earth, 163 documented on Venus, and which are also abundant on Mars (Ernst et al., 2001). The abundance of these giant swarms, as well as smaller-scale volcanic swarms (e.g. Odé, 1957; Gudmundsson, 1983; Walker, 1986; Sigurdsson, 1987; Paquet et al., 2007), indicates that the conditions for their formation are not pathological. Still, the formation of closely-spaced arrays of dikes appears to be specific to laterally-propagating, blade-like dikes that are limited in height. Drawing on a modification of the analytical hydraulic fracturing model developed by Bunger (2013), Bunger et al. (2013) have shown that the

characteristic spacing that naturally seems to arise in dike swarms is similar to the dike height, consistent with model predictions. This discovery suggests that limited height, i.e. blade-like growth, is not only a fundamental ingredient for growth of arrays of hydraulic fractures but also for the formation of dike swarms.

7. Outlook: Perspectives and challenges

Despite the many advances reviewed above, we remain far from having an ideal dike model. The single most important development that could drastically change the way we model dikes would be to move into three dimensions. While many problems are well approximated by 2D models, there are many others where a 3D model would be instrumental for the understanding of the physical process. In particular, 2D models of ascending dikes do not allow the possibility of lateral extension, while this is how dikes are observed to behave in the field (Gudmundsson, 2011b) and in experiments. The transition from vertical to horizontal propagation is very important for volcanic applications, when magma contained in dikes becomes neutrally or negatively buoyant and propagates laterally (if pressurized or driven by external gradients).

A possible strategy to solve this problem is to explore methods used in the industry to model hydraulic fractures and adapt those numerical models to dikes. It is also necessary that experimental work focuses on providing observations to constrain those models. However, large dike injections are often in areas that are infrequently monitored; for example, mid-ocean ridges, where most large dike injection are probably occurring, are deep below the ocean and are hence difficult and expensive to access. Future studies on the currently ongoing dike intrusion event at Bárạrbunga, Iceland, will certainly lead to a step in our understanding of the dynamics of dikes.

Dike models must be based on reliable estimates of large-scale crustal properties such as rock toughness and elastic moduli measured at low frequencies. On the other hand, constrains from models may provide unique insight into rock parameters that will likely be a key to progress in some far-reaching debates in geomechanics.

While waiting for progress in 3D modeling of dikes, we can focus on some outstanding questions that can be at least partially addressed with 2D models:

- The different phases of nucleation, propagation and stopping of dikes;

- Interaction between dikes and their feeding sources;
- The rifting cycle on Mid Ocean Ridges: Rifting episodes, post-diking and inter-diking deformation (in parallel with earthquakes occurring on plate boundaries);
- Interaction between faulting and diking;
- Dike-faulting/tectonics interactions (e.g. Kilauea and Etna, where large tectonic faults interact with rifts);
- Incorporation of realistic magma properties including volatile exsolution, realistic rheology (sudden changes in viscosity are critical), and magma compressibility;
- Development of volcanic conduits and vents from dikes,
- Development of magma reservoirs from dikes,
- Improved forecasts of the time, size and location of potential eruptions;
- Understanding the effect of dikes on local or large-scale crustal properties (thermal effects, permeability changes, mechanical response of the medium, seismic properties),
- Understanding the role played by magma in the development of major tectonic features such as rifts, subduction zones, volcanic arcs.

Each individual application may be best solved with a tailored approach. The details of tip processes or of the velocity of dikes may be studied most effectively by including only the fluid flow within the dike. On the other hand, the trajectory of dikes or other geometrically complex processes may be studied by simplifying or neglecting any viscous flow within the crack.

The complementarity of methods (laboratory and numerical modeling) has proven very useful in the past and will remain so in the future. It would be very helpful also to increase communication between disciplines, in particular between geophysics, petrology and field geology; more communication with industry would be beneficial in order to take advantage of the complementarity of diking and hydraulic fracturing.

8. Acknowledgements

Constructive reviews by Roger Buck and Thierry Menand helped improving the manuscript. ER was funded by the European Union through the ERC Starting Grant project CCMP-POMPEI, Grant N. 240583. RK received funding from the Leverhulme Trust.

References

A. H.-D. Cheng, A.J.A.L., 1984. Boundary integral equation method for linear porous-elasticity with applications to fracture propagation. International journal for numerical methods in engineering 20, 279–296.

an A. P. Peirce, B.L., Detournay, E., Zhang, X., Chen, Z., Bunger, A.P., Detournay, C., Napier, J., Abbas, S., Garagash, D., Cundall, P., 2013. The impact of the near-tip logic on the accuracy and convergence rate of hydraulic fracture simulators compared to reference solutions, in: Bunger, A.P., McLennan, J., Jeffrey, R.G. (Eds.), Effective and Sustainable Hydraulic Fracturing. Intech, Rijeka, Croatia. chapter 43.

Abbas, S., Lecampion, B., Prioul, R., 2013. Competition between transverse and axial hydraulic fractures in horizontal wells, in: Proceedings SPE Hydraulic Fracturing Technology Conference and Exhibition, The Woodlands, Texas, USA. SPE 163848.

Acocella, V., Neri, M., 2009. Dike propagation in volcanic edifices: Overview and possible developments. Tectonophysics 471, 67–77.

Acocella, V., Tibaldi, A., 2005. Dike propagation driven by volcano collapse: A general model tested at stromboli. Geophys. Res. Lett. 32, doi:10.1029/2004GL022248.

Albino, F., Pinel, V., Sigmundsson, F., 2010. Influence of surface load variations on eruption likelihood: Application to two Icelandic subglacial volcanoes, Griímsvötn and Katla. Geophys. J. Int. 181, 1510–1524.

Ali, S., Feigl, K., Carr, B., Masterlark, T., Sigmundsson, F., 2014. Geodetic measurements and numerical models of rifting in Northern Iceland for 19932008. Geophys. J. Int. , in press.

Aloisi, M., Bonaccorso, A., Gambino, S., 2006. Imaging composite dike propagation (Etna, 2002 case). J. Geophys. Res. 111, B06404.

Amoruso, A., Crescentini, L., 2009. Shape and volume change of pressurized ellipsoidal cavities from deformation and seismic data. J. Geophys. Res. 114, B02210.

Anderson, E., 1951. Oliver and Boyd, Edinburgh.

Aoki, Y., Segall, P., Kato, T., Cervelli, P., Shimada, S., 1999. Imaging Magma Transport During the 1997 Seismic Swarm off the Izu Peninsula, Japan. Science 286, 927–930.

van As, A., Jeffrey, R.G., 2002. Hydraulic fracture growth in naturally fractured rock: mine through mapping and analysis, in: Proceedings NARMS-TAC, pp. 1461–1469.

Atkinson, B.K., 1984. Subcritical crack growth in geological materials. J. Geophys. Res. 89, 4077–4114.

Atkinson, B.K., Meredith, P.G., 1987. Experimental fracture mechanics data for rocks and minerals, in: Atkinson, B.K. (Ed.), Fracture Mechanics of Rock. Academic Press, London, pp. 477–525.

Ayele, A., Keir, D., Ebinger, C., Wright, T.J., Stuart, G.W., R, B.W., Jacques, E., Ogubazghi, G., Sholan, J., 2009. September 2005 mega-dike emplacement in the Manda-Harraro nascent oceanic rift (Afar depression). Geophys. Res. Lett. 36.

Baer, G., 1991. Mechanisms of dike propagation in layered rocks and in massive, porous sedimentary rocks. J. Geophys. Res. 96, 11911–11929.

Baer, G., Hamiel, Y., 2010. Form and growth of an embryonic continental rift: Insar observations and modelling of the 2009 western arabia rifting episode. Geophys. J. Int. 182, 155–167.

Bagnardi, M., Amelung, F., 2012. Space-geodetic evidence for multiple magma reservoirs and subvolcanic lateral intrusions at Fernandina Volcano, Galápagos Islands. J. Geophys. Res. 117, B10406.

Bagnardi, M., Amelung, F., Poland, M.P., 2013. A new model for the growth of basaltic shields based on deformation of Fernandina volcano, Galápagos Islands. Earth and Planetary Science Letters , 1–9.

Balme, M., Rocchi, V., Jones, C., Sammonds, P., Meredith, P., Boon, S., 2004. Fracture toughness measurements on igneous rocks using a high-pressure, high-temperature rock fracture mechanics cell. J. Volc. Geoth. Res. 132, 159–172.

Barenblatt, G., 1962. The mathematical theory of equilibrium cracks in brittle fracture. Adv. Appl. Mech. VII, 55–129.

Barton, C.A., Zoback, M.D., Burns, K.L., 1988. In-situ stress orientation and magnitude at the Fenton Geothermal Site, New Mexico, determined from wellbore breakouts. Geophysical Research Letters 15, 467–470.

Batchelor, G.K., 2000. An Introduction to Fluid Dynamics.

Battaglia, J., Ferrazzini, V., Staudacher, T., Aki, K., Cheminee, J., 2005. Pre-eruptive migration of earthquakes at the Piton de la Fournaise volcano (reunion island). Geophys. J. Int. 161, 549–558.

Battaglia, M., Gottsmann, J., Carbone, D., Fernández, J., 2008. 4d volcano gravimetry. Geophysics 73, WA3–WA18.

Bažant, Z., 1997. Scaling of quasibrittle fracture: asymptotic analysis. Int. J. Fracture 83, 19–40.

Belachew, M., Ebinger, C., Cote, D., Keir, D., Rowland, J.V., Hammond, J., Ayele, A., 2011. Comparison of dike intrusions in an incipient seafloor-spreading segment in Afar, Ethiopia: Seismicity perspectives. J. Geophys. Res. 116, B06405.

Bercovici, D., Ricard, Y., Schubert, G., 2001. A two-phase model for compaction and damage: 1. General theory. J. Geophys. Res. 106.

Bialas, R.W., Buck, W.R., Qin, R., 2010. How much magma is required to rift a continent? Earth and Planetary Science Letters 292, 68–78.

Blake, S., 1981. Volcanism and the dynamics of open magma chambers. Nature 289, 783–785.

Bolchover, P., Lister, J.R., 1999. The effect of solidification on fluid-driven fracture, with application to bladed dykes. Proc. R. Soc. Lond. A 455, 2389–2409.

Bonaccorso, A., Currenti, G., Del Negro, C., Boschi, E., 2010. Dike deflection modelling for inferring magma pressure and withdrawal, with application to etna 2001 case. Earth and Planetary Science Letters 293, 121–129.

Bonafede, M., Rivalta, E., 1999a. On tensile cracks close to and across the interface between two welded elastic half-spaces. Geophys. J. Int. 138, 410–434. Cited by 34.

Bonafede, M., Rivalta, E., 1999b. The tensile dislocation problem in a layered elastic medium. Geophys. J. Int. 136, 341–356.

Borodich, F., 1999. Fractals and fractal scaling in fracture mechanics. Int. J. Fracture 95, 239–259.

Brace, W., Walsh, J., Frangos, W., 1968. Permeability of granite under high pressure. J. Geophys. Res. 73, 2225–2236.

Brandsdóttir, B., Einarsson, P., 1979. Seismic activity associated with the September 1977 deflation of the Krafla central volcano in North-Eastern Iceland. J. Volc. Geoth. Res. 6, 197–212.

Bruce, P.M., Huppert, H.E., 1990. Solidification and melting along dykes by the laminar flow of basaltic magma, in: Magma transport and storage. John Wiley & Sons. chapter 6, M. p. ryan edition. pp. 87–101.

Buck, W., Einarsson, P., Brandsdóttir, B., 2006. Tectonic stress and magma chamber size as controls on dike propagation: Constraints from the 19751784 Krafla rifting episode. Journal of Geophysical Research - Solid Earth 112.

Buck, W.R., Lavier, L.L., Poliakov, A.N.B., 2005. Modes of faulting at mid-ocean ridges. Nature 434, 719–723.

Bunger, A.P., 2013. Analysis of the power input needed to propagate multiple hydraulic fractures. International Journal of Solids and Structures 50, 1538–1549.

Bunger, A.P., Cruden, A.R., 2011. Modeling the growth of laccoliths and large mafic sills : Role of magma body forces. J. Geophys. Res. 116, B02203.

Bunger, A.P., Menand, T., Cruden, A.R., Zhang, X., 2013. Analytical predictions for a natural spacing within dyke swarms. Earth and Planetary Science Letters 375, 270–279. Doi: 10.1016/j.epsl.2013.05.044.

Bunger, A.P., Zhang, X., Jeffrey, R.G., In Press. Constraints on simultaneous growth of hydraulic fractures from multiple perforation clusters in horizontal wells. SPE Journal .

Carbone, D., 2003. Bulk processes prior to the 2001 Mount Etna eruption, highlighted through microgravity studies. J. Geophys. Res. 108.

Carbotte, S., Macdonald, K., 1990. Causes of variation in fault-facing direction on the ocean floor. Geology 18, 749–752.

Carpinteri, A., 1994. Scaling laws and renormalization groups for strength and toughness of disordered materials. Int. J. Solids Struct. 31, 291–302.

Chadima, M., Cajza, V., Týcovád, P., 2008. On the interpretation of normal and inversemagneticfabric in dikes: Examples from the Eger Graben, NW Bohemian Massif. Tectonophysics 466, 47–63.

Chen, Z., 2013. An ABAQUS implementation of the XFEM for hydraulic fracture problems, in: Bunger, A.P., McLennan, J., Jeffrey, R.G. (Eds.), Effective and Sustainable Hydraulic Fracturing. Intech, Rijeka, Croatia. chapter 36.

Choi, E., Buck, W.R., 2010. Constraints on shallow mantle viscosity from morphology and deformation of fast-spreading ridges. Geophysical Research Letters 37.

Cocco, M., Nostro, C., Ekström, G., 2000. Static stress changes and fault interaction during the 1997 umbria-marche earthquake sequence. J. Seism. 4(4), 501–516.

Cooke, M.L., Pollard, D.D., 1996. Fracture propagation paths under mixed mode loading within rectangular blocks of polymethyl methacrylate. Journal of Geophysical Research: Solid Earth 101, 3387–3400.

Corbi, F., Rivalta, E., Pinel, V., Maccaferri, F., Bagnardi, M., Acocella, V., 2014. Magma propagation and storage at calderas controlled by decompression stresses. submitted .

Correa-Gomes, L., Souza Filhoa, C., Martins, C., Oliveira, E., 2001. Development of symmetrical and asymmetrical fabrics in sheet-like igneous bodies: the role of magma flow and wall-rock displacements in theoretical and natural cases. Journal of Structural Geology 23, 1415–1428.

Costa, A., Melnik, O., Sparks, R.S., Voight, B., 2007. Control of magma flow in dykes on cyclic lava dome extrusion. Geophys. Res. Lett. 34, L02303.

Costa, A., Wadge, G., Melnik, O., 2012. Cyclic extrusion of a lava dome based on a stick-slip mechanism. Earth and Planetary Science Letters 337–338, 39–46.

Council, N.R., 2012. Induced Seismicity Potential in Energy Technologies. Technical Report. National Academies Press. New York.

Craddock, J.P., Kennedy, B.C., Cook, A.L., Pawlisch, M.S., Johnston, S.T., Jackson, M., 2008. Anisotropy of magnetic susceptibility studies in Tertiary ridge-parallel dykes (Iceland), Tertiary margin-normal Aishihik dykes (Yukon), and Proterozoic KenoraKabetogama composite dykes (Minnesota and Ontario). Tectonophysics 448, 115–124.

Crouch, S., Starfield, A., 1983. Boundary element methods in solid mechanics. George Allen and Unwin Ltd, London.

Dahi-Taleghani, A., Olson, J., 2011. Numerical modeling of multistranded-hydraulic-fracture propagation: Accounting for the interaction between induced and natural fractures. SPE Journal 16, 575–581.

Dahm, T., 2000a. Numerical simulations of the propagation path and the arrest of fluid-filled fractures in the Earth. Geophysical Journal International 141, 623–638.

Dahm, T., 2000b. On the shape and velocity of fluid-filled fractures in the Earth. Geophysical Journal International 142, 181–192.

Dahm, T., Becker, T., 1998. On the elastic and viscous properties of media containing strongly interacting in-plane cracks. Pure Appl. Geophys. 151, 1–16.

Dahm, T., Hainzl, S., Fischer, T., 2010. Bidirectional and unidirectional fracture growth during hydrofracturing: Role of driving stress gradients. J. Geophys. Res. 115.

Damjanac, B., Gil, I., Pierce, M., Sanchez, M., van As, A., McLennan, J., 2010. A new approach to hydraulic fracturing modeling in naturally fractured reservoirs, in: Proceedings 44th U.S. Rock Mechanics Symposium, Salt Lake City, Utah, USA. ARMA 10-400.

Daniels, J., Waters, G., LeCalvez, J., Lassek, J., Bentley, D., 2007. Contacting more of the Barnett Shale through and integration of real-time microseismic monitoring, petrophysics, and hydraulic fracture design, in: Proceedings SPE Annual Technical Conference and Exhibition, Anaheim, California, USA. SPE 110562.

Daniels, K., Bastow, I., Keir, D., Sparks, R., Menand, T., 2014. Thermal models of dyke intrusion during development of Continent-Ocean Transition. Earth and Planetary Science Letters 385, 145–153.

Daniels, K., Kavanagh, J., Menand, T., Sparks, R., 2012. The shapes of dikes: Evidence for the influence of cooling and inelastic deformation. GSA Bull. 124, 1102–1112.

Davis, P., Knopoff, L., 1995. The elastic modulus of media containing strongly interacting antiplane cracks. J. Geophys. Res. 100, 18253–18258.

Deichmann, N., Giardini, D., 2009. Earthquakes induced by the stimulation of an enhanced geothermal system below Basel (Switzerland). Seismological Research Letters 80, 784–798.

Del Negro, C., Currenti, G., Napoli, R., Vicari, A., 2003. Volcanomagnetic signals associated with the 2001 flank eruption of Mt. Etna (Italy). Geophys. Res. Lett. 30.

Delaney, P., Pollard, D., 1981. Deformation of host rocks and flow of magma during growth of minette dikes and breccia-bearing intrusions near Ship Rock, New Mexico. U.S. Geol. Surv. Prof. Pap. 1202.

Delaney, P., Pollard, D., Ziony, J., McKee, E., 1986. Field relations between dikes and joints: Emplacement processes and paleostress analysis. J. Geophys. Res. 91, 4920–4938.

Delaney, P.T., Pollard, D.D., 1982. Solidification of basaltic magma during flow in a dike. American Journal of Science 282, 856–885.

Desmarais, E., Segall, P., 2007. Transient deformmation following the 30 January 1997 dike intrusion at Kilauea volcano, Hawaii. Bull. Volcanol. 69, 353–363.

Di Giuseppe, E., Funiciello, F., Corbi, F., Ranalli, G., Mojoli, G., 2009. Gelatins as rock analogs: a systematic study of their rheological and physical properties. Tectonophysics 473, 391–403.

Diamond, W.P., Oyler, D.C., 1987. Effects of Stimulation Treatments on Coalbeds and Surrounding Strata. Technical Report Report of Investigations 9083. United States Bureau of Mines.

Dieterich, J., 1994. A constitutive law for rate of earthquake production and its application to earthquake clustering. J. Geophys. Res. 99, 2601–618.

Dieterich, J., Cayol, V., Okubo, P., 2000. The use of earthquake rate changes as a stress meter at Kilauea volcano. Nature 408, 457–460.

Dobran, F., 2001. Kluwer Academic.

Dyskin, A., 1997. Crack growth criteria incorporating non-singular stresses: Size effect in apparent fracture toughness. Int. J. Fracture 83, 193–206.

Dziak, R., Fox, C., Schreiner, A., 1995. The June-July1993 seismo-acoustic event at CoAxial segment, Juan de Fuca Ridge: Evidence for a lateral dike injection. Geophys. Res. Lett. 22, 135–138.

Economides, M., Nolte, K. (Eds.), 2000. Reservoir Stimulation. John Wiley & Sons, Chichester UK. 3rd edition.

Einarsson, P., Brandsdóttir, B., 1978. Seismological evidence for lateral magma intrusion during the July 1978 deflation of the Krafla Volcano in NE-Iceland. osti.gov .

Elder, C.H., 1977. Effects of Hydraulic Stimulation on Coalbeds and Assciated Strata. Technical Report Report of Investigations 8260. United States Bureau of Mines.

van der Elst, N.J., Savage, H.M., Keranen, K.M., Abers, G.A., 2013. Enhanced remote earthquake triggering at fluid-injection sites in the midwestern united states. Science 341, 164–167. http://www.sciencemag.org/content/341/6142/164.full.pdf.

EPA, 2004. Evaluation of Impacts to Underground Sources of Drinking Water by Hydraulic Fracturing of Coalbed Methane Reservoirs. Technical Report EPA 816-R-04-003. United States Environmental Protection Agency. Washington, D.C.

Erdogan, F., Sih, G., 1963. On the crack extension in plates under plane loading and transverse shear. J Basic Eng - T ASME 85, 519–527.

Ernst, R.E., Grosfils, E.B., Mège, D., 2001. Giant Dike Swarms: Earth, Venus, and Mars. Annu. Rev. Earth Planet. Sci. 29, 489–534.

Ernst, R.E., Head, J.W., Parfitt, E., Grosfils, E., Wilson, L., 1995. Giant radiating dyke swarms on earth and venus. Earth Science Reviews 39, 1–58.

Evans, K., Moriya, H., Niitsuma, H., Jones, R., Phillips, W., Genter, A., Sausse, J., Jung, R., Baria, R., 2005. Microseismicity and permeability enhancement of hydrogeologic structures during massive fluid injections into granite at 3 km depth at the Soultz HDR site. Geophysical Journal International 160, 389–412.

Fialko, Y., Rubin, A., 1998. Thermodynamics of lateral dike propagation-Implications for crustal accretion at slow spreading mid-ocean ridges. Journal of Geophysical Research 103.

Fialko, Y., Rubin, A., 1999. Thermal and mechanical aspects of magma emplacements in giant dike swarms. J. Geophys. Res. 104, 23033–23049.

Fisher, K., Warpinski, N., 2012. Hydraulic fracture height growth: Real data. SPE Production and Operations 27, 8–19. SPE 145949.

Fisher, M.K., Heinze, J.R., Harris, C.D., Davidson, B.M., Wright, C.A., Dunn, K.P., 2004. Optimizing horizontal completion techniques in the barnett shale using microseismic fracture mapping, in: Proceedings SPE Annual Technology Conference and Exhibition, Houston, Texas, USA. SPE 90051.

Funatsu, T., Seto, M., Shimada, H., Matsui, K., Kuruppu, M., 2004. Combined effects of increasing temperature and confining pressure on the fracture toughness of clay bearing rocks. International Journal of Rock Mechanics and Mining Sciences 41, 927 – 938.

Geertsma, J., de Klerk, F., 1969. A rapid method of predicting width and extent of hydraulic induced fractures. J. Pet. Tech 246, 1571–1581. (SPE 2458).

Geshi, N., Kusumoto, S., Gudmundsson, A., 2012. Effects of mechanical layering of host rocks on dike growth and arrest. J. Volc. Geoth. Res. 223-224, 74–82.

Gillard, D., Rubin, A., Okubo, P., 1996. Highly concentrated seismicity caused by deformation of kilauea's deep magma system. Nature 384, 343–346.

Gordeliy, E., Peirce, A., 2013. Coupling schemes for modeling hydraulic fracture propagation using the xfem. Computer Methods in Applied Mechanics and Engineering 253, 305–322.

Grandin, R., Socquet, A., Binet, R., Klinger, Y., Jacques, E., de Chebalier, J.B., King, G., Lasserre, C., Tait, S., Tapponier, P., Delorme, A., Pinzuti, P., 2009. The September 2005 Manda Hararo-Dabbahu rifting event, Afar (Ethiopia): constraints provided by geodetic data. J. Geophys. Res. 114, B08404.

Grandin, R., Socquet, A., Doin, M.P., Jacques, E., de Chebalier, J.B., King, G., 2010a. Transient rift opening in response to multiple dike injections in the Manda Hararo rift (Afar, Ethiopia) imaged by time-dependent elastic inversion of interferometric synthetic aperture radar data. J. Geophys. Res. 115, B09403.

Grandin, R., Socquet, A., Jacques, E., Mazzoni, N., de Chebalier, J.B., King, G., 2010b. Sequence of rifting in Afar, Manda-Hararo rift, Ethiopia, 2005-2009: Time-space evolution and interactions between dikes from interferometric synthetic aperture radar and static stress change modeling. J. Geophys. Res. 115, B10413.

Gu, H., Siebrits, E., 2008. Effect of formation modulus contrast on hydraulic fracture height containment. SPE Production & Operations 23, 170–176.

Gudmundsson, A., 1983. Form and dimensions of dykes in eastern Iceland. Tectonophysics 95, 295–307.

Gudmundsson, A., 2002. Emplacement and arrest of sheets and dykes in central volcanoes. J. Volc. Geoth. Res. 116, 279–298.

Gudmundsson, A., 2003. Surface stresses associated with arrested dykes in rift zones. Bull. Volcanol. 65, 606–619.

Gudmundsson, A., 2005. The effects of layering and local stresses in composite volcanoes on dyke emplacement and volcanic hazards. Comptes Rendus Geoscience 337, 1216–1222.

Gudmundsson, A., 2011a. Deflection of dykes into sills at discontinuities and magma-chamber formation. Tectonophysics 500, 50–64.

Gudmundsson, A., 2011b. Deflection of dykes into sills at discontinuities and magma-chamber formation. Tectonophysics 500, 50–64.

Gudmundsson, A., Loetveit, I.F., 2005. Dyke emplacement in a layered and faulted rift zone. Journal of Volcanology and Geothermal Research 144, 311–327.

Gudmundsson, A., Marinoni, L.B., Marti, J., 1999. Injection and arrest of dykes: implications for volcanic hazards. Journal of Volcanology and Geothermal Research 88, 1–13.

Guest, A., Settari, A., 2012. Relationship between microseismic activity, hydrofracture and stimulated zone growth based on a numerical damage model: an example from Bossier Sands, in: Proceedings SPE Annual Technical Conference and Exhibition, San Antonio, Texas, USA. SPE 159711.

Hainzl, S., Steacy, S., Marsan, D., 2010. Seismicity models based on Coulomb stress calculations. Community online resource for statistical seismicity analysis (CORSSA) .

Hamling, I.J., 2010. Measuring and modelling deformation during the Dabbahu (Afar) rifting episode. PhD thesis , 1–177.

Harris, R., 1998. Introduction to special section: Stress triggering, stress shadows, and implication for seismic hazards. J. Geophys. Res. 103, 24347–24347.

Havlin, C., Parmentier, E.M., Hirth, G., 2013. Dike propagation driven by melt accumulation at the lithosphere–asthenosphere boundary. Earth and Planetary Science Letters 376, 20–28.

Hayashi, Y., Morita, Y., 2003. An image of magma intrusion process inferred from precise hypocentral migration of the earthquake swarm east of the Izu Peninsula. Geophys. J. Int. 153, 159–174.

Heimpel, M., Olson, P., 1994. Buoyancy-driven fracture and magma transport through the lithosphere: models and experiments, in: Ryan, M. (Ed.), Magmatic Systems. Academic Press, pp. 223–240.

Hill, D.P., 1977. A model for earthquake swarms. Journal of Geophysical Research 82, 1347–1352.

Hooper, A., Ófeigsson, B., Sigmundsson, F., Lund, B., Einarsson, P., Geirsson, H., Sturkell, E., 2011. Increased capture of magma in the crust promoted by ice-cap retreat in Iceland. Nature Geoscience 4, 783–786.

Hughes, G., 2010. Investigations of magmatic end-members: silicic magma chambers and mafic dikes. Ph.D. thesis. Stanford University.

Huppert, H., Woods, A., 2002. The role of volatiles in magma chamber dynamics. Nature 420, 493–493.

Ida, Y., 1992. Width change of a planar magma path: implication for the evolution and style of volcanic eruptions. Physics of the earth and planetary interiors 74, 127–138.

Ida, Y., 1999. Effects of the crustal stress on the growth of dikes: Conditions of intrusion and extrusion of magma. Journal of Geophysical Research-Solid Earth 104, 17897–17909.

Irwan, M., Kimata, F., Fujii, N., 2006. Time dependent modeling of magma intrusion during the early stage of the 2000 Miyakejima activity. Journal of Volcanology and Geothermal Research 150, 202–212.

Ito, G., Martel, S., 2002. Focusing of magma in the upper mantle through dike interaction. J. Geophys. Res. 107 B10.

Jakobsdóttir, S., Roberts, M., Gudmundsson, G., Geirsson, H., Slunga, R., 2008. Earthquake swarms at Upptyppingar, north-east Iceland: A sign of magma intrusion? Studia Geophysica et Geodaetica 52 (4), 513–528.

Jeffrey, R.G., Brynes, R.P., Ling, D.J., 1992. An analysis of hydraulic fracture and mineback data for a treatment in the german creek coal seam, in: Proceedings SPE Rocky Mountain Regional Meeting, Casper, Wyoming, USA. SPE 24362.

Jeffrey, R.G., Bunger, A.P., Lecampion, B., Zhang, X., Chen, Z.R., van As, A., Allison, D., Beer, W.D., Dudley, J.W., Siebrits, E., Thiercelin, M., Mainguy, M., 2009. Measuring hydraulic fracture growth in naturally fractured rock, in: Proceedings SPE Annual Technical Conference and Exhibition, New Orleans, Louisiana, USA. SPE 124919.

Jeffrey, R.G., Settari, A., Smith, N.P., 1995. A comparison of hydraulic fracture field experiments, including mineback geometry data, with numerical fracture model simulations, in: Proceedings SPE Annual Technical Conference and Exhibition, Dallas, Texas, USA. SPE 30508.

Jin, Z.H., Johnson, S., 2008. Magma-driven multiple dike propagation and fracture toughness of crustal rocks. J. Geophys. Res. 113.

Johnson, D., Sigmundsson, F., Delaney, P., 2000. Comment on" Volume of magma accumulation or withdrawal estimated from surface uplift or subsidence, with application to the 1960 collapse of Kilauea volcano by P. T. Delaney and D. F. McTigue. Bulletin of Volcanology 61, 491–493.

Jolly, R.J.H., Sanderson, D.J., 1995. Variation in the form and distribution of dykes in the Mull swarm, Scotland. Journal of Structural Geology 17, 1543–1557.

Julian, B.R., 1983. Evidence for dyke intrusion earthquake mechanisms near Long Valley caldera, California. Nature 303, 323–325.

Jung, R., 2013. EGS goodbye or back to the future, in: Bunger, A.P., McLennan, J., Jeffrey, R.G. (Eds.), Effective and Sustainable Hydraulic Fracturing. Intech, Rijeka, Croatia. chapter 5.

Katz, R., 2008. Magma dynamics with the enthalpy method: Benchmark solutions and magmatic focusing at mid-ocean ridges. Journal of Petrology .

Katz, R., Weatherley, S., 2012. Consequences of mantle heterogeneity for melt extraction at mid-ocean ridges. Earth and Planetary Science Letters 335-336, 226–237.

Kavanagh, J.L., Menand, T., Daniels, K., 2013. Gelatine as a crustal analogue: Determining elastic properties for modelling magmatic intrusions. Tectonophysics 582, 101–111.

Kavanagh, J.L., Menand, T., Sparks, R.S.J., 2006. An experimental investigation of sill formation and propagation in layered elastic media. Earth and Planetary Science Letters 245, 799–813.

Kavanagh, J.L., Sparks, R.S.J., 2011. Insights of dyke emplacement mechanics from detailed 3D dyke thickness datasets. Journal of the Geological Society, London 168, 965–978.

Keir, D., Hamling, I., Ayele, A., Calais, E., Ebinger, C., 2009. Evidence for focused magmatic accretion at segment centers from lateral dike injections captured .... Geology 37, 59–62. - Velocita' del dicco che si propaga deve fittare il modello? - Questo e' un altro problema cmq - Ipotesi del perche' rallenta cmq sono elencate: + drop in magma pressure as dike grows + along-rift gradients in tectonic stress + decrease in driving pressure gradient as size increases + resistance to flow from dike freezing.

Keller, T., May, D.A., Kaus, B.J.P., 2013. Numerical modelling of magma dynamics coupled to tectonic deformation of lithosphere and crust. Geophys. J. Int. .

Kervyn, M., Ernst, G., van Wyk de Vries, B., Mathieu, L., Jacobs, P., 2009. Volcano load control on dyke propagation and vent distribution: Insights from analogue modeling. J. Geophys. Res. 114, B03401.

Khristianovic, S., Zheltov, Y., 1955. Formation of vertical fractures by means of highly viscous fluids, in: Proc. 4th World Petroleum Congress, Carlo Colombo, Rome, Rome. pp. 579–586.

King, G.E., 2010. Thirty years of gas shale fracturing: What have we learned?, in: Proceedings SPE Annual Technical Conference and Exhibition, Florence, Italy. SPE 133256.

Kirton, S.R., Donato, J.A., 1985. Some buriedTertiary dykes of Britain and surrounding waters deduced by magnetic modelling and seismic reflection methods. J. Geol. Soc. London 142, 1047–1057.

Klein, F.W., Koyanagi, R.Y., Nakata, J.S., Tanigawa, W.R., 1987. The seismicity of Kilauea's magma system. Volcanism in Hawaii, U.S. Geological Survey Professional Paper 1350 Chapter 43, 1019–1185.

Knight, M.D., Walker, G.P.L., 1988. Magma flow directions in dykes of the Koolao complex, O'ahu, determined from magnetic fabric studies. J. Geophys. Res. 96, 19,539–19,544.

Kresse, O., Weng, X., Gu, H., Wu, R., 2013. Numerical modeling of hydraulic fractures interaction in complex naturally fractured formations. Rock Mechanics and Rock Engineering 46, 555–568.

Kühn, D., Dahm, T., 2004. Simulation of magma ascent by dykes in the mantle beneath mid-ocean ridges. Journal of Geodynamics 38, 147–159.

Kühn, D., Dahm, T., 2008. Numerical modelling of dyke interaction and its influence on oceanic crust formation. Tectonophysics 447, 53–65.

Lambert, S.W., Trevits, M.A., Steidl, P.F., 1980. Vertical Borehole Design and Completion Practices to Remove Methane Gas from Mineable Coalbeds. Technical Report DOE/CMTC/TR-80/2. United States Department of Energy.

Le Corvec, N., Menand, T., Lindsay, J., 2013. Interaction of ascending magma with pre-existing crustal fractures in monogenetic basaltic volcanism: an experimental approach. J. Geophys. Res.-Solid Earth 118, 968–984.

Lecampion, B., 2009. An extended finite element method for hydraulic fracture problems. Communications in Numerical Methods in Engineering 25, 121–133.

Li, L., Tang, C., Li, G., Wang, S., Liang, Z., Zhang, Y., 2012. Numerical simulation of 3D hydraulic fracturing based on an improved flow-stress-damage model and a parallel FEM technique. Rock mechanics and rock engineering 45, 801–818.

Linde, A., Agustsson, K., Sacks, I., Stefánsson, R., 1993. Mechanism of the 1991 eruption of Hekla from continuous borehole strain monitoring. Nature 365, 737–740.

Lister, J.R., 1990a. Buoyancy-driven fluid fracture: similarity solutions for the horizontal and vertical propagation of fluid-filled cracks. J. Fluid Mech. 217, 213–239.

Lister, J.R., 1990b. Buoyancy-driven fluid fracture: the effects of material toughness and of low-viscosity precursors. J. Fluid Mech. 210, 263–280.

Lister, J.R., 1991. Steady solutions for feeder dykes in a density-stratified lithosphere. Earth Planet. Sci. Lett. 107, 233–242.

Lister, J.R., 1994a. The solidification of buoyancy-driven flow in a flexible-walled channel. Part 1. Constant-volume release. J. Frac. Mech. 272, 21–44.

Lister, J.R., 1994b. The solidification of buoyancy-driven flow in a flexible-walled channel. Part 2. Continual release. J. Frac. Mech. 272, 44–65.

Lister, J.R., Kerr, R.C., 1991. Fluid-mechanical models of crack propagation and their application to magma transport in dykes. J. Geophys. Res. 96, 10049–10077.

Maccaferri, F., Bonafede, M., Rivalta, E., 2010. A numerical model of dyke propagation in layered elastic media. Geophys. J. Int. 180, 1107–1123. Cited by 15.

Maccaferri, F., Bonafede, M., Rivalta, E., 2011. A quantitative study of the mechanisms governing dike propagation, dike arrest and sill formation. J. Volc. Geoth. Res. 208, 39–50. Cited by 6.

Maccaferri, F., Rivalta, E., Keir, D., Acocella, V., 2014. Unloading-driven off-axis volcanism in rift zones. Nat. Geosci. 7, 297–300.

Maccaferri, F., Rivalta, E., Passarelli, L., Jónsson, S., 2013. The stress shadow induced by the 1975-1984 krafla rifting episode. J. Geophys. Res. 118, 1109–1121.

Maimon, O., Lyakhovsky, V., Melnik, O., Navon, O., 2012. The propagation of a dyke driven by gas-saturated magma. Geophysical Journal International 189, 956–966.

Mastin, L., Ghiorso, M., 2000. A Numerical Program for Steady-State Flow of Magma-Gas Mixtures Through Vertical Eruptive Conduits. Technical Report 00–209. U.S. Geological Survey Open-File Report.

Maxwell, S., Urbancic, T., Steinsberger, N., Zinno, R., 2002. Microseismic imaging of hydraulic fracture complexity in the Barnett shale, in: Proceedings SPE Annual Technical Conference and Exhibition, San Antonio, Texas, USA. SPE 77440.

McKenzie, D., 1984. The generation and compaction of partially molten rock. Journal of Petrology 25.

Menand, T., 2011. Physical controls and depth of emplacement of igneous bodies: A review. Tectonophysics 500, 11–19.

Menand, T., Daniels, K.A., Benghiat, P., 2010. Dyke propagation and sill formation in a compressive tectonic environment. J. Geophys. Res. 115, B08201.

Menand, T., Tait, S., 2002. The propagation of a buoyant liquid-filled fissure from a source under constant pressure: An experimental approach. J. Geophys. Res. 107, B11, 2306,doi:10.1029/2001JB000589.

Menand, T., Tait, S.R., 2001. A phenomenological model for precursor volcanic eruptions. Nature 411, 678–680.

Mériaux, C., Jaupart, C., 1995. Simple fluid dynamic models of volcanic rift zones. Earth and Planetary Science Letters 136, 223–240.

Meriaux, C., Jaupart, C., 1998. Dike propagation through an elastic plate. J. Geophys. Res. 103, 18295–18314.

Meyer, B., Bazan, L., 2011. A discrete fracture network model for hydraulically induced fractures-theory, parametric and case studies, in: Proceedings SPE Hydraulic Fracturing Technology Conference and Exhibition, The Woodlands, Texas, USA. SPE 140514.

Minson, S.E., Dreger, D.S., Bürgmann, R., Kanamori, H., Larson, K.M., 2007. Seismically and geodetically determined nondouble-couple source mechanisms from the 2000 Miyakejima volcanic earthquake swarm. Journal of Geophysical Research 112, B10308.

Mogi, K., 1958. Relations between the eruptions of various volcanoes and the deformations of the ground surfaces around them. Bulletin of the Earthquake Research Institute, University of Tokyo 36, 99–134.

Montagna, C.P., Gonnermann, H.M., 2013. Magma flow between summit and Pu'u 'O'o at Kilauea volcano, Hawai'i. Geophys. Geochem. Geosys. .

Montgomery-Brown, E.K., Sinnett, D.K., Larson, K.M., Poland, M.P., Segall, P., Miklius, A., 2011. Spatiotemporal evolution of dike opening and décollement slip at Kīlauea Volcano, Hawai'i. Journal of Geophysical Research 116.

Montgomery-Brown, E.K., Sinnett, D.K., Poland, M.P., Segall, P., Orr, T., Miklius, A., 2010. Geodetic evidence for en echelon dike emplacement and concurrent slow slip during the June 2007 intrusion and eruption at Kilauea volcano, Hawai'i. J. Geophys. Res. 115.

Morita, Y., Nakao, S., Hayashi, Y., 2006. A quantitative approach to the dike intrusion process inferred from a joint analysis of geodetic and seismological data for the 1998 earthquake swarm off the east coast of Izu Peninsula, central Japon. J. Geophys. Res. 111.

Mukuhira, Y., Nozaki, H., Asanuma, H., Niitsuma, H., Wyborn, D., Häring, M., 2010. Interpretation of microseismic events of large magnitudes collected at Cooper Basin, Australia and at Basel, Switzerland, in: Proceedings World Geothermal Congress, Bali, Indonesia.

Muller, J., Ito, G., Martel, S., 2001. Effects of volcano loading on dike propagation in an elastic half-space. Journal of Geophysical Research 106, 11101–11113.

Muskhelishvili, N.I., 1953. Singular Integral Equations. Nordhoff, the Netherlands.

Naceur, K.B., Thiercelin, M., Touboul, E., 1990. Simulation of fluid flow in hydraulic fracturing: Implications for 3D propagation. SPE Production Engineering 5, 133–141.

Nagel, N., Sanchez-Nagel, M., Zhang, F., Garcia, X., Lee, B., 2013. Coupled numerical evaluations of the geomechanical interactions between a hydraulic fracture stimulation and a natural fracture system in shale formations. Rock Mechanics and Rock Engineering , 1–29.

Nakamura, K., 1977. Volcanoes as possible indicators of tectonic stress orientation – principle and proposal. J. Volc. Geoth. Res. 2, 1–16.

Nakashima, Y., 1993. Static Stability and Propagation of a Fluid-Filled Crack in Rock: Implication for Fluid Transport in Magmatism and Metamorphism. J. Phys. Earth 41, 189–202.

Neres, M., Bouchez, J.L., Terrinha, P., Font, E., Moreira, M., Miranda, R., Launeau, P., Carvallo, C., 2014. Magnetic fabric in a Cretaceous sill (Foz da Fonte, Portugal): flow model and implications for regional magmatism. Geophys. J. Int. 199, 78–101.

Nishimura, T., Ozawa, S., Murakami, M., Sagiya, T., Tada, T., Kaidzu, M., Ukawa, M., 2001. Crustal deformation caused by magma migration in the northern Izu Islands, Japan. Geophys. Res. Lett. 28, 3745–3748.

Nobile, A., Pagli, C., Keir, D., Wright, T.J., Ayele, A., Ruch, J., Acocella, V., 2012. Dike-fault interaction during the 2004 Dallol intrusion at the northern edge of the Erta Ale Ridge (Afar, Ethiopia). Geophys. Res. Lett 39.

Nordgren, R., 1972. Propagation of vertical hydraulic fractures. J. Pet. Tech 253, 306–314. (SPE 3009).

Nuismer, R.J., 1975. An energy release rate criterion for mixed mode fracture. Int. J. Fracture 11, 245–250.

Nunn, J., 1996. Buoyancy-driven propagation of isolated fluid-filled fractures: implications for fluid transport in Gulf of Mexico geopressured sediments. Journal of Geophysical Research 101, 2963–2970.

Odé, H., 1957. Mechanical analysis of the dike pattern of the Spanish Peaks area, Colorado. Bulletin of the Geological Society of America 68, 567–576.

Okada, Y., 1985. Surface deformation due to shear and tensile faults in a half-space. Bull. Seism. Soc. Am. 75, 1135–1154.

Okada, Y., 1992. Internal deformation due to shear and tensile faults in a half-space. Bull. Seism. Soc. Am. 82, 1018–1040.

Okada, Y., Yamamoto, E., 1991. Dyke intrusion model for the 1989 seismo-volcanic activity off Ito, central Japan. Journal of Geophysical Research 96, 10361–10376.

Olson, J.E., 2003. Sublinear scaling of fracture aperture versus length: An exception or the rule? J. Geophys. Res. 108, 2413.

Olson, J.E., Dahi-Taleghani, A., 2009. Modeling simultaneous growth of multiple hydraulic fractures and their interaction with natural fractures, in: Proceedings SPE Hydraulic Fracturing Technology Conference and Exhibition, The Woodlands, Texas, USA. SPE 119739.

Olson, J.E., Schultz, R.A., 2011. Comment on "A note on the scaling relations for opening mode fractures in rock" by C.H. Scholz. J. Struct. Geol 33, 1523–1524.

Pallister, J.S., McCausland, W.A., Jónsson, S., Lu, Z., Zahran, H.M., El Hadidy, S., Aburukbah, A., Stewart, I.C.F., Lundgren, P., White, R.A., Moufti, M.R.H., 2010. Broad accommodation of rift-related extension recorded by dyke intrusion in Saudi Arabia. Nature Geoscience 3, 705–712.

Paquet, F., Dauteuil, O., Hallot, E., Moreau, F., 2007. Tectonics and magma dynamics coupling in a dyke swarm of Iceland. Journal of Structural Geology 29, 1477–1493.

Parotidis, M., Shapiro, S., Rothert, E., 2004. Back front of seismicity induced after termination of borehole fluid injection. Geophysical Research Letters 31, L02612.

Parsons, T., Sleep, N.H., Thompson, G.A., 1992. Host rock rheology controls on the emplacement of tabular intrusions: Implications for underplating of extending crust. Tectonics 11, 1348–1356.

Pascal, K., Neuberg, J., Rivalta, E., 2013. On precisely modelling surface deformation due to 2 interacting magma chambers and dikes. Geophys. J. Int. , under review.

Passarelli, L., Rivalta, E., Cesca, S., Aoki, Y., 2014a. A statistical analysis of the focal mechanisms for the earthquakes induced by the 2000 dike intrusion at miyakejima (japan). J. Geophys. Res. submitted.

Passarelli, L., Rivalta, E., Shuler, A., 2014b. Dike intrusions during rifting episodes obey scaling relationships similar to earthquakes. Sci. Rep. 4.

Patanè, D., Chiarabba, C., Cocina, O., De Gori, P., Moretti, M., Boschi, E., 2002. Tomographic images and 3D earthquake locations of the seismic swarm preceding the 2001 Mt. Etna eruption: Evidence for a dyke intrusion. Geophys. Res. Lett. 29, 4 pp.

Pearson, C., 1981. The relationship between microseismicity and high pore pressures during hydraulic stimulation experiments in low permeability granitic rocks. Journal of Geophysical Research: Solid Earth 86, 7855–7864.

Pedersen, R., Sigmundsson, F., Einarsson, P., 2007. Controlling factors on earthquake swarms associated with magmatic intrusions; Constraints from Iceland. J. Volc. Geoth. Res. 162, 73–80.

Pedersen, R., Sigmundsson, F., Masterlark, T., 2009. Rheologic controls on inter-rifting deformation of the Northern Volcanic Zone, Iceland. Earth and Planetary Science Letters 281, 14–26.

Peirce, A., Detournay, E., 2008. An implicit level set method for modeling hydraulically driven fractures. Computer Methods in Applied Mechanics and Engineering 197, 2858–2885.

Peltier, A., Ferrazzini, V., Staudacher, T., Bachèlery, P., 2005. Imaging the dynamics of dyke propagation prior to the 2000-2003 flank eruptions at Piton de La Fournaise, Reunion Island. Geophys. Res. Lett. 32, 22302.

Perkins, T., Kern, L., 1961. Widths of hydraulic fractures. J. Pet. Tech., Trans. AIME 222, 937–949.

Pinel, V., Jaupart, C., 2004. Magma storage and horizontal dyke injection beneath a volcanic edifice. Earth and Planetary Science Letters 221, 245–262.

Pinel, V., Poland, M., Hooper, A., 2014. Volcanology: Lessons learned from synthetic aperture radar imagery. J. Volc. Geoth. Res. , in press.

Pollard, D., 1976. On the form and stability of open hydraulic fractures in the earth's crust. Geophys. Res. Lett. 3, 513–516.

Pollard, D., 1987. Elementary fracture mechanics applied to the structural interpretation of dykes, in: H.C. Halls, W.F. (Ed.), Mafic Dyke Swarms. volume 34, pp. 5–24.

Pollard, D., Holzhausen, G., 1979. On the mechanical interaction between a fluid-filled fracture and the earth's surface. Tectonophysics 53, 27–57.

Pollard, D., Muller, O., 1976. The effect of gradients in regional stress and magma pressure on the form of sheet intrusions in cross section. J. Geophys. Res. 81, 975–984.

Pollard, D., Segall, P., Delaney, P., 1982. Formation and interpretation of dilatant echelon cracks. Bull. Geol. Soc. America 93, 1291–1303. http://gsabulletin.gsapubs.org/content/93/12/1291.full.pdf+html.

Pollard, D.D., Muller, O.H., Dockstader, D.R., 1975. The form and growth of fingered sheet intrusions. Bull. Geol. Soc. America 86, 351–363.

Qin, R., Buck, W., 2008. Why meter-wide dikes at oceanic spreading centers? Earth and Planetary Science Letters 265, 466–474.

Reches, Z., Fink, J., 1988. The mechanism of intrusion of the Inyo Dike, Long Valley Caldera, California. Journal of Geophysical Research 93, 4321–4334.

Reynolds, M., Thomson, S., Peyman, F., Hung, A., Quirk, D., Chen, S., 2012. A direct comparison of hydraulic fracture geometry and well performance between cemented liner and openhole packer completed horizontal wells in a tight gas reservoir, in: Proceedings SPE Hydraulic Fracturing Technology Conference, The Woodlands, Texas, USA. SPE 152185.

Rivalta, E., 2010. Evidence that coupling to magma chambers controls the volume history and velocity of laterally propagating intrusions. Journal of Geophysical Research 115, B07203.

Rivalta, E., Böttinger, M., Dahm, T., 2005. Buoyancy-driven fracture ascent: Experiments in layered gelatin. J. Volc. Geoth. Res. 144, 273–285.

Rivalta, E., Böttinger, M., Schnese, M., Dahm, T., 2013a. Supplement to: A review of numerical models of dike propagation: schools of thought, results and applications.

Rivalta, E., Böttinger, M., Schnese, M., Dahm, T., 2013b. Supplement to: Acceleration of buoyancy-driven fractures and magmatic dikes beneath the free surface.

Rivalta, E., Böttinger, M., Schnese, M., Dahm, T., 2013c. Supplement to: Buoyancy-driven fracture ascent: Experiments in layered gelatin.

Rivalta, E., Dahm, T., 2004. Dyke emplacement in fractured media: application to the 2000 intrusion at Izu islands, Japan. Geophys. J. Int. 157, 283–292.

Rivalta, E., Dahm, T., 2006. Acceleration of buoyancy-driven fractures and magmatic dikes beneath the free surface. Geophys. J. Int. 166, 1424–1439.

Rivalta, E., Mangiavillano, W., Bonafede, M., 2002. The edge dislocation problem in a layered elastic medium. Geophys. J. Int. 149, 508–523. Cited by 12.

Rivalta, E., Segall, P., 2008. Magma compressibility and the missing source for some dike intrusions. Geophys. Res. Lett. 35, L04306.

Roman, D.C., Cashman, K.V., 2006. The origin of volcano-tectonic earthquake swarms. Geology 34, 457.

Roman, D.C., Moran, S.C., Power, J.A., Cashman, K.V., 2004. Temporal and spatial variation of local stress fields before and after the 1992 eruptions of Crater Peak Vent, Mount Spurr volcano, Alaska. Bull. Seism. Soc. Am. 94, 2366–2379.

Roper, S., Lister, J., 2005. Buoyancy-driven crack propagation from an overpressured source. Journal of Fluid Mechanics 536, 79–98.

Roper, S., Lister, J., 2007. Buoyancy-driven crack propagation: the limit of large fracture toughness. Journal of Fluid Mechanics 580, 359–380.

Roult, G., Peltier, A., Taisne, B., Staudacher, T., Ferrazzini, V., Di Muro, A., 2012. A new comprehensive classification of the Piton de la Fournaise activity spanning the 1985-2010 period. Search and analysis of short-term precursors from a broad-band seismological station. Journal of Volcanology and Geothermal Research 241, 78–104.

Ru, Z., Zhao, H., Wang, M., 2013. Numerical modeling of hydraulic fracture propagation using Extended Finite Element Method, in: Hellmich, C., Pichler, B., Adam, D. (Eds.), Poromechanics V: Proceedings of the Fifth Biot Conference on Poromechanics, Vienna, Austria.

Rubin, A., 1993a. Dikes vs. diapirs in viscoelastic rocks. Earth and Planetary Science Letters 19, 641–659.

Rubin, A., 1993b. On the thermal viability of dikes leaving magma chambers. Geophys. Res. Lett. 20, 257–260.

Rubin, A., 1993c. Tensile fracture of rock at high confining pressure: implications for dike propagation. J. Geophys. Res. 98, 15919–935.

Rubin, A., 1995. Propagation of magma-filled cracks. Annual Review of Earth and Planetary Sciences 23, 287–336.

Rubin, A., Gillard, D., 1998. Dike-induced earthquakes— Theoretical considerations. Journal of Geophysical Research 103, 10017–10030.

Rubin, A., Gillard, D., Got, J.L., 1998. A reinterpretation of seismicity associated with the January 1983 dike intrusion at Kilauea volcano, Hawai'i. J. Geophys. Res. 103, 10003–10015.

Rutledge, J.T., Phillips, W.S., 2003. Hydraulic stimulation of natural fractures as revealed by induced microearthquakes, Carthage Cotton Valley gas field, east Texas. Geophysics 68, 441–452.

Sahagian, D., 2005. Volcanic eruption mechanisms: Insights from intercomparison of models of conduit processes. J. Volc. Geoth. Res. 143, 1–15.

Savage, J., Cockerham, R., 1984. Earthquake swarm in Long Valley caldera, California, January 1983: Evidence for dike inflation. Journal of Geophysical Research: Solid Earth 89, 8315–8324.

Savage, J., Yu, S., 2007. Postearthquake relaxation and aftershock accumulation linearly related after the 2003 M 6.5 Chengkung, Taiwan, and the 2004 M 6.0 Parkfield, California, earthquakes. Bulletin of the Seismological Society of America 97, 1632.

Schmidt, R., Huddle, C., 1977. Effect of confining pressure on fracture toughness of indiana limestone. International Journal of Rock Mechanics and Mining Sciences and Geomechanics Abstracts 14, 289 – 293.

Scholtz, C., 2010. A note on the scaling relations for opening mode fractures in rock. Journal of Structural Geology 106, 1485–1487.

Scott, D., Stevenson, D., 1986. Magma ascent by porous flow. J. Geophys. Res. 91.

Secor, Jr., D.T., Pollard, D.D., 1975. On the stability of open hydraulic fractures in the Earth's crust. Geophys. Res. Lett. 2, 510–513.

Segall, P., 2013. Volcano deformation and eruption forecasting. Geological Society, London, Special Publications , in press.

Segall, P., Cervelli, P., Owen, S., Lisowski, M., Miklius, A., 2001. Constraints on dike propagation from continuous GPS measurements. Journal of Geophysical Research 106, 19301–19317.

Segall, P., Desmarais, E.K., Shelly, D., Miklius, A., Cervelli, 2006. Earthquakes triggered by silent slip events on Kilauea volcano, Hawaii. Nature 442, 71–74.

Segall, P., Llenos, A.L., Yun, S.H., Bradley, A.M., Syracus, E.M., 2013. Time-dependent dike propagation from joint inversion of seismicity and deformation data. J. Geophys. Res. 118.

Shapiro, S., Dinske, C., Rothert, E., 2006. Hydraulic-fracturing controlled dynamics of microseismic clouds. Geophysical Research Letters 33, L14312.

Shapiro, S.A., Huenges, E., Borm, G., 1997. Estimating the crust permeability from fluid-injection-induced seismic emission at the ktb site. Geophysical Journal International 131, F15–F18.

Shapiro, S.A., Rothert, E., Rath, V., Rindschwentner, J., 2002. Characterization of fluid transport properties of reservoirs using induced microseismicity. Geophysics 67, 212–220.

Shlyapobersky, J., Issa, M.A., Issa, M.A., Islam, M.S., Dudley, J.W., Shulkin, Y., Chudnovsky, A., 1998. Scale effects on fracture growth resistance in poroelastic materials, in: Proceedings SPE Annual Technical Conference and Exhibition, New Orleans, Louisiana, USA. SPE 48929.

Sibson, R.H., 1996. Structural permeability of fluid-driven fault-fracture meshes. Journal of Structural Geology 18, 1031–1042.

Sigmundsson, F., 2006. Magma does the split. Nature 442, 251–252.

Sigmundsson, F., Einarsson, P., Bilham, R., 1992. Magma chamber deflation recorded by the global positioning system: the Hekla 1991 eruption. Geophys. Res. Lett. 19, 1483–1486.

Sigmundsson, F., Hreinsdóttir, H., Hooper, A., Árnadóttir, T., Pedersen, R., Roberts, M.J., Óskarsson, N., Auriac, A., Decriem, J., Einarsson, P., Geirsson, H., Hensch, M., Ófeigsson, B.G., Sturkell, E., Sveinbjörnsson, H., Feigl, K.L., 2010. Intrusion triggering of the 2010 Eyjafjallajökull explosive eruption. Nature 468, 426–432.

Sigurdsson, H., 1987. Dyke injection in Iceland: A review, in: Halls, H.C., Fahrig, W.F. (Eds.), Mafic Dyke Swarms, pp. 55–64.

Silva, P.F., Marques, F.O., Henry, B., Madureira, P., Hirt, A.M., Font, E., Lourenco, N., 2010. Thick dyke emplacement and internal flow: A structural and magnetic fabric study of the deep-seated dolerite dyke of Foum Zguid (southern Morocco). Journal of Geophysical Research 115, 26 pp.

Simonson, E.R., Abou-Sayed, A.S., Clifton, R.J., 1978. Containment of massive hydraulic fractures. SPE Journal 18, 27–32.

Siniscalchi, A., Tripaldi, S., Neri, M., Balasco, M., Romano, G., Ruch, J., Schiavone, D., 2012. Flank instability structure of Mt. Etna inferred by a

magnetotelluric survey. Journal of Geophysical Research — Atmosphere 117.

Skempton, A., 1960. Effective stress in soils, concrete and rocks, in: Proceedings of the conference on pore pressure and suction in soils, pp. 4–16.

Sommer, E., 1969. Formation of fracture lances in glass. Engineering Fracture Mechanics 1, 539 – 546.

Sparks, D., Baker, L., Brown, R., Field, M., Schumacher, j., Stripp, G., Walters, A., 2006. Dynamical constraints on kimberlite volcanism. J. Volc. Geoth. Res. 155, 18–48.

Sparks, D., Parmentier, E., 1991. Melt extraction from the mantle beneath spreading centers. Earth and Planetary Science Letters 105, 368–377.

Spence, D., Sharp, P., 1985. Self-similar solution for elastohydrodynamic cavity flow. Proc. Roy. Soc. London A 400, 289–313.

Spence, D.A., Sharp, P.W., Turcotte, D.L., 1987. Buoyancy-driven crack propagation: a mechanism for magma migration. J. Fluid Mech. 174, 135–153.

Spence, D.A., Turcotte, D.L., 1990. Buoyancy-driven magma fracture: a mechanism for ascent through the lithosphere and the emplacement of diamonds,. J. Geophys. Res. 95, 5133–5139.

Spera, F., 2000. Physical properties of magma, in: Sigurdsson, H. (Ed.), Encyclopedia of Volcanoes. Academic, San Diego, California, p. 171190.

Spiegelman, M., McKenzie, D., 1987. Simple 2-D models for melt extraction at mid-ocean ridges and island arcs. Earth and Planetary Science Letters 83.

Steidl, P.F., 1991. Inspection of induced fractures intercepted by mining in the Warrior Basin, Alabama, in: Proceedings Coalbed Methane Symposium, Tuscaloosa, Alabama, USA. Paper 9162.

Stein, R., 1999. The role of stress transfer in earthquake occurrence. Nature 402, 605–609.

Sturkell, E., Sigmundsson, F., Slunga, R., 2006. 19832003 decaying rate of deflation at Askja caldera: Pressure decrease in an extensive magma plumbing system at a spreading plate boundary. Bull. Volcanol. 68, 727–735.

Sumita, I., Ota, Y., 2011. Experiments on buoyancy-driven crack around the brittle-ductile transition. Earth and Planetary Science Letters 304, 337–346.

Taisne, B., Brenguier, F., Shapiro, N.M., Ferrazzini, V., 2011a. Imaging the dynamics of magma propagation using radiated seismic intensity. Geophys. Res. Lett. 38, 4304.

Taisne, B., Jaupart, C., 2009. Dike propagation through layered rocks. Journal of Geophysical Research (Solid Earth) 114, 9203.

Taisne, B., Jaupart, C., 2011. Magma expansion and fragmentation in a propagating dyke. Earth and Planetary Science Letters 301, 146–152.

Taisne, B., Tait, S., 2009. Eruption versus intrusion? Arrest of propagation of constant volume, buoyant, liquid-filled cracks in an elastic, brittle host. Journal of Geophysical Research (Solid Earth) 114, 6202.

Taisne, B., Tait, S., 2011. Effect of solidification on a propagating dike. Journal of Geophysical Research (Solid Earth) 116, 1206.

Taisne, B., Tait, S., Jaupart, C., 2011b. Conditions for the arrest of a vertical propagating dyke. Bulletin of Volcanology 73, 191–204.

Tait, S., Taisne, B., 2013. Experimental models of hydraulic fissures with application to the propagation of magmatic dykes, in: S. A. Fagents, T. K. P. Gregg and R. M. C. Lopes (Ed.), Modeling Volcanic Processes: The Physics and Mathematics of Volcanism. Cambridge University Press. chapter 3.

Takada, A., 1989. Magma transport and reservoir formation by a system of propagating cracks. Bulletin of Volcanology 52, 118–126.

Takada, A., 1990. Experimental study on propagation of liquid-filled crack in gelatin: shape and velocity in hydrostatic stress conditions. J. Geophys. Res. 95, 8471–8481.

Takada, A., 1994a. Accumulation of magma in space and time by crack interaction, in: Ryan, M. (Ed.), Magmatic systems. Academic Press, pp. 241–257.

Takada, A., 1994b. Development of a subvolcanic structure by the interaction of liquid-filled cracks. J. Volc. Geoth. Res. 62, 207–224.

Tarasewicz, J., White, R., Woods, A., Brandsdóttir, B., Gudmundsson, M., 2012. Magma mobilization by downward-propagating decompression of the Eyjafjallajökull volcanic plumbing system. Geophys. Res. Lett. 39, L19309.

Terzaghi, K., 1943. Theoretical soil mechanics. John Wiley.

Tester, J.W., Anderson, B., Batchelor, A., Blackwell, D., DiPippo, R., Drake, E., Garnish, J., Livesay, B., Moore, M., Nichols, K., et al., 2006. The future of geothermal energy. Technical Report 358. Massachusetts Institute of Technology. Cambridge, MA, USA.

Teufel, L.W., Clark, J.A., 1984. Hydraulic fracture propagation in layered rock: Experimental studies of fracture containment. SPE Journal 24, 19–32.

Thordarson, T., Self, S., 1993. The Laki (Skaftar Fires) and Grimsvötn eruptions in 1783–1785. Bull. Volcanol. 55, 233–263.

Toda, S., Stein, R., 2002. Evidence from the AD 2000 Izu islands earthquake swarm that stressing rate governs seismicity. Nature 419, 58–61.

Toda, S., Stein, R., Beroza, G., Marsan, D., 2012. Aftershocks halted by static stress shadows. Nature Geosci. 419, 410–413.

Toda, S., Stein, R.S., Sagiya, T., 2002. Evidence from the AD 2000 Izu islands earthquake swarm that stressing rate governs seismicity. Nature 419, 58–61.

Touvet, T., Balmforth, N.J., Craster, R.V., Sutherland, B.R., 2011. Fingering instability in buoyancy-driven fluid-filled cracks. Journal of Fluid Mechanics 672, 60–77.

Traversa, P., Pinel, V., Grasso, J.R., 2010. A constant influx model for dike propagation: Implications for magma reservoir dynamics. Journal of Geophysical Research 115, B01201.

Tryggvason, E., 1984. Widening of the Krafla fissure swarm during the 1975–1981 volcano-tectonic episode. Bulletin of Volcanology 47, 47–69.

Tryggvason, E., 1986. Multiple magma reservoirs in a rift zone volcano: Ground deformation and magma transport during the September 1984 eruption of Krafla, Iceland. Journal of Volcanology and Geothermal Research 28, 1–44.

Uhira, K., Baba, T., Mori, H., Katayama, H., Hamada, N., 2005. Earthquake swarms preceding the 2000 eruption of Miyakejima volcano, Japan. Bulletin of Volcanology 67, 219–230.

Valentine, G.A., Krogh, K.E.C., 2006. Emplacement of shallow dikes and sills beneath a small basaltic volcanic center 17The role of pre-existing structure (Paiute Ridge, southern Nevada, USA) . EPSL 246, 217–230.

Valley, B., Evans, K.F., 2007. Stress state at Soultz-sous-Forêts to 5 km depth from wellbore failure and hydraulic observations, in: Proceedings 32nd Stanford Workshop on Geothermal Reservoir Engineering, Stanford, CA, USA.

Vandamme, L., Curran, J.H., 1989. A three-dimensional hydraulic fracturing simulator. International journal for numerical methods in engineering 28, 909–927.

Vermilye, J.M., Scholz, C.H., 1995. Relation between vein length and aperture. J. Struct. Geol. 17, 423–434.

Walker, G.P.L., 1986. Koolau dike complex, Oahu: Intensity and origin of a sheeted-dike complex high in a Hawaiian volcanic edifice. Geology 14, 310–313.

Walker, H., Wutherich, K., Terry, J., 2012. Engineered perforation design improves fracture placement and productivity in horizontal shale gas wells, in: Proceedings SPE Americas Unconventional Resources Conference, Pittsburgh, PA, USA. SPE 154582.

Wangen, M., 2011. Finite element modeling of hydraulic fracturing on a reservoir scale in 2D. Journal of Petroleum Science and Engineering 77, 274–285.

Warpinski, N., 1985. Measurement of width and pressure in a propagating hydraulic fracture. SPE Journal 25, 46–54. SPE 11648.

Warpinski, N., Du, J., Zimmer, U., 2012a. Measurements of hydraulic-fracture-induced seismicity in gas shales. SPE Production and Operations 27, 240–252.

Warpinski, N., Mayerhofer, M., Agarwal, K., Du, J., 2012b. Hydraulic fracture geomechanics and microseismic source mechanisms, in: Proceedings SPE Annual Technical Conference and Exhibition, San Antonio, Texas, USA. SPE 158935.

Warpinski, N., Schmidt, R., Northrop, D., 1982. In-situ stresses: the predominant influence of hydraulic fracture containment. J. Petroleum Technology 34, 653–664. SPE 8932.

Warpinski, N.R., 2013. Understanding hydraulic fracture growth, effectiveness, and safety through microseismic monitoring, in: Bunger, A.P., McLennan, J., Jeffrey, R.G. (Eds.), Effective and Sustainable Hydraulic Fracturing. Intech, Rijeka, Croatia. chapter 6.

Warpinski, N.R., Teufel, L.W., 1987. Influence of geologic discontinuities on hydraulic fracture propagation. J. Petroleum Technology 39, 209–220. SPE 13224.

Watanabe, T., Masuyama, T., Nagaoka, K., 2002. Analog experiments on magma-filled cracks: Competition between external stresses and internal pressure. Earth Planets and Space 54, 1247–1261.

Weber, N., Siebert, P., Willbrand, K., Feinendegen, M., Clauser, C., Fries, T., 2013. The XFEM with an explicit-implicit crack description for hydraulic fracture problems, in: Bunger, A.P., McLennan, J., Jeffrey, R.G. (Eds.), Effective and Sustainable Hydraulic Fracturing. Intech, Rijeka, Croatia. chapter 35.

Weertman, J., 1971a. Theory of water-filled crevasses in glaciers applied to vertical magma transport beneath oceanic ridges. J. Geophys. Res. 76, 1171–1183.

Weertman, J., 1971b. Velocity at which liquid-filled cracks move in the Earth's crust or in glaciers. J. Geophys. Res. 76, 8544–8553.

Weertman, J., 1973. Can a water-filled crevasse reach the bottom surface of a glacier? IASH Publishing (Proc. Symp. on the Hydrology of Glaciers, Cambridge, 7–13 September 1969) 1973 76, 139–145.

Weertman, J., 1980. The stopping of a rising, liquid-filled crack in the Earth's crust by a freely slipping horizontal joint. J. Geophys. Res. 85, 967–976.

White, R., Drew, J., Martens, H., Key, J., 2011. Dynamics of dyke intrusion in the mid-crust of Iceland. Earth and Planetary Science Letters 304, 300–312.

Wong, T., Ko, S., Olgaard, D., 1997. Generation and maintenance of pore pressure excess in a dehydrating system. 2. theoretical analysis. J. Geophys. Res. 102, 841–852.

Wright, T., Ebinger, C., Biggs, J., Ayele, A., Yirgu, G., 2006. Magma-maintained rift segmentation at continental rupture in the 2005 Afar dyking episode. Nature 442, 291–294.

Wright, T., Sigmundsson, F., Pagli, C., Belachew, M., Hamling, I., Brandsdóttir, B., Keir, D., Pedersen, R., Ayele, A., Ebinger, C., Einarsson, P., Lewi, E., Calais, E., 2012. Geophysical constraints on the dynamics of spreading centres from rifting episodes on land. Nature Geoscience 5, 242–250.

Wu, R., Germanovich, L.N., Hurt, R.S., 2009. Experimental and theoretical study of mixed-mode i+iii crack propagation and segmentation, in: Proceedings 43rd U.S. Rock Mechanics Symposium, Asheville, North Carolina, USA. ARMA 09-142.

Xu, W., Jónsson, S., 2014. The 2007–8 volcanic eruption on Jebel at Tair island (Red Sea) observed by satellite radar and optical images. Bulletin of Volcanology 76, 795.

Yamakawa, N., 1955. On the strain produced in a semi-infinite elastic solid by an interior source of stress. Journal of the Seismological Society of Japan 8, 84–98.

Yun, S., Segall, P., H, Z., 2006. Constraints on magma chamber geometry at Sierra Negra Volcano, Galápagos Islands, based on InSAR observations. J. Volc. Geoth. Res. 150, 232173.

Zhang, X., Jeffrey, R.G., Thiercelin, M., 2009. Mechanics of fluid-driven fracture growth in naturally fractured reservoirs with simple network geometries. J. Geophys. Res. 114, B08416.

Ziv, A., Rubin, A., Agnon, A., 2000. Stability of dike intrusion along preexisting fractures. Journal of Geophysical Research 105, 5947–5961.